

**Elucidation of Structural Factors Controlling Thermal Stability
of Bulk and Metal-Oxide Supported Phosphonium Ionic Liquids**

by

Volkan Balci

**A Thesis Submitted to the
Graduate School of Sciences and Engineering
in Partial Fulfillment of the Requirements for
the Degree of**

**Master of Science
in
Chemical and Biological Engineering**

Koc University

September 2014

Koc University
Graduate School of Sciences and Engineering

This is to certify that I have examined this copy of a master's thesis by

Volkan Balci

and have found that it is complete and satisfactory in all respects,
and that any and all revisions required by the final
examining committee have been made.

Committee Members:

Alper Uzun, Ph. D. (Advisor)

Seda Keskin, Ph. D.

Melis Şerefođlu, Ph. D.

Date:

ABSTRACT

Ionic liquids (ILs) are a novel class of green solvents recognized as potential replacements for conventional volatile organic compounds. They have attracted great attention in the last decade because of their unique physicochemical properties, such as extremely low volatility, low melting point ($<100\text{ }^{\circ}\text{C}$), high solvating ability, and high thermal stability. These physicochemical properties can be tailored by integrating almost endless number of different combinations of anions and cations; hence they are often called “designer” or “task-specific” solvents. Their tailor-made characteristics offer a wide range of applications in numerous research fields, such as synthesis, separation, electrochemistry, and catalysis. Their applicability in these fields primarily depends on whether they protect their structural integrity at the operating conditions. In catalysis, for example, ILs are immobilized on metal-oxide surfaces, thus, they directly interact with these surfaces. Therefore, application of ILs in such supported-catalyst concepts is limited with their thermal stabilities on corresponding support materials. Though most of the ILs are thermally stable at elevated temperatures ($> 300\text{ }^{\circ}\text{C}$) in their pure state, they become less stable when coated on metal-oxide supports because of the interactions between IL and metal-oxide. Thus, it is crucial to elucidate structural factors controlling the thermal stability of bulk and supported ILs for choosing the best ILs for specific processes.

In the first part of thesis, such structural factors controlling thermal stability limits of bulk phosphonium ILs were determined by combining experiments with Density Functional Theory (DFT) calculations. Decomposition mechanisms were elucidated by utilizing DFT calculated ^1H NMR chemical shifts of individual protons quantifying electron density around them. Data illustrated that electron density around terminal protons of the alkyl group closest to the anion present a perfect correlation with the stability limits. Based on this finding, a general thermal decomposition mechanism for phosphonium ILs

was postulated and confirmed by on-line mass spectrometry monitoring decomposition products of a representative phosphonium IL. Accordingly, reaction involves nucleophilic substitution of the anion at α -carbon of its closest neighboring alkyl chain on the cation. Identification of structural factors controlling thermal stability limits and elucidation of decomposition mechanism create opportunities for rational design of ILs with superior thermal stability.

In the same manner, structural factors governing the thermal stability limits of phosphonium ILs supported on SiO_2 , $\gamma\text{-Al}_2\text{O}_3$, and MgO were investigated using thermogravimetric analysis. Results indicated that thermal stability limits of these ILs diverge greatly from the corresponding bulk values when they are immobilized on metal-oxide supports. More pronounced effect of the support was observed for ILs immobilized on MgO . This higher deviation from bulk values was attributed to stronger interactions between basic MgO surface and ILs than those with other support materials. Thus, surface acidity was identified as one of the factors controlling the stability limits. The other factors were characterized as the size of IL, and electronegativity and aromaticity of the anion. Once these structural factors are fully identified, it would be, therefore, possible to select an optimum phosphonium IL that retains its performance and functional activity at designed operating temperatures in supported-IL processes.

Consequently, interaction energies between anions and cations of some imidazolium ILs with 1-butyl-1-methylimidazolium ($[\text{BMIM}]^+$) cation were determined using DFT calculations. These interaction energies were further used to be associated with experimental stretching frequencies of the acidic proton on the imidazolium ring (C2–H). Results illustrated that experimental C2–H stretching frequencies correlate proportionally with calculated interaction energies. Therefore, this correlation renders a quick estimation of interaction energies between anions and cations of $[\text{BMIM}]^+$ -based imidazolium ILs by simply utilizing experimental C2–H stretching frequencies. This information together with

those acquired on phosphonium ILs throughout this thesis will set the basis for future work focusing on atomic-scale understanding of structure-performance relationship in IL-assisted metal catalysts for energy related applications.

ÖZET

İyonik sıvılar (İS'ler), klasik uçucu organik çözücülerin yerini alacağı düşünülen yeni bir çevreci çözücü sınıfıdır. Son derece düşük uçuculuk, düşük erime noktası (<100 °C), yüksek çözdürücü yeteneği ve yüksek ısı kararlılık gibi kendilerine özgü fizikokimyasal özellikleri sebebiyle son on yılda büyük ilgi görmüşlerdir. Bu fizikokimyasal özellikler, anyon ve katyonun neredeyse sonsuz sayıdaki farklı kombinasyonları birleştirilerek tasarlanabilir; bundan dolayı genellikle "tasarımcı" veya "göreve özel" çözücüler olarak adlandırılırlar. İS'lerin tasarlanabilen bu özellikleri; sentez, ayırma, elektrokimya ve kataliz gibi çok sayıda araştırma alanında geniş bir yelpazede kullanılabilme imkanı sunmaktadır. Bu alanlardaki uygulanabilirlikleri, öncelikli olarak, çalışma koşullarında yapısal bütünlüklerini korumalarına bağlıdır. Örneğin, kataliz alanında, İS'ler metal oksit yüzeyler üzerinde sabitlenirler; dolayısıyla bu yüzeyler ile etkileşirler. Bu nedenle, İS'lerin bu tür destekli katalizör konseptlerinde uygulanması, ilgili destek malzemeleri üzerindeki ısı kararlılıkları ile sınırlıdır. Çoğu İS, saf hallerinde yüksek sıcaklıklarda (> 300 °C) ısı olarak kararlı olmalarına rağmen metal oksitler üzerine kaplandıklarında, İS ve metal oksit arasındaki etkileşimlerden dolayı daha az kararlı olurlar. Bu sebeple; saf ve destekli İS'lerin ısı kararlılıklarını kontrol eden yapısal faktörleri belirlemek, belirli proseslerde kullanmak üzere en uygun İS'yi seçmek için son derece önemlidir.

Tezin ilk bölümünde, saf fosforyum İS'lerinin ısı kararlılık limitlerini kontrol eden bu yapısal faktörler, Yoğunluk Fonksiyonel Teorisi (YFT) hesaplamaları ile deneysel çalışmaların birleştirilmesi ile belirlendi. Bozunma mekanizmaları, her bir protonun etrafındaki elektron yoğunluğunu ölçen YFT ile hesaplanmış ¹H NMR kimyasal kaymaları kullanılarak ortaya çıkarılmıştır. Anyona en yakın alkil grubunun terminal protonları etrafındaki elektron yoğunluğu, kararlılık limitleri ile mükemmel bir korelasyon göstermiştir. Bu bulguya dayanarak, fosforyum İS'leri için genel bir ısı bozunma

mekanizması öne sürülmüştür ve temsili bir fosfonyum İS'sinin ısıl bozunma ürünlerini on-line olarak izleyen kütle spektrometresi ile teyit edilmiştir. Buna göre, reaksiyon, anyonun katyondaki ona en yakın komşu alkil zincirinin α -karbonuna nükleofilik katılmasını içerir. Isıl kararlılık limitlerini kontrol eden yapısal faktörlerin belirlenmesi ve bozunma mekanizmasının ortaya çıkarılması, üstün ısıl kararlı İS'lerin akılcı tasarımına yönelik fırsatlar yaratmaktadır.

Aynı şekilde, SiO_2 , $\gamma\text{-Al}_2\text{O}_3$ ve MgO üzerinde desteklenmiş fosfonyum İS'lerinin ısıl kararlılık limitlerini düzenleyen yapısal faktörler termogravimetrik analiz ile incelenmiştir. Sonuçlar, bu İS'lerin ısıl kararlılık limitlerinin, metal oksitler üzerinde desteklendiklerinde, ilgili saf değerlerinden büyük oranda saptığını göstermiştir. MgO ile desteklenen İS'ler üzerinde, destek malzemesinin etkisinin daha belirgin olduğu gözlemlenmiştir. Bu saf değerlerden daha yüksek sapmanın, MgO yüzeyi ile İS'ler arasında, diğer destek malzemelerine kıyasla, daha güçlü etkileşimlerden kaynaklandığına atfedilmiştir. Bu nedenle, yüzey asitliği, kararlılık limitlerini kontrol eden faktörlerden biri olarak tanımlanmıştır. Diğer faktörler, İS'nin boyutu, anyonun elektronegatifliği ve aromatikliği olarak karakterize edilmiştir. Bu yapısal unsurlar tümüyle tespit edildikten sonra, destekli İS proseslerinin tasarlanan çalışma sıcaklıklarında, performansını ve fonksiyonel aktivitesini koruyan en uygun fosfonyum İS'sini seçmek dolayısıyla mümkün olacaktır.

Sonuç olarak, 1-bütül-1-metil-imidazolyum ($[\text{BMIM}]^+$) katyonuna sahip bazı imidazolyum İS'lerinin anyonları ve katyonları arasındaki etkileşim enerjileri, YFT hesaplamaları kullanılarak belirlendi. Daha sonra bu etkileşim enerjileri, imidazolyum halkasında bulunan asidik protonun (C2-H) deneysel gerilme frekansları ile ilişkilendirilmek için kullanılmıştır. Sonuçlar, deneysel C2-H gerilme frekanslarının hesaplanmış etkileşim enerjileri ile orantısal bir ilişkide olduğunu göstermiştir. Dolayısıyla, bu ilişki, $[\text{BMIM}]^+$ bazlı imidazolyum İS'lerinin anyonları ve katyonları arasındaki etkileşim enerjilerinin, sadece deneysel C2-H gerilme frekanslarını kullanarak hızlı bir

tahminini mümkün kılar. Bu bilgi ve bu tez boyunca fosfonyum İS'leri üzerine elde edilenlerle birlikte, İS-destekli metal katalizörlerinin enerji uygulamalarındaki yapı-performans ilişkisini atomik ölçekte anlamaya odaklı gelecekteki çalışmalara temel teşkil edecektir.

ACKNOWLEDGEMENTS

My most sincere thanks go to my advisor Asst. Prof. Dr. Alper Uzun for giving me the opportunity to pursue my master degree in his research group, and for his excellent guidance, valuable advices and constant support during this study.

I am also grateful to Dr. Rıza Kızılel for always providing assistance and doing a great job in maintaining KÜTEM for its smooth and efficient functioning.

I would like to express my thanks to my group members Aslı Akçay and Melike Babucci for their kind support and friendship.

I want to express my gratitude to Hüseyin Özbey for providing help with the computing clusters that I used during DFT calculations.

My special thanks go to my beloved friends Yaprak Özbakır, Ayşe Dilan Çelebi, Selma Bulut, Deniz Şanlı, Fatih Rahim, Sinan Yüçetürk, İbrahim Şahin, Ehsan Sarayloo, Amir Hossein Habibi, Metin Karayılan and Okan Yalçın for their encouragement and sincere friendships. Thank you for being source of motivation and happiness all the time.

Most importantly, this thesis would not have been possible without unconditional love, care and continuous support of my family. Their belief in me has always given me the strength and confidence along this arduous journey to carry on my graduate studies.

To my mother and sister

TABLE OF CONTENTS

List of Tables	xiii
List of Figures	xiv
Chapter 1: Introduction	1
Chapter 2: Literature Review	4
2.1 Ionic Liquids: Definition and Applications.....	4
2.2 Physicochemical Properties of Ionic Liquids.....	6
2.3 Catalysis in Ionic Liquids.....	10
2.4 Thermal Stability of Ionic Liquids	12
Chapter 3: Experimental and Computational Methods	17
3.1 Chemicals	17
3.2 Sample Preparation	17
3.3 Thermogravimetric Analysis (TGA)	19
3.4 Monitoring of Decomposition Products by Mass Spectrometry	19
3.5 FTIR Spectroscopy.....	20
3.6 Computational Methods	21
Chapter 4: Thermal Stability of Bulk Phosphonium Ionic Liquids	23
4.1 Introduction	23
4.2 Characterization and Modeling of Phosphonium ILs	25
4.3 Thermal Stability of Phosphonium ILs	31

4.4 Structural Factors Controlling Thermal Stability Limits and Decomposition Mechanism	35
Chapter 5: Thermal Stability of Metal-Oxide Supported Phosphonium Ionic Liquids	41
5.1 Introduction	41
5.2 Thermal Stability Limits of Metal-Oxide Supported Phosphonium Ionic Liquids.....	42
Chapter 6: Probing Cation-Anion Interaction Energies in Imidazolium Ionic Liquids	47
6.1 Introduction	47
6.2 Conformational Analysis and Computation of Interaction Energies	49
6.3. Correlation between Interaction Energy and Vibration Frequency	60
Chapter 7: Conclusions and Outlook	63
Bibliography	66
Appendix	75

LIST OF TABLES

Table 2.1: Comparison of melting points of ILs with conventional salts	8
Table 3.1: Structures of phosphonium ILs investigated in this study	18
Table 4.1: Vibration frequencies assignments of phosphonium ILs.....	27
Table 4.2: Thermal stability limits of phosphonium ILs	33
Table 5.1: Thermal stability limits of bulk and supported phosphonium ILs.....	44
Table 6.1: Interaction energies and experimental C2–H stretching frequencies of ILs.....	53

LIST OF FIGURES

Figure 2.1: Some commonly used cations for ILs	5
Figure 2.2: Some commonly used anions for ILs	5
Figure 2.3: Number of ILs related publications over the years	7
Figure 2.4: Structural differences between conventional salt and ILs.....	9
Figure 2.5: The local hydrogen bonding between cation and anion of [EMIM][Cl].....	9
Figure 2.6: The correlation of melting points and interaction energies for [MMIM], [EMIM], [BMIM], [PMIM] based ILs	10
Figure 2.7: Comparison of SILP and SCILL concepts.....	11
Figure 2.8: (a) Illustration of possible IL confinement in SiO ₂ matrix pores as obtained from HF calculations (b) Equivalent ‘hinged spring’ model of IL confined in SiO ₂ nanopores	15
Figure 3.1: Determination of T _{onset} , T’ _{onset} , and T’ _{peak} values on a representative TGA data obtained for [BMIM][NTf ₂]	20
Figure 4.1: Representative optimized geometries for ILs based on [P ₄₄₄₁], [P ₄₄₄₄] and [P ₆₆₆₍₁₄₎] (a) [P ₄₄₄₁][DBP], (b) [P ₄₄₄₄][MeSO ₃], and (c) [P ₆₆₆₍₁₄₎][Br].....	29
Figure 4.2: Comparison of fast-scan TGA results of phosphonium ILs.....	32
Figure 4.3: Regression analysis results between chemical shifts of individual protons and thermal stability limits of ILs.....	36
Figure 4.4: Relationship between thermal stability limits of ILs and DFT calculated chemical shifts of T9-protons on each IL	37

Figure 4.5: TGA and MS results in the effluent stream during temperature programmed decomposition of $[P_{666(14)}][Cl]$	39
Figure 5.1: Comparison of thermal stability limits of phosphonium ILs supported on different metal oxides	43
Figure 6.1: Structures of imidazolium ILs based on [BMIM] cation	51
Figure 6.2: Conformers and relative energies of [BMIM][BF ₄].....	54
Figure 6.3: Conformers and relative energies of [BMIM][SbF ₆]	55
Figure 6.4: Conformers and relative energies of [BMIM][NTf ₂].....	56
Figure 6.5: Conformers and relative energies of [BMIM][TfO]	57
Figure 6.6: Conformers and relative energies of [BMIM][SCN]	58
Figure 6.7: Conformers and relative energies of [BMIM][DBP]	59
Figure 6.8: Relationship between experimental $\nu(C2-H)$ and interaction energies between cation and anion of corresponding ILs.....	61
Figure 6.9: Relationship between experimental $\nu(C4,5-H)$ and interaction energies between cation and anion of corresponding ILs	62

Chapter 1

INTRODUCTION

Ionic liquids (ILs) are new-generation green solvents and potential alternatives for their volatile organic counterparts. They have received tremendous attention during the last decade because of their unique physical and chemical properties, such as non-volatility, non-flammability, high chemical and thermal stability, high solvating ability and tunable miscibility. These physicochemical properties can be tailored by incorporating almost infinite combinations of different anions and cations; hence they are often called as “designer” or “task-specific” solvents. Such structural diversity and functional flexibility has led to a growing interest towards application in numerous research fields such as synthesis, electrochemistry, separation, and catalysis [1].

As one of the emergent application areas, two primary concepts have been pioneered to exploit tunable features of ILs in catalysis -*supported ionic liquid phase* (SILP) [2] and *solid catalysts with an ionic liquid layer* (SCILL) [3]. For SILP-type catalyst, a thin layer of ionic liquid containing a homogeneous catalyst is applied to the internal surface of a porous support material. Similarly, in SCILL concept, heterogeneous catalyst or catalytically active materials are coated with a thin film of IL. These promising catalytic concepts lead to enhanced selectivity, product distribution, yields, and selective solubility for intermediates and products because of promoting interactions between active sites, supports and IL. However, application of ILs in these supported-catalyst concepts is limited with their thermal stability on corresponding support materials. Though most of the

ILs are thermally stable at elevated temperatures ($> 300\text{ }^{\circ}\text{C}$) in their pure state, they become less stable when coated on metal-oxide supports because of the interactions between IL and metal-oxide.

Within the scope of this thesis, structural factors determining the thermal stability limits of nine different bulk phosphonium ILs and their thermal decomposition mechanisms were first elucidated by combining experiments with theory. Subsequently, thermal stability limits of phosphonium ILs immobilized on three of the most commonly used metal-oxide catalyst supports, namely SiO_2 , $\gamma\text{-Al}_2\text{O}_3$, and MgO , were investigated. Finally, interaction energies between cation and anion in different imidazolium ILs were computed and correlated with experimental vibration frequencies.

Chapter 2 provides background information on the nature of ILs and their types, physicochemical properties and potential applications in different research fields. Specifically, their effects on catalytic performance and applications in catalysis field are discussed in detail. It also presents a comprehensive literature review focusing on thermal stability limits of bulk and supported ILs.

Chapter 3 describes experimental methods in detail used for purification, characterization and thermal stability analyses of bulk and supported ILs. Furthermore, quantum-mechanical computational methods used for geometry optimization, vibration and Nuclear Magnetic Resonance (NMR) spectra calculations of corresponding ILs are given in this section.

Chapter 4 reports results of systematic investigation on the elucidation of structural factors determining thermal stability limits of nine bulk phosphonium ILs by combining experiments with Density Functional Theory (DFT) calculations. In addition, thermal decomposition mechanisms of corresponding bulk phosphonium ILs are elucidated in this section.

Chapter 5 reports results of elucidation of thermal stability limits of phosphonium ILs by thermogravimetric analysis complemented by spectroscopy and theory, which are immobilized on three different metal-oxide catalyst supports, *viz.*, SiO₂, γ -Al₂O₃, and MgO.

Chapter 6 discusses geometry optimization, conformational search and calculation of spectroscopic properties of imidazolium ILs based on DFT calculations. Moreover, strength of interaction between cation and anion in different imidazolium ILs is assessed and correlated by experimental vibration frequencies in combination with DFT calculations. This part of the thesis was performed to complement another study in our research group.

Chapter 7 summarizes and highlights the results presented throughout the thesis, and provides an outlook for future research in this area.

All in all, we performed a fundamental study addressing the composite interactions prevailing between anion–cation of bulk ILs as well as IL–support surfaces. An in-depth analysis of these inherent interactions is particularly crucial as they intrinsically determine the physicochemical and thermochemical properties in bulk and supported IL systems. Among these, thermal stability limit of ILs is the key fundamental element to establish an upper barrier for operating temperature in IL-integrated processes, such as SILP and SCILL involving processes. Therefore, the results of this study will serve as baseline data in selecting the optimum IL to achieve a superior performance at desired operating temperatures for the studies to be performed in our research group. Additionally, the calculated interaction energies will be further used to characterize thermal stability limits of ILs and their interactions with the active sites of the catalysts for these studies. Besides, each chapter reporting the results of this study is planned to be published in corresponding journals, hence they were written in a stand-alone article format including a short introduction and literature review excluding the experimental details, which are provided in Chapter 3.

Chapter 2

LITERATURE REVIEW

2.1 Ionic Liquids: Definition and Applications

Ionic liquids (ILs) are defined as salts composed entirely of ions (i.e., anion and cation) and possess very low melting points ($<100\text{ }^{\circ}\text{C}$) compared to conventional salts [4]. Many of them are liquid even at or below room temperature, which are called *room temperature ionic liquids* (RTILs) [5]. Some commonly used cations and anions of ILs are shown in Figure 2.1 and 2.2. ILs based on imidazolium cation have been extensively studied compared to others. With the combination of different types of cations and anions, it is estimated that 10^{18} different ILs can be designed theoretically [6].

The synthesis of first RTIL dates back to 1914, when Paul Walden reported the preparation and physical properties of ethylammonium nitrate (e.g., melting point: $13\text{--}14\text{ }^{\circ}\text{C}$) [7]. However, they have acquired major scientific and industrial popularity only in the last decade because of their unique physical and chemical properties such as low volatility, low flammability, high solvating ability, tunable miscibility, extensive electrochemical window, and high thermal stability [8].

As demonstrated in Figure 2.3, the number of ILs-related publications has exponentially increased especially after 1999. This burgeoning interest towards ILs stems from their physicochemical properties that can be tuned by incorporating almost infinite combinations

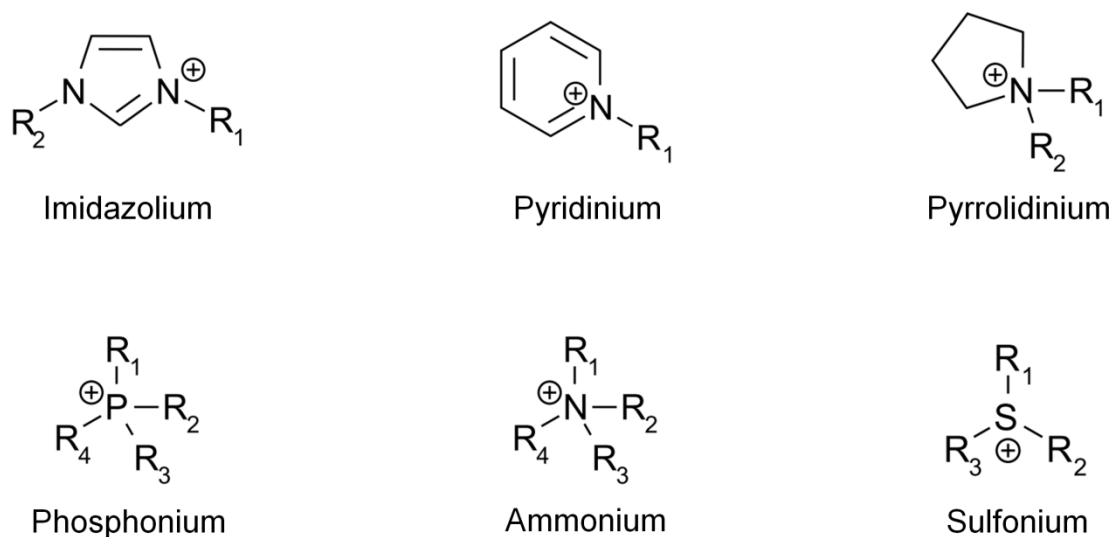


Figure 2.1: Some commonly used cations for ILs.

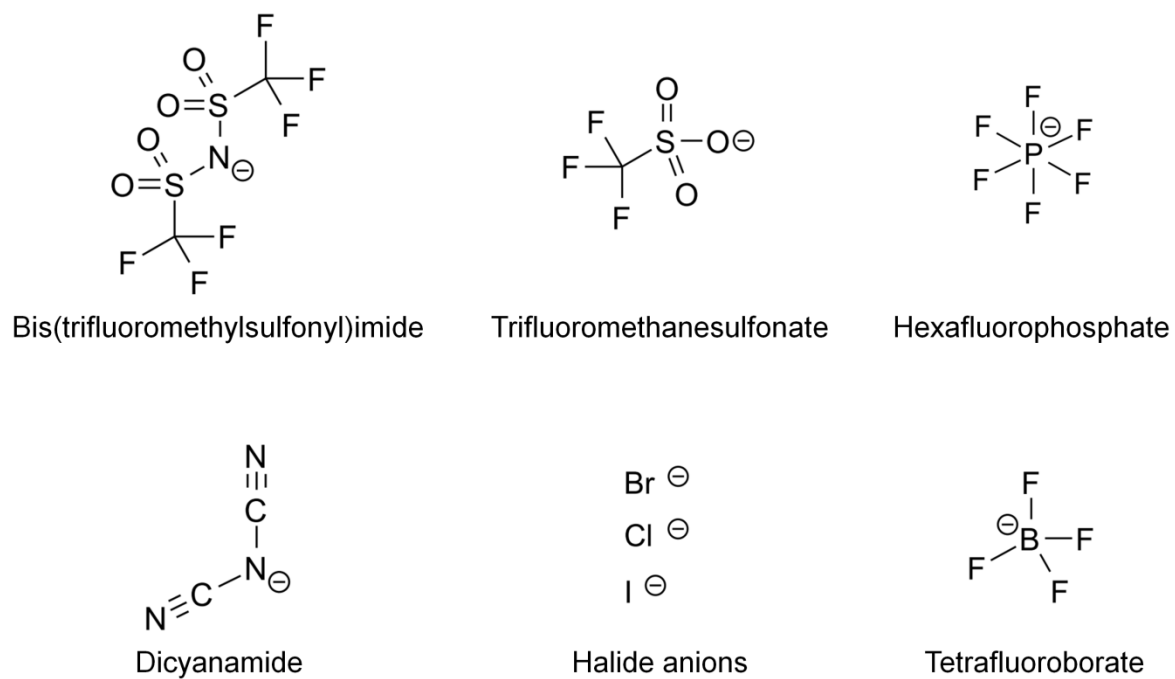


Figure 2.2: Some commonly used anions for ILs.

of different anions and cations; hence they are often called as “designer” [9] or “task-specific” [10] solvents. Such structural diversity and functional flexibility has led to a growing interest towards application in numerous research fields such as synthesis [1], electrochemistry [11], separation [12], and catalysis [5,13]. Furthermore, ILs-assisted industrial processes have been extensively developed or implemented into conventional processes, and some of the commercial processes involving ILs are as follows:

- BASF (BASIL: Biphasic Acid Scavenging utilizing Ionic Liquids process for the production of the photoinitiator precursor alkoxyphenylphosphines, breaking azeotropes, replacing phosgene, aluminum plating, cellulose dissolution)
- Institut Français du Pétrole (Difasol process for ionic liquids-supported nickel-catalyzed dimerization of alkenes)
- Degussa (hydrosilylation, paint additives)
- Linde (ionic liquid compressor for compressing gases at constant temperature and high pressure)
- Air Products (entrainment of reactive and hazardous gases in ionic liquids)
- Pionics (lithium ion batteries) [8].

2.2 Physicochemical Properties of Ionic Liquids

One of the most prominent physicochemical properties of ILs is the fact that they have negligible vapor pressures at near ambient conditions [14]. They were extensively claimed to have no measurable vapor pressure; hence ILs were erroneously assumed to be non-volatile. However, in 2006, Earle *et al.* showed that some of the ionic liquids can be even distilled at 200-300 °C and low pressure without thermal degradation of ILs [15]. For instance, they heated one of the most commonly used ILs, 1-Ethyl-3-methylimidazolium bis(trifluoromethylsulfonyl)imide, for 5 h at 300 °C and 0.1 mbar, and reported the

distillation rate for this IL as 0.12 g h^{-1} . NMR spectrum of the distillate showed that no thermal decomposition occurred during distillation process [15].

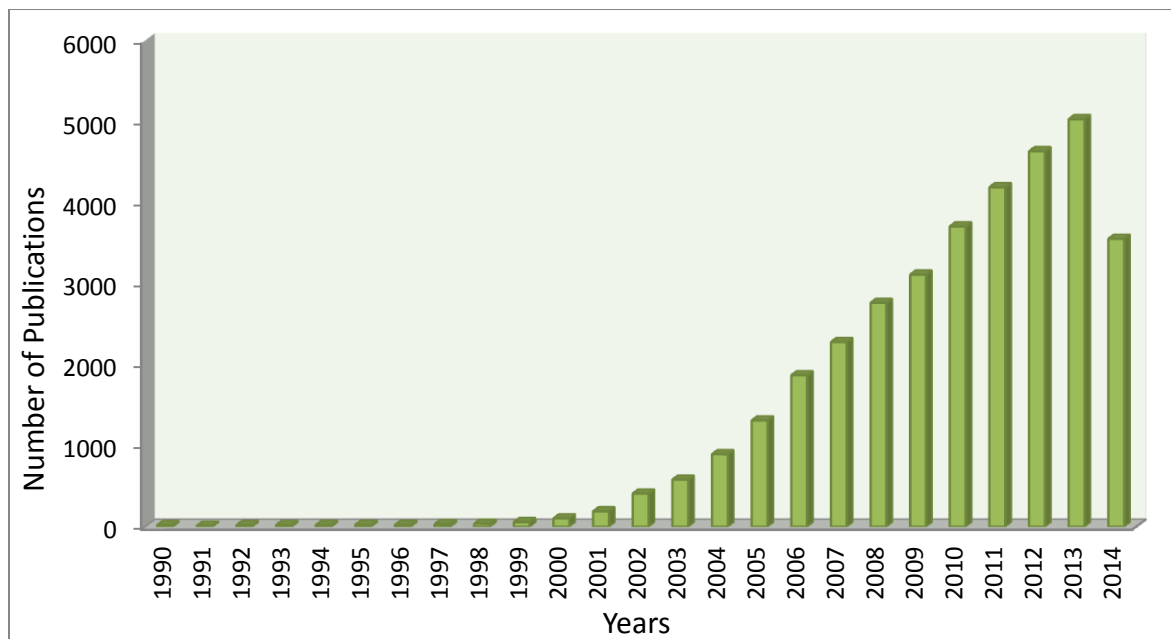


Figure 2.3: Number of ILs related publications over the years. Data taken from Scopus[®] database as of August 2014.

Another important characteristic of ILs is their low melting points (below $100 \text{ }^{\circ}\text{C}$). As seen in Table 2.1, ILs have very low melting points as compared to conventional salts (i.e., NaCl, KCl, LiCl and AlCl_3). For example, the melting points are significantly reduced from 803°C to -82°C as the conventional NaCl salt is replaced with the [OMIM][Cl] ionic liquid. Krossing *et al.* attributed this phenomenon to the fact that ILs consist of large, asymmetrical ions with high conformational flexibility and high charge delocalization [17]. These characteristics result in smaller lattice energy and lower melting points, thus preventing the packing of the cations/anions into a crystal lattice as illustrated in Figure 2.4. Zahn *et al.* theoretically compared the intermolecular forces in [MMIM][Cl] and the

conventional NaCl salt [18]. They reported that dispersion and induction interactions are the dominant forces determining the low-melting points of ILs as they exhibit more shallow energy potential curves compared to high-melting point salt of NaCl. Dispersion interactions have no effect in NaCl [18].

Table 2.1: Comparison of melting points of ILs with conventional salts.

Salt	Abbreviation	Melting Point (°C)	
Sodium chloride	NaCl	803	[8]
Potassium chloride	KCl	772	[8]
Lithium chloride	LiCl	610	[8]
Aluminum chloride	AlCl ₃	192	[8]
1-Methyl-3-methylimidazolium chloride	[MMIM][Cl]	125	[16]
1-Ethyl-3-methylimidazolium chloride	[EMIM][Cl]	87	[16]
1-Propyl-3-methylimidazolium chloride	[PMIM][Cl]	60	[16]
1-Butyl-3-methylimidazolium chloride	[BMIM][Cl]	41	[16]
1-Octyl-3-methylimidazolium chloride	[OMIM][Cl]	-82	[16]
1-Ethyl-3-methylimidazolium aluminum chloride	[EMIM][AlCl ₄]	7	[16]
1-Ethyl-3-methylimidazolium tetrafluoroborate	[EMIM][BF ₄]	6	[16]
1-Butyl-3-methylimidazolium tetrafluoroborate	[BMIM][BF ₄]	-81	[16]
1-Ethyl-3-methylimidazolium trifluoromethanesulfonate	[EMIM][TfO]	-9	[16]
1-Butyl-3-methylimidazolium trifluoromethanesulfonate	[BMIM][TfO]	16	[16]

The strength of hydrogen bonding between cation and anion of an IL structure (see Figure 2.5) influences melting point as well. Dong *et al.* reported the interaction energies (E , kJ mol⁻¹) between anion and cation for the ILs based on [MMIM], [EMIM], [BMIM], [PMIM] cations and [Cl], [Br], [BF₄], [PF₆] anions [19]. They found a linear correlation between the melting points and interactions energies for the most of the imidazolium based ionic liquids (see Figure 2.6). The results show that as the interaction energies increase the melting points of corresponding ILs decrease, and the melting points decrease when the size of the *N*-alkyl side chains increases.

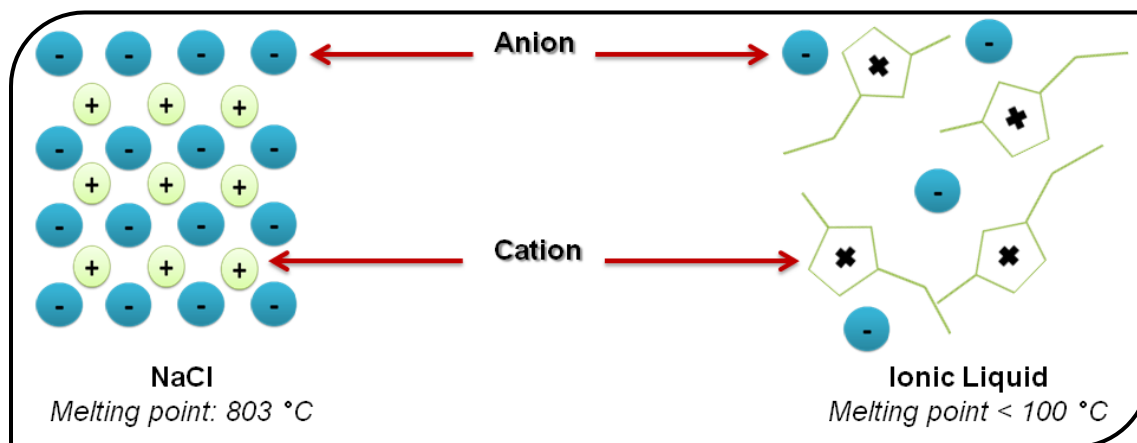


Figure 2.4: Structural differences between conventional salt and IL.

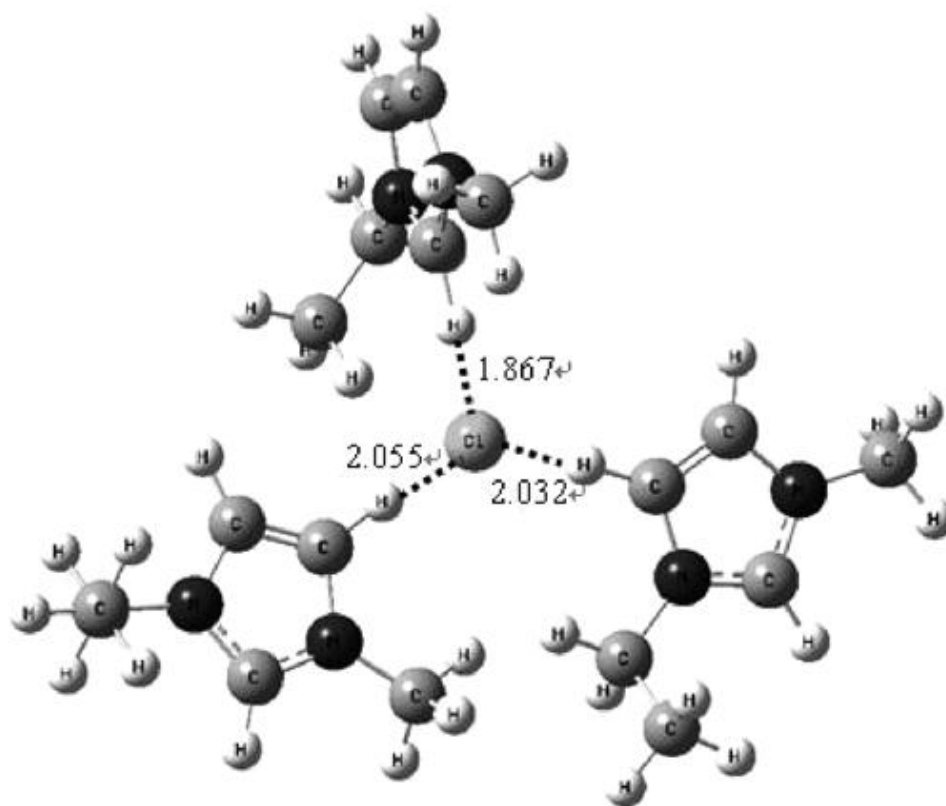


Figure 2.5: The local hydrogen bonding between cation and anion of [EMIM][Cl] [19].

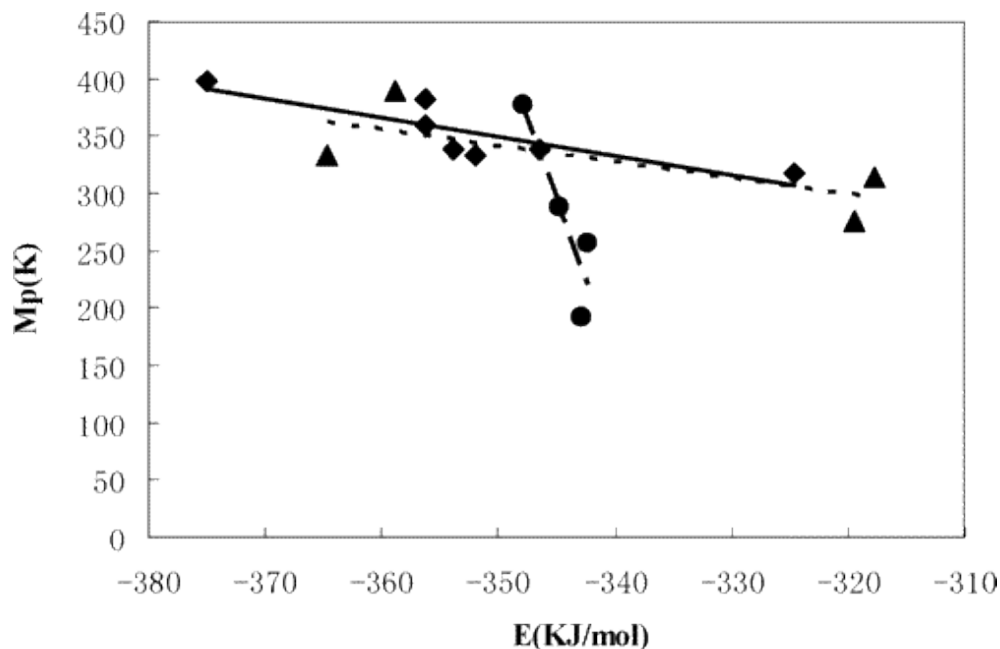


Figure 2.6: The correlation of melting points and interaction energies for [MMIM], [EMIM], [BMIM], [PMIM] based ILs: (▲) Cl and Br, (●) BF₄, and (◆) PF₆ [19].

2.3 Catalysis in Ionic Liquids

Besides their low melting point and negligible vapor pressure characteristics, ILs have drawn a great deal of attention for their remarkable catalytic performance [5,13,20]. As one of the emergent application areas, two primary concepts have been pioneered to exploit tunable features of ILs in catalysis — *supported ionic liquid phase* (SILP) and *solid catalysts with an ionic liquid layer* (SCILL). For SILP-type catalyst, a thin layer of ionic liquid containing a homogeneous catalyst is applied to the internal surface of a porous support material [2]. Similarly, in SCILL concept, heterogeneous catalyst or catalytically active materials are coated with a thin film of IL [3]. The differences in the SILP and SCILL concepts are illustrated in Figure 2.7. These promising catalytic concepts lead to

enhanced selectivity, product distribution, yields, and selective solubility for intermediates and products because of promoting interactions between active sites, supports and IL. The reasons for these enhanced catalytic performances are twofold: (1) ILs may act as co-catalyst to induce promoting chemical effects on supports and active sites, comparable to the behavior of a ligand, and ultimately improve the catalytic activity; (2) They may act as physical solvent to selectively affect the solubility of reactants, thus modifying the effective concentrations of the reactants or intermediates at the active sites. Therefore, they bolster the selectivity for desired products because of different affinity of reactants or intermediates towards solubility in ILs [3].

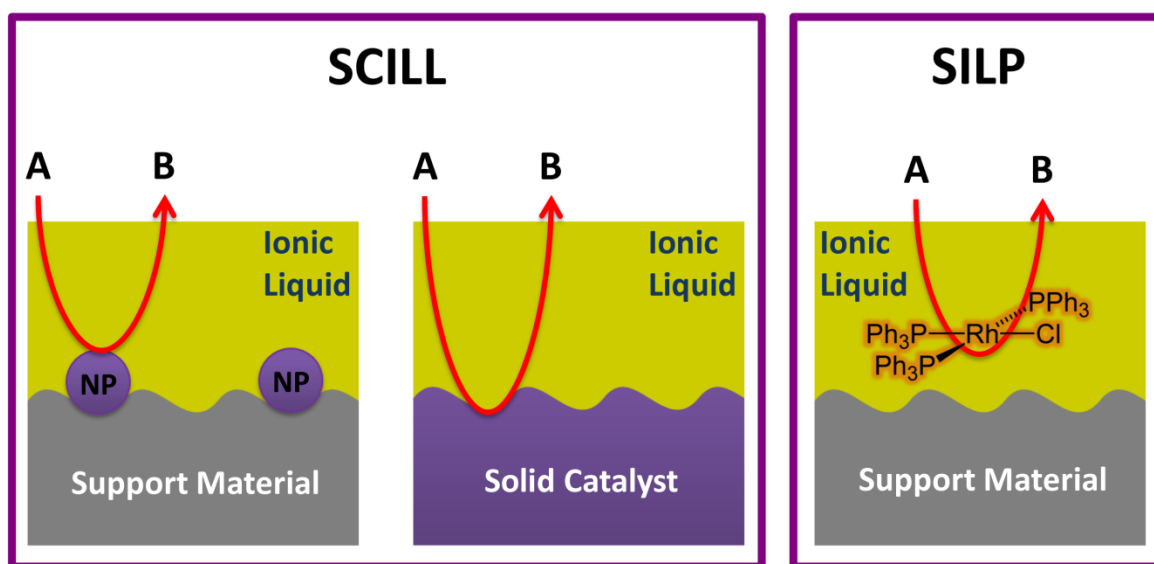


Figure 2.7: Comparison of SILP and SCILL concepts. NP represents metal nanoparticle such as Pt, Pd, and Ni. A and B represent reactant and product, respectively.

The effect of ILs on catalytic activity was studied by Knapp *et al.* [21] on hydrogenation of ethylene by SiO₂ supported platinum catalysts coated with 1-butyl-2,3-dimethyl-imidazolium trifluoromethanesulfonate (IL loading: 17 wt%). The results

demonstrated increased catalytic activity with IL-coated supported catalysts compared to uncoated catalysts. Kernchen *et al.* [3] used SCILL concept for the hydrogenation of cyclooctadiene. They used commercial nickel catalyst (i.e., Süd-Chemie; 37 wt% Ni supported on SiO₂) coated with 1-Butyl-3-methylimidazolium octylsulfate (IL loading: 6 wt%). In comparison to conventional Ni-catalyst, SCILL concept was proven to highly selective towards intermediate cyclooctene, enhanced from 40 % to 70%. Similarly, Arras *et al.* [22] used hydrogenation of citral as the model reaction to test the SCILL concept in terms of catalytic performance using SiO₂ supported palladium catalyst coated with 1-Butyl-3-methylimidazolium dicyanamide, [BMIM][DCA], (IL loading: 50 wt%). They reported that the selectivity towards citronellal increased significantly from 37 % to 99 % by using [BMIM][DCA] coated Pd/ SiO₂ catalyst. In addition, using the ionic liquid as bulk solvent resulted in higher selectivity towards citronellal up to 97 %.

2.4 Thermal Stability of Ionic Liquids

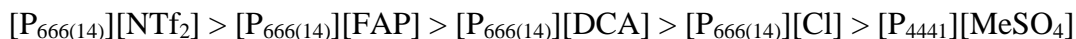
Basically, ILs are required to retain their structural integrity at the specific process conditions for these IL-integrated applications. The designated structural integrity is vanished as the IL evaporates or leaches out from the system or thermally decomposes [23]. Therefore, thermal stability of ILs is the key process parameter which determines the upper operating limits.

Thermal stability of bulk ILs has been extensively studied by thermogravimetric analysis (TGA), and usually in the rapid-scan (or ramped temperature) mode, where the samples are heated at a constant heating rate such as 10 °C min⁻¹ from room temperature to elevated temperatures. In the rapid-scan TGA measurements, T_{onset} value is determined to report the thermal stability limit of the corresponding ILs. T_{onset} is determined by “step tangent” method as the intersection of an extrapolated baseline from zero-weight loss

region with a tangent to the inflection point on the weight loss versus temperature curve [24]. However, the conditions of the TGA measurements strictly influence the obtained thermal stability limits (i.e., T_{onset} values). For example, Kosmulski *et al.* [25] reported that when the heating rate was decreased from $10\text{ }^{\circ}\text{C min}^{-1}$ to $1\text{ }^{\circ}\text{C min}^{-1}$ during TGA of 1-Decyl-3-methylimidazolium trifluoromethanesulfonate, [DMIM][TfO], T_{onset} of the IL decreased significantly as well. Additionally, increasing the amount of sample used during TGA of 1-Butyl-3-methylimidazolium hexafluoroborate, [BMIM][PF₆], from 13 mg to 30 mg at the same heating rate of $10\text{ }^{\circ}\text{C min}^{-1}$ increased the T_{onset} by $50\text{ }^{\circ}\text{C}$. They also reported that addition of silica into ILs (i.e., 1-hexyl-3-methylimidazolium phosphate and 1-methyl-3-octylimidazolium phosphate) drastically decreases thermal stability limits of the corresponding ILs. On the other hand, the effect of TiO₂ and Al₂O₃ on the thermal stability limits of the same ILs is less significant [25]. Similarly, Ngo *et al.* [26] observed that thermal stability limits of imidazolium ILs bearing the PF₆ anion decreases even more than $100\text{ }^{\circ}\text{C}$ as the pan material changed from alumina to aluminium. The type of purge gas used during TGA measurements also affects thermal stability limits of ILs. Awad *et al.* [27] performed TGA measurements under air and nitrogen atmosphere at a heating rate of $10\text{ }^{\circ}\text{C min}^{-1}$ for a series of imidazolium and ammonium ILs. They reported that thermal stability limits of the ILs decrease under air atmosphere to a variable extent. For instance, T_{onset} value of 1,2-Dimethyl-3-hexadecylimidazolium tetrafluoroborate recorded under air atmosphere is $122\text{ }^{\circ}\text{C}$ lower than that of under nitrogen atmosphere [27].

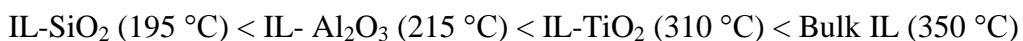
Although thermal stability of bulk nitrogen-based ILs such as imidazolium, pyridinium and ammonium has been extensively investigated, less studies have been devoted to phosphonium ILs in this context [23]. Tsunashima *et al.* reported that dicyanamide-based phosphonium ILs exhibited more than $120\text{ }^{\circ}\text{C}$ higher thermal stability than the corresponding ammonium ILs [28]. Ferreira *et al.* [29] conducted high-resolution modulated thermogravimetric analysis for a series of phosphonium ILs including

[P₆₆₆₍₁₄₎][NTf₂], [P₆₆₆₍₁₄₎][Cl], [P₆₆₆₍₁₄₎][DCA], [P₄₄₄₁][MeSO₄], and [P₆₆₆₍₁₄₎][FAP] ([FAP]: tris(pentafluoroethyl)trifluorophosphate). The results indicated that the relative thermal stability limits vary in the following order:



The same thermogravimetric analysis was also performed with [EMIM][NTf₂] for comparison reason. Data further illustrated that [EMIM][NTf₂] is up to 54 °C thermally more stable than [P₆₆₆₍₁₄₎][NTf₂] [29]. Similarly, Adamová *et al.* [30] investigated thermal stability of chloride-based alkyltrioctylphosphonium ILs, [P_{888n}][Cl] (n = 1–14). The thermal stability limits were found to be around 320 ± 20 °C, which is approximately 100 °C lower than pyridinium ILs. Nevertheless, the major shortcomings can be seen in these studies include the fact that they directly report the thermal stability limits of phosphonium ILs without delving deeper into the structural factors that really control the stability limits of these ILs.

Moreover, there is a huge gap in the literature regarding thermal stability limit of ILs on different support materials, especially for the phosphonium family. Only a few studies have focused on thermal stability limits of IL-supported matrices. As one of these studies, Lemus *et al.* [31] characterized SILP materials, where 1-methyl-3-octylimidazolium hexafluorophosphate supported on silica (SiO₂), alumina (Al₂O₃) and titania (TiO₂), and three different activated carbons. They conducted the TGA measurements at a heating rate of 10 °C min⁻¹, and found that T_{onset} values (i.e., reported inside the brackets) changed in the following order:



They attributed this significant thermal stability decrease of the IL on SiO₂ to the fact that SiO₂ is the most polar support among others [31].

Similarly, Singh *et al.* [32] reported that [BMIM][PF₆] decomposes in a multi-step pathway and earlier than the bulk case when it is supported on SiO₂. They postulated a

“hinged spring” model using Hartree–Fock (HF) calculations to explain this decline in thermal stability of IL on SiO_2 as illustrated in Figure 2.8. According to this model, the imidazolium ring was supposed to interact with the surface oxygen through its C–H groups. In other words, the imidazolium ring was presumed to be “hinged” to the SiO_2 pore walls as the butyl chain (i.e., from Alk1 to Alk4) is free to move. Therefore, it is more likely for the freely moving butyl chain (or its Alk4, Alk3 and Alk2 aliphatic fractions) to decompose first with the increase in thermal vibrations during heating process. They also claimed that the butyl chain decomposes into its fractions starting from more vulnerable constituent of Alk4, and followed by Alk3, Alk2. The ‘hinged’ imidazolium ring is more likely to decompose lastly, which also explains the multi-step decomposition mechanism [32].

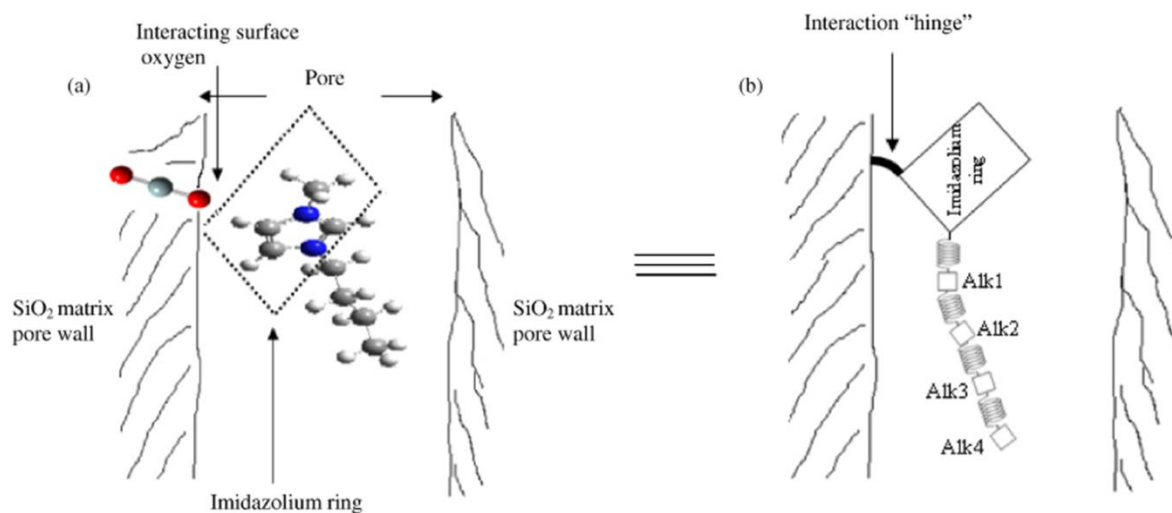


Figure 2.8: (a) Illustration of possible IL confinement in SiO_2 matrix pores as obtained from HF calculations: (gray) silicon, (red) oxygen, (blue) nitrogen, (white) hydrogen, (light gray) carbon atom. (b) Equivalent ‘hinged spring’ model of IL confined in SiO_2 nanopores [32].

These results clearly illustrate that thermal stability limits of ILs depend not only the structure of cation and anion, but also the nature and surface chemistry of the supports on

which they are immobilized. Although most of the ILs are thermally stable at elevated temperatures ($> 300\text{ }^{\circ}\text{C}$) in their pure state, they usually become less stable when coated on supports because of the mutual interactions between IL and support. Most importantly, the loss of structural robustness by the virtue of thermal decomposition of ILs on support surfaces predominantly hinders the efficiency and the activity of SILP and SCILL processes. Therefore, thermal stability limits of bulk ILs are not valid when they are immobilized on support surfaces, and elucidation of structural parameters controlling the thermal stability limits of ILs on supports is crucial to design robust and effective IL-assisted processes.

Chapter 3

EXPERIMENTAL AND COMPUTATIONAL METHODS

3.1 Chemicals

Phosponium ILs (Table 3.1) [P₄₄₄₁][DBP], [P₄₄₄₁][MeSO₄], [P₄₄₄₄][MeSO₃], [P₄₄₄₄][TOS], [P₆₆₆₍₁₄₎][Br], [P₆₆₆₍₁₄₎][Cl], [P₆₆₆₍₁₄₎][NTf₂], [P₆₆₆₍₁₄₎][DCA], and [P₆₆₆₍₁₄₎][TMPP] were purchased from Sigma-Aldrich with the highest purity commercially available, and used without further purification except for drying. All ILs were dried at 70 °C in air for 24 h prior to use. The validity of such drying procedure was justified by Clough *et al.* [33]. Furthermore, SiO₂, γ -Al₂O₃, MgO, acetone and methanol were purchased from Sigma-Aldrich with the highest purity commercially available.

3.2 Sample Preparation

The metal-oxide supports, SiO₂, γ -Al₂O₃, MgO, were calcined at 520 °C, 500 °C and 700 °C, respectively. All calcination processes were performed at a heating rate of 3 °C min⁻¹ under oxygen flow, and the temperatures were kept constant at the designated calcination temperatures for 5 h. 200 mg of corresponding IL was dissolved in 5 ml of either acetone or methanol. 1 g freshly calcined SiO₂, γ -Al₂O₃, or MgO was immersed into prepared IL-solvent mixture. Resulting mixture was dried in an oven for 24 h at 70 °C, and powder IL-coated metal-oxide samples were obtained. Such drying procedure was checked

Table 3.1: Structures of phosphonium ILs investigated in this study.

Structure	Name	Abbreviation
	Tributylmethylphosphonium dibutylphosphate	[P ₄₄₄₁][DBP]
	Tributylmethylphosphonium methylsulfate	[P ₄₄₄₁][MeSO ₄]
	Tetrabutylphosphonium methanesulfonate	[P ₄₄₄₄][MeSO ₃]
	Tetrabutylphosphonium p-toluenesulfonate	[P ₄₄₄₄][TOS]
	Trihexyltetradecylphosphonium bromide	[P ₆₆₆₍₁₄₎][Br]
	Trihexyltetradecylphosphonium chloride	[P ₆₆₆₍₁₄₎][Cl]
	Trihexyltetradecylphosphonium bis(trifluoromethylsulfonyl)amide	[P ₆₆₆₍₁₄₎][NTf ₂]
	Trihexyltetradecylphosphonium dicyanamide	[P ₆₆₆₍₁₄₎][DCA]
	Trihexyltetradecylphosphonium bis(2,4,4- trimethylpentyl)phosphinate	[P ₆₆₆₍₁₄₎][TMPP]

by inspecting the derivative onset temperature of each compound, which was significantly higher than 70 °C as suggested by Clough *et al.* [33]. The corresponding IL loading was approximately 16.7 wt. %.

3.3 Thermogravimetric Analysis (TGA)

TGA measurements were conducted at ambient pressure using a Seiko Instruments Inc. (SII) EXSTAR TG/DTA 6300 analyzer at a heating rate of 10 °C min⁻¹ from 25 to 600 °C under an argon flow of 100 ml min⁻¹. Samples between 15 and 20 mg were placed in aluminum pans and purged with argon for 1 h. The onset temperature (T_{onset}) was determined by the intersection of an extrapolated baseline from zero weight loss region with a tangent to the inflection point on the weight loss versus temperature curve (i.e., TG curve), as shown in Figure 3.1. Similarly, the derivative onset temperature (T'_{onset}) and the derivative peak temperature (T_{peak}) were determined from the derivative of TG curve (i.e., DTG curve). T_{onset} typically overestimates the thermal decomposition temperature, thus all of our discussions are based on T'_{onset} values. All reported temperatures are reproducible within an error range of ± 3 °C.

3.4 Monitoring of Decomposition Products by Mass Spectrometry

Analysis of decomposition products was done by an MKS Cirrus 2 mass spectrometer (MS) connected to a Micromeritics AutoChem II 2920 equipment performing temperature programmed decomposition measurements. Samples (approximately 10 mg) were first dried at 70 °C for 1 h under a nitrogen flow of 100 ml min⁻¹, and heated to 500 °C at a heating rate of 10 °C min⁻¹. The effluent gas stream passed through a heated silica capillary (heated to 120 °C) to the mass spectrometer, where it was ionized at 70 eV. Mass spectra

were recorded in the range of 1–200 atomic mass units (amu) continuously (each scan took 13 s from 1 to 200 amu). National Institute of Standards and Technology (NIST) library database was utilized for mass spectra interpretation [35].

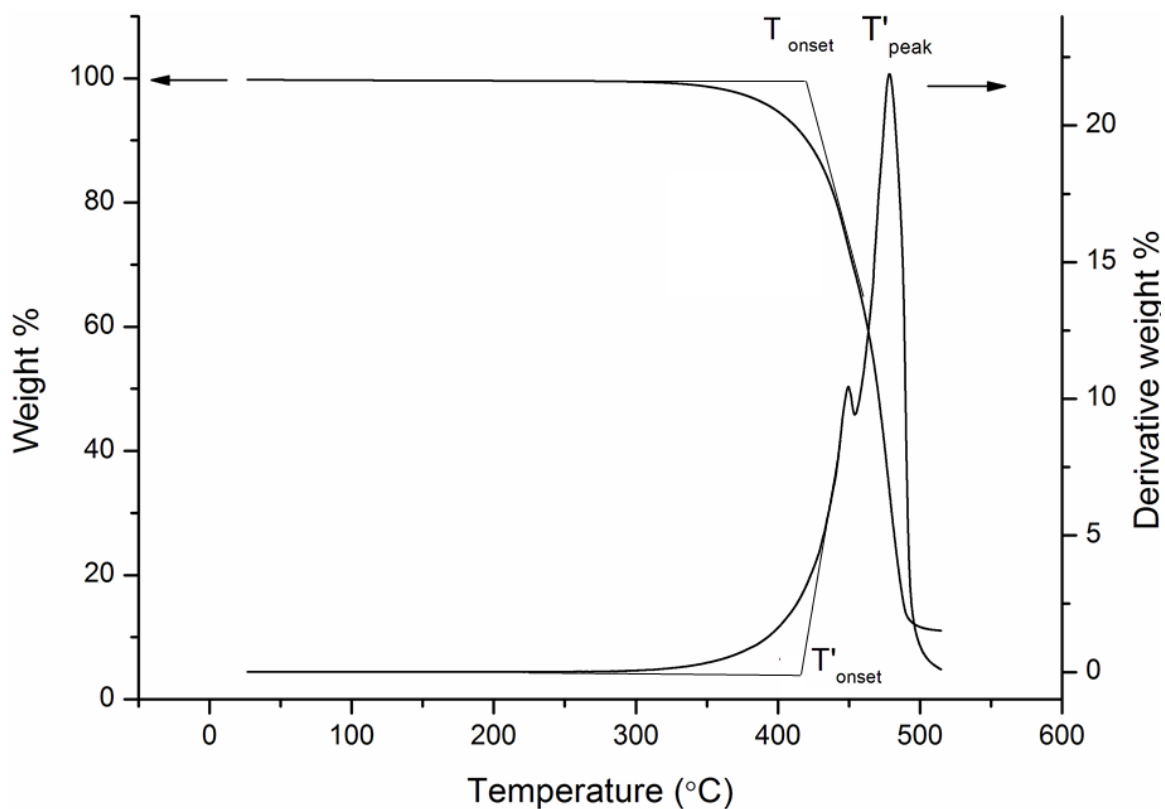


Figure 3.1: Determination of T_{onset} , T'_{onset} , and T'_{peak} values on a representative TGA data obtained for [BMIM][NTf₂] [34].

3.5 FTIR Spectroscopy

FTIR measurements were performed by a Thermo Scientific Nicolet iS10 model FTIR spectrometer with an attenuated total reflection (ATR) cell. IR spectra with an average of 512 scans were collected in air at room temperature with a resolution of 4 cm⁻¹. At the

beginning of each measurement, background scans were collected using an average of 32 scans. IR bands were deconvoluted using Voigt function with Thermo Scientific OMNIC™ Spectra software.

3.6 Computational Methods

Density Functional Theory (DFT) calculations were performed using Gaussian 09 software [36]. Geometries representing the structures of ILs were fully optimized at the Becke's three parameter hybrid exchange functional [37] and the Lee-Yang-Parr correlation functional [38] (B3LYP) method along with the 6-31+G(d) basis set. Since that 6-31+G(d) basis set is not applicable for Sb atom, DGDZVP basis set was employed for IL bearing Sb atom. The “tight” convergence criteria (10^{-7} on energy) and the “ultrafine” numerical integration grid (99 radial shells and 590 angular points per shell) were employed for all calculations to enhance numerical accuracy and reliability. Vibration frequencies were calculated at the same level of theory to confirm that all optimized geometries corresponded to true minima on the potential energy surface (i.e., no imaginary frequencies). ^1H NMR chemical shifts were calculated on the optimized geometries at the same level of theory using gauge-independent atomic orbital (GIAO) [39] method and reported relative to TMS (chemical shielding 31.88 ppm calculated at B3LYP/6-311+G(2d,p)).

Moreover, the interaction energies, $E_{\text{interaction}}$, (also binding or cohesive energy) between anions and cations were calculated at the same level of theory using following formula [40]:

$$E_{\text{interaction}} = E_{\text{IL}} - E_{\text{cation}} - E_{\text{anion}} + \Delta\text{ZPVE} \quad \text{Eq. 3.1}$$

where E_{IL} , E_{cation} , and E_{anion} are the energies of ionic liquid, cation and anion at their lowest energy conformers, respectively. ΔZPVE is the zero-point vibrational energies of ILs, and it was scaled for B3LYP/6-31+G(d) using a scaling factor of 0.9829 [41].

Chapter 4

THERMAL STABILITY OF BULK PHOSPHONIUM IONIC LIQUIDS

4.1 Introduction

Ionic liquids (ILs) have received tremendous attention during the last decade because of their unique physicochemical properties, such as extremely low volatility, high solvating ability, and high thermal stability. These physicochemical properties can be tuned by incorporating numerous combinations of different anions and cations; hence they are often called “designer” or “task-specific” solvents [42]. Such structural diversity and functional flexibility has led to a growing interest towards application in many research fields, such as synthesis, separation/storage, and catalysis, specifically in energy and sustainability applications [1,5,43]. Understanding their structure-property relationship is crucial to tune their structures for optimum performance and to fully exploit their favorable features for these applications. Among various families of ILs, phosphonium ILs offer higher degree of rational design because of possible variation in their four functional groups attached to the cation with a diverse range of anions [44-46]. This family of ILs lack acidic protons, thus they are chemically stable along with strong bases, such as in reactions involving Grignard reagents [47]. In contrast, imidazolium ILs are prone to form *N*-heterocyclic carbenes under basic conditions [48]. Furthermore, commercial availability of phosphonium ILs in bulk at relatively low prices renders designing feasible processes [45]. Despite these

favorable properties, phosphonium ILs are less studied in the IL literature relative to other families such as imidazolium [23,49].

Thermal stability of ILs is one of the primary parameters that restrict their application conditions. For practical point of view, ILs are required to preserve their structural integrity and functional activity at specific operating conditions. The structural integrity is considered to be lost when the IL evaporates or leaches out from the system or it chemically decomposes [34]. Thermal stability of nitrogen-based ILs [23,50,51] and, to a lesser extent, phosphonium ILs [29,46] have been investigated widely by thermogravimetric analysis (TGA). As Luo *et al.* reported, phosphonium ILs exhibit significantly higher thermal stability than ammonium ILs [49], and comparable thermal stability with nitrogen-based ILs such as pyridinium and imidazolium ILs [23]. One of the main drawbacks of these studies is the fact that they directly report the results of thermogravimetric measurements without focusing on elucidating general criteria on structural factors really controlling the stability limits. Ferreira *et al.* reported that it is not possible to designate such general criteria for assessing the thermal stability limits of ILs [29]. Nonetheless, understanding of such factors is crucial for their selection or rational design for specific applications requiring harsh operating conditions.

Here, we report the results of our systematic investigation on the elucidation of structural factors determining thermal stability limits of nine commercially-available phosphonium ILs. The ILs were chosen with three different tetraalkylphosphonium cations, (ranging from a relatively small size tributylmethylphosphonium, $[P_{4441}]^+$, to symmetric tetrabutylphosphonium, $[P_{4444}]^+$, and to large trihexyltetradecylphosphonium, $[P_{666(14)}]^+$) incorporating different anions (Table 3.1). Structures of ILs were first investigated at the molecular level and structural factors were correlated with variations in corresponding thermal stability limits. Atomic level structural parameters, such as electron densities on individual protons on alkyl chains, were determined by DFT calculations at the

B3LYP level of theory, and thermal stability limits were measured by TGA. A strong correlation between the electron density of a terminal proton on a specific alkyl chain and the corresponding thermal stability limit was elucidated. Based on this correlation a decomposition mechanism for tetraalkylphosphonium ILs was postulated and confirmed by on-line mass spectrometry monitoring decomposition products of a representative phosphonium IL.

4.2 Characterization and Modeling of Phosphonium ILs

FTIR spectra of individual ILs were measured to identify fingerprints of structural features. IR spectra of all ILs investigated are given in appendix. Deconvoluted IR bands in $\nu(\text{CH})$ region of individual ILs, given in Table 4.1, show a slight variation with changes in the IL structure. Such variation is mainly based on electron density disparities on individual protons along the alkyl chains of phosphonium cation generally caused by the presence of different anions [52]. To be able to map these electronic structural variations, we performed DFT calculations at B3LYP/6-31+G(d) level of theory to obtain optimized geometries. Moreover, vibration frequencies of all optimized geometries were calculated, and no imaginary frequencies were detected confirming that the optimized geometries correspond to local minima structures [53]. Furthermore, these calculated frequencies were utilized to assign deconvoluted peaks in experimentally measured IR spectra as summarized in Table 4.1. Geometry optimization of these ionic liquids was a challenging and time consuming process, and led to a high computational cost because they constitute large number of atoms up to 154. Therefore, studies focused on the modeling of these ILs by DFT are rare [54-58], and smaller size models were used previously to optimize such bulky ILs. For instance, Dwan *et al.* optimized $[\text{P}_{666(14)}][\text{Cl}]$ IL with a simplest model bearing tetramethyl phosphonium cation [54]. Similarly, Fraser *et al.* used a smaller cation

of $[P_{4444}]^+$ to model the bulky $[P_{666(14)}]^+$ cation [55]. Only very recently, Morco *et al.* focused on larger ILs and obtained optimized geometries of six ILs based on $[P_{666(14)}]^+$ to correlate some bulk phase properties such as melting point and viscosity to atomic level structures [58]. Here, to reach fast convergence, structures of cations and anions were first optimized separately, starting with a smaller 3-21G basis set. Subsequently, ILs were optimized as ion pairs employing 6-31G(d) basis set. Finally, these ion pairs were optimized using 6-31+G(d) basis set [33].

Figure 4.1 presents representative local minima geometries of individual ILs with three different cations investigated, $[P_{4441}]^+$, $[P_{4444}]^+$, and $[P_{666(14)}]^+$ (those of all ILs investigated are given in appendix). The optimized geometries of these ILs have the following orientation of anion/cation pair. $[P_{4441}]^+$ (Figure 4.1a) has one short methyl chain and three relatively long butyl chains attached to the central phosphorous atom. In ILs with this cation, $[DBP]^-$ and $[MeSO_4]^-$ are located facing the methyl chain of the cation. $[P_{4444}]^+$, on the other hand, has four identical butyl chains bonded to the central phosphorous atom. Anions of the ILs with this cation align along with the opposite direction of one of the butyl chains and the other three butyl groups remaining almost coplanarly with respect to the anion (Figure 4.1b). As demonstrated in Figure 4.1c, $[P_{666(14)}]^+$ is composed of three hexyl chains and one very long tetradecyl chain bonded to the central phosphorous atom. For all ILs with this cation, $[P_{666(14)}][Br]$, $[P_{666(14)}][Cl]$, $[P_{666(14)}][NTf_2]$, $[P_{666(14)}][DCA]$, and $[P_{666(14)}][TMPP]$, the corresponding anions are located near the central phosphorous atom. For each case, two hexyl chains and a long tetradecyl chain are located coplanarly with the anions. Consistent with these structures, Abdallah *et al.* [59] investigated crystal structures of tetraalkylphosphonium IL containing 10-18 carbon atoms, and found that alkyl chains have linear conformations.

Table 4.1: Vibration frequencies assignments of phosphonium ILs.

Ionic Liquids	Assignments	$\nu_{\text{exp}} (\text{cm}^{-1})$	$\nu_{\text{exp}} (\text{cm}^{-1})^{[62]}$	$\nu_{\text{comp}} (\text{cm}^{-1})$	$\nu_{\text{exp}}/\nu_{\text{comp}}$	Average ($\nu_{\text{exp}}/\nu_{\text{comp}}$)
[P ₄₄₄₁][DBP]	$\nu_{\text{as}}(\text{CH}_3)$	2959		3104	0.9533	0.9480
	$\nu_{\text{as}}(\text{CH}_2)$	2933		3095	0.9477	
	$\nu_{\text{as}}(\text{CH}_2)$	2909		3075	0.9460	
	$\nu_{\text{s}}(\text{CH}_2)$	2871		3025	0.9491	
	$\nu_{\text{s}}(\text{CH}_2)$	2837		3006	0.9438	
[P ₄₄₄₁][MeSO ₄]	$\nu_{\text{as}}(\text{CH}_3)_{\text{anion}}$	2991		3145	0.9510	0.9469
	$\nu_{\text{as}}(\text{CH}_3)$	2960		3116	0.9499	
	$\nu_{\text{as}}(\text{CH}_2)$	2935		3106	0.9449	
	$\nu_{\text{as}}(\text{CH}_2)$	2912		3075	0.9470	
	$\nu_{\text{s}}(\text{CH}_2)$	2871		3026	0.9488	
	$\nu_{\text{s}}(\text{CH}_2)$	2827		3008	0.9398	
[P ₄₄₄₄][MeSO ₃]	$\nu_{\text{as}}(\text{CH}_3)_{\text{anion}}$	3005		3177	0.9459	0.9457
	$\nu_{\text{as}}(\text{CH}_3)$	2957		3109	0.9511	
	$\nu_{\text{as}}(\text{CH}_2)$	2931		3100	0.9455	
	$\nu_{\text{as}}(\text{CH}_2)$	2908		3085	0.9426	
	$\nu_{\text{s}}(\text{CH}_2)$	2869		3023	0.9491	
	$\nu_{\text{s}}(\text{CH}_2)$	2821		3001	0.9400	
[P ₄₄₄₄][TOS]	$\nu(\text{CH})_{\text{anion}}$	3074		3172	0.9691	0.9531
	$\nu(\text{CH})_{\text{anion}}$	3041		3167	0.9602	
	$\nu_{\text{as}}(\text{CH}_3)_{\text{anion}}$	3020		3113	0.9701	
	$\nu_{\text{as}}(\text{CH}_3)$	2959		3107	0.9524	
	$\nu_{\text{as}}(\text{CH}_2)$	2931		3100	0.9455	
	$\nu_{\text{as}}(\text{CH}_2)$	2906		3088	0.9411	
	$\nu_{\text{s}}(\text{CH}_2)$	2870		3031	0.9469	
	$\nu_{\text{s}}(\text{CH}_2)$	2820		3002	0.9394	
[P ₆₆₆₍₁₄₎][Br]	$\nu_{\text{as}}(\text{CH}_3)$	2956		3105	0.9520	0.9449
	$\nu_{\text{as}}(\text{CH}_2)$	2923		3082	0.9484	

	$\nu_{\text{as}}(\text{CH}_2)$	2896		3070	0.9433	
	$\nu_{\text{s}}(\text{CH}_3)$	2871		3035	0.9460	
	$\nu_{\text{s}}(\text{CH}_2)$	2853		3023	0.9438	
	$\nu_{\text{s}}(\text{CH}_2)$	2802		2993	0.9362	
[P ₆₆₆₍₁₄₎][Cl]	$\nu_{\text{as}}(\text{CH}_3)$	2957	2955	3104	0.9526	0.9456
	$\nu_{\text{as}}(\text{CH}_2)$	2923	2924	3083	0.9481	
	$\nu_{\text{as}}(\text{CH}_2)$	2896		3070	0.9433	
	$\nu_{\text{s}}(\text{CH}_3)$	2871		3035	0.9460	
	$\nu_{\text{s}}(\text{CH}_2)$	2853	2854	3023	0.9438	
	$\nu_{\text{s}}(\text{CH}_2)$	2804		2984	0.9397	
[P ₆₆₆₍₁₄₎][NTf ₂]	$\nu_{\text{as}}(\text{CH}_3)$	2959		3107	0.9524	0.9471
	$\nu_{\text{as}}(\text{CH}_2)$	2926	2929	3085	0.9485	
	$\nu_{\text{as}}(\text{CH}_2)$	2899		3072	0.9437	
	$\nu_{\text{s}}(\text{CH}_3)$	2873		3036	0.9463	
	$\nu_{\text{s}}(\text{CH}_2)$	2855	2858	3022	0.9447	
[P ₆₆₆₍₁₄₎][DCA]	$\nu_{\text{as}}(\text{CH}_3)$	2957	2955	3099	0.9542	0.9475
	$\nu_{\text{as}}(\text{CH}_2)$	2925	2925	3084	0.9484	
	$\nu_{\text{as}}(\text{CH}_2)$	2899		3070	0.9443	
	$\nu_{\text{s}}(\text{CH}_3)$	2871		3033	0.9466	
	$\nu_{\text{s}}(\text{CH}_2)$	2854	2854	3024	0.9438	
	$\nu_{\text{comb}}(\text{CN})$	2225	2225			
	$\nu_{\text{s}}(\text{CN})$	2188	2188	2272	0.9630	
	$\nu_{\text{as}}(\text{CN})$	2126	2126	2231	0.9529	
[P ₆₆₆₍₁₄₎][TMPP]	$\nu_{\text{as}}(\text{CH}_3)$	2954	2954	(*)		
	$\nu_{\text{as}}(\text{CH}_2)$	2926	2927			
	$\nu_{\text{as}}(\text{CH}_2)$	2900				
	$\nu_{\text{s}}(\text{CH}_3)$	2871				
	$\nu_{\text{s}}(\text{CH}_2)$	2855	2857			

ν : stretching frequency, as: antisymmetrical, s: symmetrical, comb: combination of symmetric and antisymmetrical stretching. (*) IR frequencies could not be calculated successfully because of exceptionally large size. Assignments were done according to assignments of other ILs.

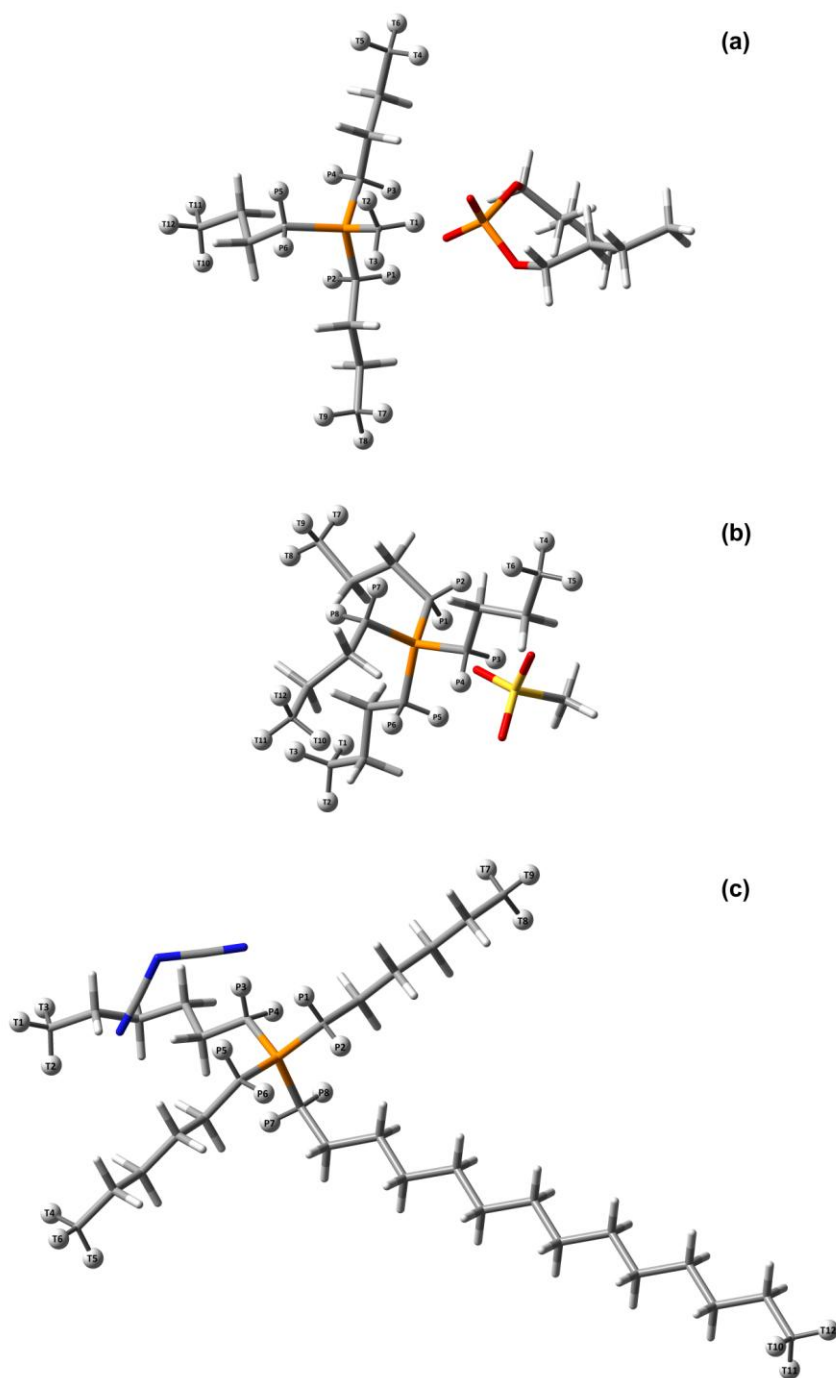


Figure 4.1: Representative optimized geometries for ILs based on $[P_{4441}]$, $[P_{4444}]$ and $[P_{666(14)}]$ (a) $[P_{4441}][DBP]$, (b) $[P_{4444}][MeSO_3]$, and (c) $[P_{666(14)}][Br]$.

IR fingerprints are calculated on these optimized geometries and compared with the experimentally measured spectra to confirm the validity of calculated geometries. These values together with ratios of experimental stretching frequencies (ν_{exp}) to the computed unscaled frequencies (ν_{comp}) are given in Table 2. The average of $\nu_{\text{exp}}/\nu_{\text{comp}}$ values obtained for individual ILs varies between 0.9449 and 0.9531. The average of these $\nu_{\text{exp}}/\nu_{\text{comp}}$ values of all ILs is 0.9473, a reasonable scaling factor to compensate for harmonic effects [41]. When corrected for harmonic effects, these calculated $\nu(\text{CH})$ bands perfectly match with the experimentally measured counterparts. Thus, we infer that these optimized geometries satisfactorily represent actual structures of the corresponding phosphonium ILs.

Once the optimized geometries of individual ILs satisfactorily representing the actual structures were obtained, we examined variation in electronic structures of individual alkyl groups on phosphonium cations. To differentiate these groups in a comparable manner, each alkyl group was named from A1 to A4 with respect to their distance to the anion from closest to farthest in each IL, respectively. Moreover, protons on each of these alkyl groups were grouped with respect to their distance to the anion as well. The protons bonded to the terminal carbon atoms at each alkyl end were labeled from T1 to T12. α -Protons, on the other hand, were labeled from P1 to P8. These protons, T1 to T12 and P1 to P8, are highlighted with ball and tube type representation in Figure 4.1 (and in appendix). In order to relatively quantify electron densities on these individual protons ^1H NMR calculations were performed on the optimized geometries. Calculated chemical shifts of highlighted protons, T1 to T2 and P1 to P8, are given in appendix. Although such calculations were restricted with the optimized ion-pair geometries, it is still a valuable tool to relatively quantify and compare the electron densities on individual protons [60]. Calculated chemical shifts of individual protons are directly correlated with their electron density. In general, the higher the electron density near a proton, the more shielding of the external magnetic field resulting in lower chemical shift values [61]. In the following section, we first

measured the stability limits of these ILs. Then, we focused on identifying the location of a common proton for each IL whose electron density strongly correlated with these limits. Consequently, we postulated a common mechanism for the decomposition of tetraalkylphosphonium ILs based on this correlation.

4.3 Thermal Stability of Phosphonium ILs

Thermal stability limits of phosphonium ILs were investigated by fast-scan thermogravimetric analysis (TGA) performed at a heating rate of $10\text{ }^{\circ}\text{C min}^{-1}$ (Figure 4.2). Typically, results obtained by such fast-scan TGA measurements depend mainly on sample amount and purity, type of pan material, heating rate, and type of carrier gas [23]. As these parameters directly govern the outcomes of these dynamic measurements, comparison of data collected under different experimental conditions is quite difficult. Here, we performed TGA measurements under identical experimental conditions to achieve reproducible and consistent results for assessing the relationship between structural parameters and thermal stability limits. Because we utilized a relatively high heating rate ($10\text{ }^{\circ}\text{C min}^{-1}$), stability limits that we measured are rather short-term limits. These short-term limits are in general 75 to $100\text{ }^{\circ}\text{C}$ higher than the results of isothermal TGA measurements [62]. Although fast-scan TGA method overestimates the thermal stability limits [63], it serves as a valuable tool to relatively compare thermal stability limits of different ILs under identical and dynamic analysis conditions [34]. Since, we aim to reveal the structural parameters controlling stability limits, and the decomposition mechanism, it is crucial to obtain more explicit and comparable data that better reflect the differences in these stability limits under identical conditions [34]. A heating rate of $10\text{ }^{\circ}\text{C min}^{-1}$ can characterize such direct structural dependency, which otherwise would not be possible to distinguish by isothermal TGA or slow heating dynamic measurements. Besides, as Heym

et al. reported, slow heating rates make the evaporation dominate over thermal decomposition [64]. Similarly, Clough *et al.* [33] performed TGA-MS experiments to elucidate decomposition mechanism of carboxylate ILs utilizing the same heating rate of $10\text{ }^{\circ}\text{C min}^{-1}$. Thus, we solely focused on short-term thermal stability limits rather than long-term limits and compared the results relative to each other to find correlations between the structural parameters and stability limits.

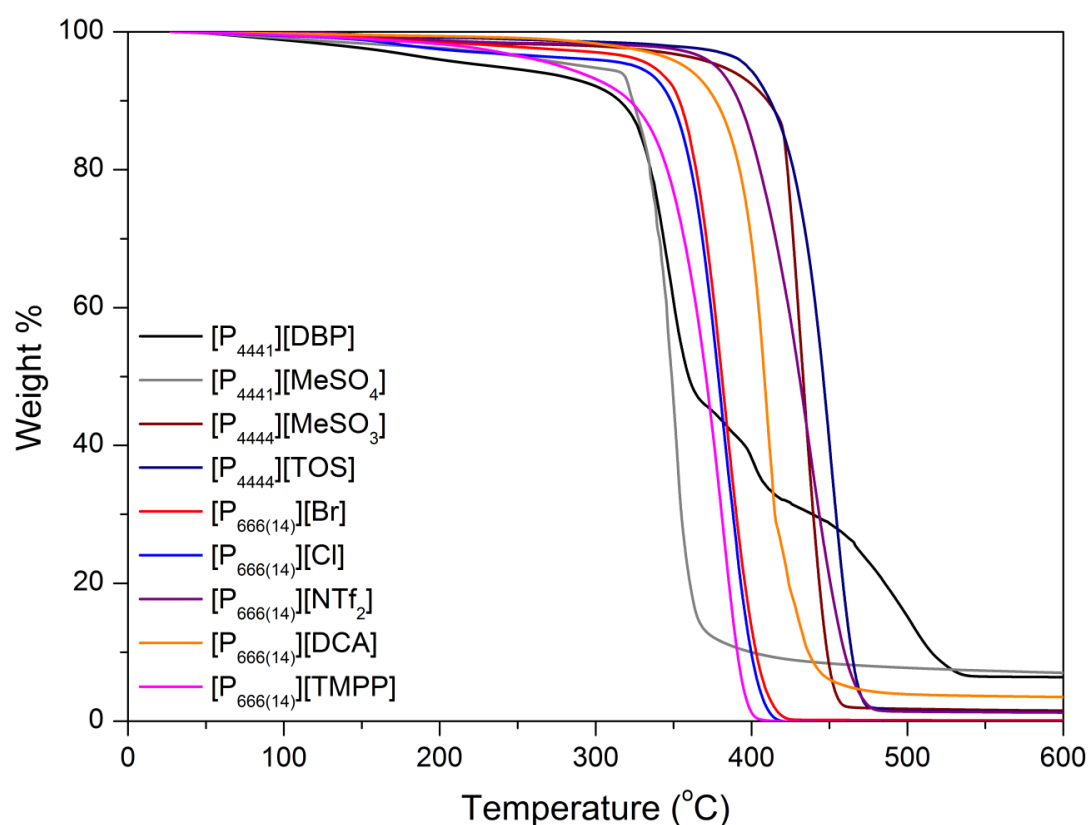


Figure 4.2: Comparison of fast-scan TGA results of phosphonium ILs.

For each IL investigated here, T_{onset} and T'_{onset} were determined. Table 4.2 summarizes these values along with the literature data. Here, we focus on T'_{onset} as they provide more

conservative thermal stability limits compared to the conventional T_{onset} values. Note that T'_{onset} values are up to 47 °C lower than that of T_{onset} .

Table 4.2: Thermal stability limits of phosphonium ILs.

Ionic Liquids	T_{onset} (°C)	T'_{onset} (°C)	T_{peak} (°C)	Literature T_{onset} (°C)
[P ₄₄₄₁][DBP]	327	312	350	-
[P ₄₄₄₁][MeSO ₄]	318	313	353	288 ^[29a]
[P ₄₄₄₄][MeSO ₃]	418	387	437	-
[P ₄₄₄₄][TOS]	423	396	453	-
[P ₆₆₆₍₁₄₎][Br]	357	344	389	320 ^[45b] , 353 ^[65c] , 356 ^[50c]
[P ₆₆₆₍₁₄₎][Cl]	357	345	391	350 ^[45] , 331 ^[29]
[P ₆₆₆₍₁₄₎][NTf ₂]	391	369	437	400 ^[46d] , 363 ^[29] , 402 ^[66e]
[P ₆₆₆₍₁₄₎][DCA]	389	371	414	395 ^[46] , 359 ^[29] , 399 ^[66] , 396 ^[67f]
[P ₆₆₆₍₁₄₎][TMPP]	339	292	384	340 ^[45]

^aPlatinum pan, under nitrogen flow with a heating rate of 2 °C min⁻¹; ^bUnder nitrogen flow; ^cPlatinum pan, under nitrogen flow with a heating rate of 10 °C min⁻¹; ^d No info available; ^eUnder nitrogen flow with a heating rate of 10 °C min⁻¹; ^fAluminum pan, under nitrogen flow with a heating rate of 10 °C min⁻¹.

As illustrated in Table 4.2, thermal stability limits change significantly with changes in IL structure. ILs investigated here are thermally stable at temperatures higher than 300 °C, except for [P₆₆₆₍₁₄₎][TMPP] decomposing at 292 °C, most probably because of its extraordinarily large size. In particular, ILs based on symmetrical [P₄₄₄₄]⁺ exhibit enhanced thermal stability compared to those based on asymmetrical [P₄₄₄₁]⁺ and [P₆₆₆₍₁₄₎]⁺. For instance, thermal stability limits of [P₄₄₄₄][MeSO₃] and [P₄₄₄₄][TOS] approach to temperatures as high as 400 °C, whereas those of ILs with [P₆₆₆₍₁₄₎]⁺ and [P₄₄₄₁]⁺ go down to 300 °C region.

To further investigate the effect of ILs' size on their thermal stability limits, variation of stability limits with molar volumes was considered (given in appendix). It is evident that

there is no significant correlation between the size of phosphonium ILs and their corresponding thermal stability limits. Thus, the size effect was ruled out in our investigation, unless the IL is exceptionally large, such as $[P_{666(14)}][TMPP]$. Besides, when structures of $[P_{4444}][MeSO_3]$ and $[P_{4444}][TOS]$ were compared, they have similar anions with the same cation. The only difference is the aromatic ring in $[TOS]^-$. Normally, one would expect somehow lower thermal stability limit for $[P_{4444}][TOS]$, because $[TOS]^-$ is larger than $[MeSO_3]^-$. However, data reveal that thermal stability limit increases with aromatic addition on anion. We infer that addition of aromatic ring further stabilizes delocalized charge resulting in enhanced thermal stability.

Another directly comparable structural factor was anion electronegativity. For this purpose, we compared stability limits of $[P_{666(14)}][Br]$ and $[P_{666(14)}][Cl]$ because they have exactly the same cation and similar anion in size. The only difference is the electronegativity of $[Br]^-$ and $[Cl]^-$, 2.96 and 3.16 (on Pauling scale [68]), respectively. Although $[Cl]^-$ has a higher electronegativity than $[Br]^-$, thermal stability limits of these two analogues ILs are the same within the error range of our measurements (344 °C for $[P_{666(14)}][Br]$ and 345 °C for $[P_{666(14)}][Cl]$). The difference was not sufficient enough to elucidate the effect of anion electronegativity. However, these effects were found to be more obvious for imidazolium ILs. According to the results reported by Cao and Mu [50], thermal stability limits of ILs based on 1-butyl-3-methylimidazolium, $[BMIM]$, decrease from 278 °C for $[BMIM][I]$ to 272 °C for $[BMIM][Br]$ and to 257 °C for $[BMIM][Cl]$, as the electronegativity of anions increases in the order of $[I]^- < [Br]^- < [Cl]^-$.

Table 4.2 shows that stability limits of ILs based on $[P_{666(14)}]^+$ increase along with different anions as $[TMPP] \ll [Br] \cong [Cl] < [NTf_2] \cong [DCA]$. Similarly, Green *et al.* reported that anion structure controls the stability limits of phosphonium ILs [69]. However, as in the case of other studies reporting the thermal stability limits of ILs, they directly reported their raw data without providing any insights into thermal decomposition

mechanism. However, elucidation of correlations between stability limits with structural factors and the decomposition mechanism is extremely crucial for the rational design of thermally superior ILs, which can withstand harsh operating conditions.

4.4 Structural Factors Controlling Thermal Stability Limits and Decomposition Mechanism

As discussed above, direct comparison of IL structures is not truly appropriate to discover correlations between stability limits and the structural factors. This is mainly because of the fact that number of structurally comparable phosphonium ILs is limited.

It has been reported that ILs undergo thermal decomposition by a nucleophilic attack of the anion at the cation, such as E2 Hofmann elimination or S_N2 nucleophilic substitution mechanisms, or by the reaction of anion fragments with the cation [33,67,70]. Identification of structural centers involving in decomposition reaction is required to elucidate the decomposition mechanism in detail. Once this center is identified, it could be possible to rationally design novel ILs for high-temperature applications. For such centers, it is expected to have correlations between electron density and thermal stability limit of corresponding IL. Thus, we applied calculated ¹H NMR chemical shifts as a tool to map the electron densities around individual protons of phosphonium cations (appendix). Correlations between stability limits and chemical shifts of individual protons located at the identical position on each IL were considered individually. Results of linear regression analysis for these individual cases searching correlations between stability limits and chemical shifts of protons (i.e., T1 to T12 and P1 to P9) are given in Figure 4.3. Accordingly, R² value of 0.9921 obtained with protons located at T9 position of each IL exhibited a perfectly good fit as illustrated in Figure 4.4. This terminal proton is located on the closest alkyl chain to the anion, A1 alkyl chain. Specifically, it is the farthest terminal

proton to the anion on this specific alkyl chain. Data show that as the chemical shift value of this proton (T9) increases, thermal stability limit of the corresponding IL increases linearly (Figure 4.4).

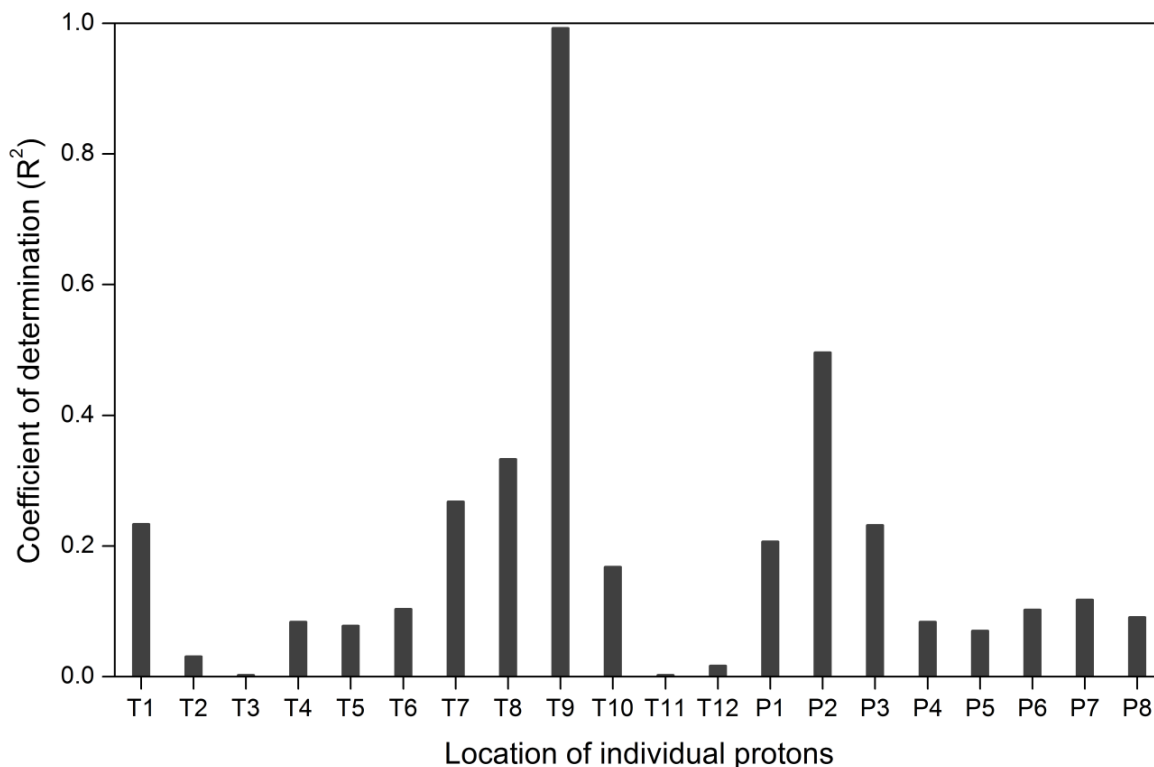


Figure 4.3: Regression analysis results between chemical shifts of individual protons and thermal stability limits of ILs (See Figure 4.1 and appendix for labeling).

As discussed before, there is a reverse relationship between chemical shift of a specific proton and its corresponding electron density. Thus, thermal stability limit of an IL increases with a decrease in electron density around its T9 proton on A1 chain. Decrease in electron density on the terminal end of A1 chain is accompanied by an increase in electron density allocated for bonding between P center and α -carbon of this alkyl chain. Therefore,

our data suggest that ILs with larger electron density for bonding between P center and α -carbon have higher thermal stability limits. High electron density around α -carbon makes the P–C bond stronger and induces a higher barrier for nucleophilic substitution by anion. This barrier hinders P–C bond cleavage and it becomes harder for anion to attack at α -carbon, resulting in an increase in the thermal stability limit. Thus, we infer that decomposition mechanism involves nucleophilic substitution of anion at the α -carbon of A1 chain.

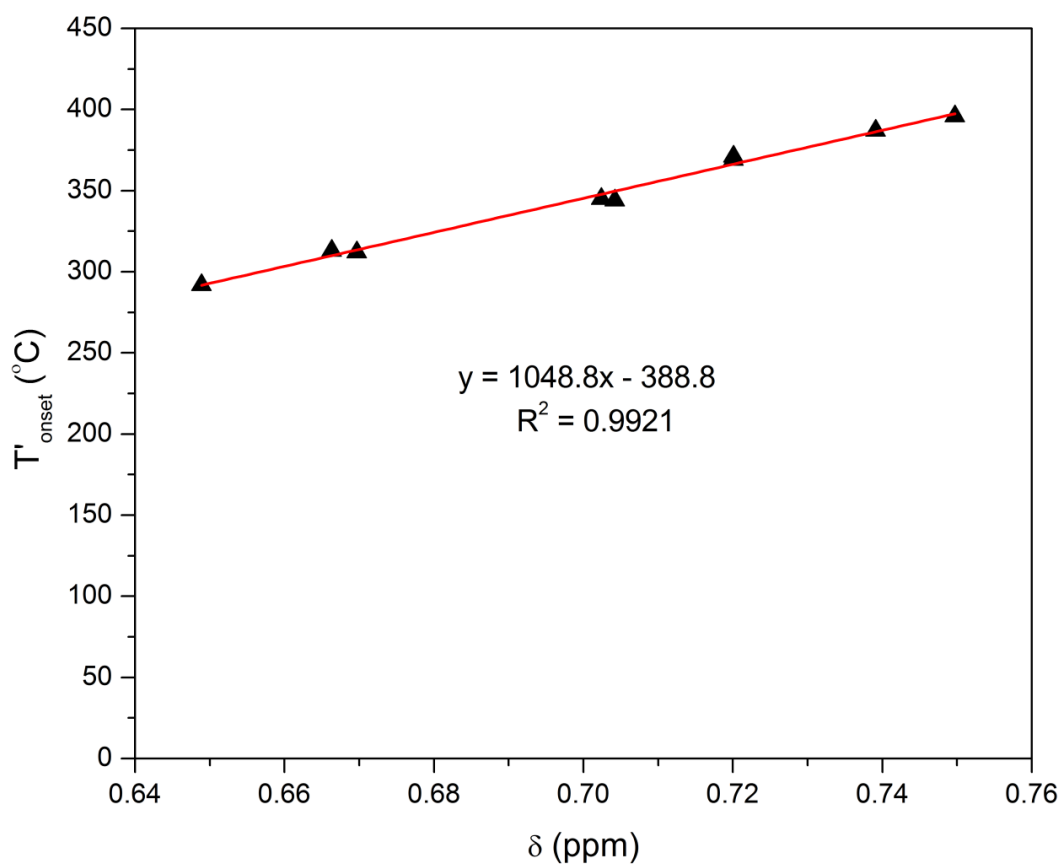


Figure 4.4: Relationship between thermal stability limits of ILs and DFT calculated chemical shifts of T9-protons on each IL.

To further confirm this postulated decomposition mechanism we have performed temperature programmed decomposition measurements with online mass spectrometry monitoring the effluent stream. The measurement was performed on $[\text{P}_{666(14)}][\text{Cl}]$, as it has the simplest anion structure, and thus, providing opportunities to identify individual decomposition products. Results show that m/z values of 39, 41, 42, 43, 55, 56, 57, 69, 70, 91, and 93 (given in appendix) were detected in the effluent stream as the decomposition products. These m/z values are assigned to $\text{C}_6\text{H}_{13}\text{Cl}$ fragments according to NIST database [35], confirming the nucleophilic substitution of anion at the α -carbon of the shorter alkyl chain. As illustrated in Figure 4.5, peak temperature at which the intensities of these m/z values reach the maximum was consistent with the TGA results. To check whether the longer alkyl chain ($\text{C}_{14}\text{H}_{29}$) undergoes nucleophilic substitution by $[\text{Cl}]^-$, we examined data closely at $m/z = 105$, which is the characteristic to $\text{C}_{14}\text{H}_{29}\text{Cl}$ fragments as reported in the NIST database [35]. However, within the noise level of our measurements, none of this mass could be detected as the decomposition product. Our DFT results also confirmed that the longer alkyl chain, $\text{C}_{14}\text{H}_{29}$, align opposite to $[\text{Cl}]^-$, hence it is not favorable for $[\text{Cl}]^-$ to access and react with the α -carbon on this alkyl chain because of steric hindrance.

Another possible decomposition mechanism was the β -elimination. For such mechanism one would expect to observe HCl with m/z values of 36 and 38 in the effluent stream. However, our data do not provide any evidence on the formation of such fragments during thermal decomposition. Thus, we infer that MS results strongly confirm our postulated mechanism for thermal decomposition of tetraalkylphosphonium ILs. The postulated mechanism given in Scheme 1 summarizes that decomposition starts with nucleophilic substitution of the anion at α -carbon of A1 alkyl, which is the closest neighbor of the anion.

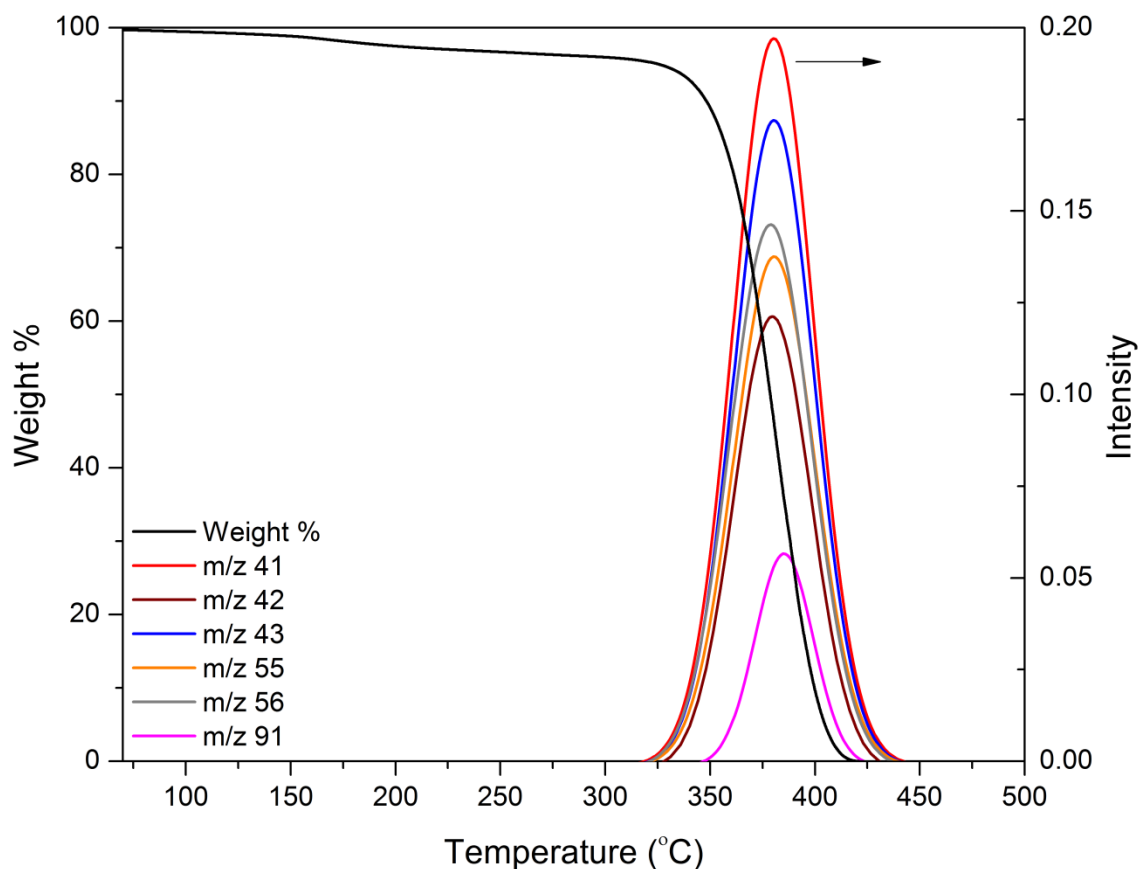
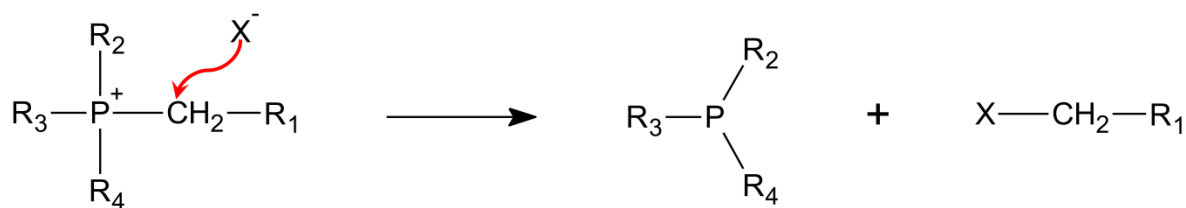


Figure 4.5: TGA and MS results in the effluent stream during temperature programmed decomposition of $[P_{666(14)}][Cl]$. Primary y-axis shows TGA thermograph, the colored lines on the secondary y-axis represent the intensities of certain m/z values that were detected in the effluent stream.



Scheme 1: Mechanism for nucleophilic substitution of anion, $[X]^-$, at α -carbon.

Xie *et al.* [71] investigated thermal degradation mechanism of tetraalkylphosphonium IL-modified montmorillonites by TGA coupled with pyrolysis/GC-MS. For tributyl-octadecylphosphonium bromide, they postulated four different thermal decomposition reaction mechanisms, such as nucleophilic substitution at the α -carbon, and β -elimination, and in the presence of a strong base, substitution at phosphorus, and α -elimination. Consistent with our results, they concluded that nucleophilic substitution at the α -carbon reaction mechanism is more favored among others. Moreover, Gross [72] studied trihexyl(tetradecyl)phosphonium, [P₆₆₆₍₁₄₎], tris(pentafluoroethyl)trifluorophosphate by liquid injection field desorption/ionization (LIFDI) mass spectrometry. Their results on this specific IL revealed that the bulky [P₆₆₆₍₁₄₎]⁺ fragments by homolytic cleavages at C–C and P–C bonds. P–C bond cleavage is found to be more favorable because of the major peaks appeared at m/z values of 398.4, [C₂₆H₅₅P], and 286.3, [C₁₈H₃₉P], as a result of hexyl and tetradecyl losses from the cation, respectively. These findings further confirm our postulated decomposition mechanism involving nucleophilic substitution at the α -carbon. We note that our decomposition mechanism postulated here can be valid for a wide range of tetraalkylphosphonium ILs, not only limited with those listed in Table 3.1. Moreover, we suggest that our data in Figure 4.4 can be utilized to estimate short-term decomposition temperatures of tetraalkylphosphonium ILs, provided that their structures and corresponding ¹H NMR spectra is calculated by DFT with the identical basis sets as utilized here. For designing phosphonium ILs with superior thermal stability, we suggest that structures should be tailored to increase electron density allocated for the bonding between central P atom and its substituents. Consistent with this suggestion, Cassity *et al.* [73] replaced alkyl substituents on the phosphonium cation with aryl groups. These ILs were reported to have the record high thermal stability limits up to date [73].

Chapter 5

THERMAL STABILITY OF METAL-OXIDE-SUPPORTED PHOSPHONIUM IONIC LIQUIDS

5.1 Introduction

Ionic liquids (ILs) are new-generation green solvents and potential alternatives for their volatile organic counterparts. They have received tremendous attention during the last decade because of their unique physical and chemical properties such as non-volatility, non-flammability, high chemical and thermal stability, high solvating ability and tunable miscibility. These physicochemical properties can be tailored by incorporating almost infinite combinations of different anions and cations; hence they are often called as “designer” or “task-specific” solvents. Such structural diversity and functional flexibility has led to a growing interest towards application in numerous research fields such as synthesis, electrochemistry, separation, and catalysis.

As one of the emergent application areas, two primary concepts have been pioneered to exploit tunable features of ILs in catalysis -*supported ionic liquid phase* (SILP) and *solid catalysts with an ionic liquid layer* (SCILL). For SILP-type catalyst, a thin layer of ionic liquid containing a homogeneous catalyst is applied to the internal surface of a porous support material. Similarly, in SCILL concept, heterogeneous catalyst or catalytically active materials are coated with a thin film of IL. These promising catalytic concepts lead to enhanced selectivity, product distribution, yields, and selective solubility for

intermediates and products because of promoting interactions between active sites, supports and IL. However, application of ILs in these supported-catalyst concepts is limited with their thermal stability on corresponding support materials. For instance, data gathered by Lemus *et al.* [31] provide confirmatory evidence corroborating the notion that thermal stability of ILs is an issue when they are immobilized on metal-oxide supports. They reported that thermal stability of 1-methyl-3-octylimidazolium hexafluorophosphate decreased by 40 °C on TiO₂, 135 °C on Al₂O₃, and 155 °C on SiO₂ as compared to bulk value [31]. On this basis it may be inferred that even though most of the ILs are thermally stable at elevated temperatures (> 300 °C) in their bulk case, they become less stable when coated on metal-oxide supports because of the interactions between IL and metal-oxide.

Here we report the results of a systematic investigation on the elucidation of structural factors determining the thermal stability limits of 9 different phosphonium ILs on three of the most commonly used catalyst supports, SiO₂, γ -Al₂O₃, and MgO.

5.2. Thermal Stability Limits of Metal-Oxide Supported Phosphonium Ionic Liquids

Thermal stability limits of phosphonium ionic liquids supported on SiO₂, γ -Al₂O₃, and MgO were determined using TGA measurements at a heating rate of 10 °C min⁻¹. The results were illustrated in Figure 5.1 and tabulated in Table 5.1. The ILs studied here have three different cations bearing different alkyl groups attached to the central P atom, and showing symmetrical (e.g., [P₄₄₄₄]) and asymmetrical cation geometries (e.g., [P₄₄₄₁], [P₆₆₆₍₁₄₎]). These cations are incorporated with 9 different anions, ensuring different physicochemical and thermochemical properties for each IL.

As illustrated in Figure 5.1, thermal stability limits change with variations in ILs' structures. Bulk ILs are thermally stable at temperatures higher than 300 °C (see Table 5.1), except for [P₆₆₆₍₁₄₎][TMPP], which is because of its extremely large size as discussed in the

previous chapter. However, when these ILs were supported on SiO_2 , $\gamma\text{-Al}_2\text{O}_3$, and MgO , their corresponding thermal stability limits decrease appreciably. Especially on MgO , thermal stability limits of ILs are much lower than that of on SiO_2 and $\gamma\text{-Al}_2\text{O}_3$. For example, thermal stability limit of $[\text{P}_{4444}][\text{MeSO}_3]$ is significantly deviated from bulk value to the extent of 39 °C on SiO_2 , 128 °C on $\gamma\text{-Al}_2\text{O}_3$, and most drastically, 185 °C on MgO (see Table 5.1).

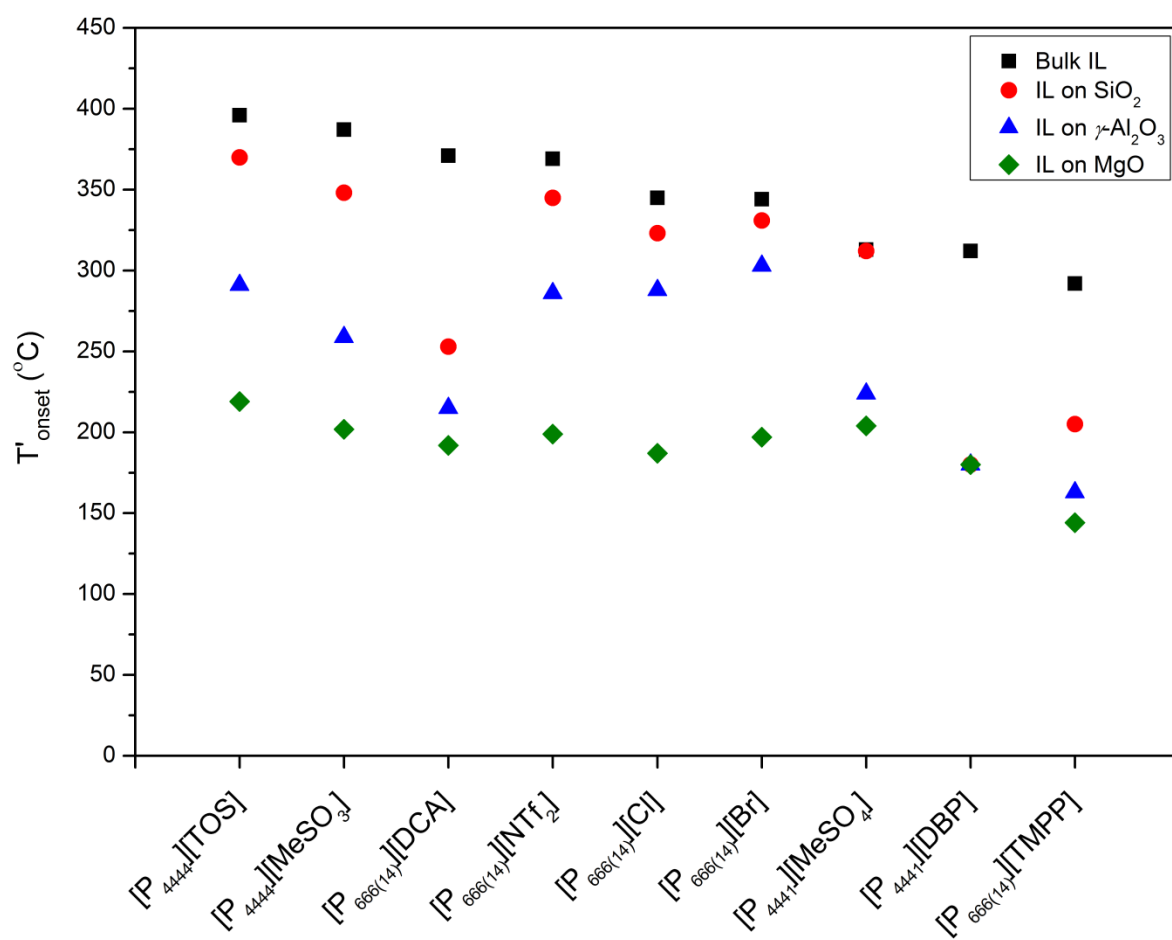


Figure 5.1: Comparison of thermal stability limits of phosphonium ILs supported on different metal oxides.

Here the ILs with similar structures are directly compared with each other with respect to the differences between their thermal stability limits to identify the structural parameters controlling thermal stabilities.

As discussed before, [P₆₆₆₍₁₄₎][TMPP] has the lowest thermal stability limit among other bulk ILs, which was attributed to its extremely large size. When [P₆₆₆₍₁₄₎][TMPP] is coated on metal oxides, its thermal stability decreases significantly on each support. Its thermal stability decreases further by 87 °C on SiO₂, 129 °C on γ -Al₂O₃, and 148 °C on MgO (see Table 5.1). Thus, these results confirm that the effect of IL size on thermal stability still prevails and even more dominant on metal oxides.

Table 5.1: Thermal stability limits of bulk and supported phosphonium ILs.

Ionic Liquids	T' _{onset} (°C)			
	Bulk IL	IL on SiO ₂	IL on γ -Al ₂ O ₃	IL on MgO
[P ₄₄₄₄][TOS]	396	370	291	219
[P ₄₄₄₄][MeSO ₃]	387	348	259	202
[P ₆₆₆₍₁₄₎][DCA]	371	253	215	192
[P ₆₆₆₍₁₄₎][NTf ₂]	369	345	286	199
[P ₆₆₆₍₁₄₎][Cl]	345	323	288	187
[P ₆₆₆₍₁₄₎][Br]	344	331	303	197
[P ₄₄₄₁][MeSO ₄]	313	312	224	204
[P ₄₄₄₁][DBP]	312	180	180	180
[P ₆₆₆₍₁₄₎][TMPP]	292	205	163	144

Moreover, as discussed in previous chapter, normally we would expect somehow lower thermal stability limit for [P₄₄₄₄][TOS], because [TOS]⁻ is larger than [MeSO₃]⁻. However, thermal stability limit further increases on metal oxides with aromatic addition on anion.

For instance, thermal stability limit increases 32 °C on γ -Al₂O₃ with aromatic addition on anion (i.e., for [P₄₄₄₄][TOS]) as compared to IL with aliphatic anion. It is evident that addition of aromatic ring further stabilizes delocalized charge resulting in enhanced thermal stability of ILs even on metal oxides.

Another structural parameter that can be directly elucidated is the electronegativity of anion. We first compared the thermal stability limits of [P₆₆₆₍₁₄₎][Br] and [P₆₆₆₍₁₄₎][Cl], because they have the same cation with different electronegative anions of comparable size. As discussed in Chapter 4, although [Cl]⁻ has a higher electronegativity than [Br]⁻, electronegativity effect of anions on thermal stability limits of bulk ILs are vaguely discernible. However, when these ILs are coated on metal-oxide supports, the differences in thermal stability limits on the same support increase evidently. On MgO surface, for example, thermal stability limit decreases from 197 °C to 187 °C as [P₆₆₆₍₁₄₎][Br] is substituted with [P₆₆₆₍₁₄₎][Cl]. Therefore, the effect of electronegativity on thermal stability of ILs becomes more apparent when they are confined on support surfaces. Thermal stability decreases with more electronegative anion (i.e., [Cl]⁻) on supports, as it is more favorable for the more electronegative anion to promote elimination reactions, which is considered as the dominant decomposition pathway, at lower reaction temperatures on immobilized-IL matrices [71]. Especially on γ -Al₂O₃, the difference in thermal stability limits of these two ILs is 15 °C.

Finally, data further illustrate that [P₄₄₄₁][DBP] decomposes at 180 °C on SiO₂, γ -Al₂O₃, and MgO. We believe that there is a different decomposition mechanism for [P₄₄₄₁][DBP] regardless of type of metal oxide support. For this case, the relatively bulky [DBP] anion may decompose first on metal oxides. Nevertheless, the decomposition of [P₄₄₄₁][DBP] on supports should be investigated by mass spectroscopy in detail.

In conclusion, results presented here set the first steps towards revealing the structural factors determining thermal stability limits of phosphonium-type ILs on three of the most

commonly used metal-oxide catalyst supports. These structural parameters are characterized as size of IL, electronegativity of anion, and aromatic ring addition in anion. Thermal stability limits of ILs decrease when they are coated on metal oxides. The more pronounced effect of support on thermal stability limits of ILs is observed on MgO. These stability limits serve as the basis for the selection of suitable phosphonium-type ILs according to the application conditions of IL-assisted supported catalysts.

This part of the study will be further complemented by mass spectroscopy analyses to postulate a thermal decomposition mechanism for metal-oxide supported phosphonium ILs by characterizing corresponding thermal degradation products.

Chapter 6

PROBING CATION-ANION INTERACTION ENERGIES IN IMIDAZOLIUM IONIC LIQUIDS

6.1 Introduction

Ionic liquids (ILs) offer high degree of tunability in their corresponding physicochemical properties by incorporating myriad combinations of different anions and cations. These physicochemical properties, such as vapor pressure, melting point, density, viscosity, surface tension, predominantly depend on interactions between anion and cation [74]. Therefore, elucidation of inter-ionic interactions in ILs is crucial to rationally design novel ILs to obtain target bulk physicochemical properties.

Such interactions are evolved from a complex interplay of Coulombic interactions, hydrogen bonding and dispersion forces among cations and anions, and ultimately determine the bulk properties of ILs [75]. Determination of these pronounced interactions in ILs is quite difficult [75]. Experimental and computational studies have been carried out to determine these inter-ionic interactions in ILs, and to correlate them with their bulk properties. Ludwig *et al.* studied interaction energies between cations and anions of [EMIM][SCN], [EMIM][DCA], [EMIM][EtSO₄], and [EMIM][NTf₂] by combination of far infrared (FIR) spectroscopy with *ab initio* calculations [76]. Their results revealed that the low frequency vibrational bands between 50 cm⁻¹ and 120 cm⁻¹ are attributed to bending and stretching modes of hydrogen bonds between anions and cations of the

corresponding ILs. These vibrational frequencies were found to be shifted to higher frequencies with increasing ionic strength of the anion, and correlated well with the calculated interaction energies [76].

Furthermore, Gao *et al.* [77] utilized attenuated total reflection infrared spectroscopy (ATR-IR) and density functional theory calculation to reveal the hydrogen-bond interactions between cation and anions of different ILs based on [BMIM] cation. They reported that C2–H stretching frequency determines electron density of hydrogen-bonding between anion and cation of corresponding ILs. As the electron density of hydrogen-bonding between cation and anion increases, the C2–H stretching frequency decreases leading to a stronger cation-anion interaction. Thus, C2–H stretching frequency predicts reasonably well the strength of cation-anion interaction. Additionally, they claimed that calculated interaction energies partially explain the cation-anion interaction. Size and position of anion is also important in determining the strength of cation-anion interaction [77]. One drawback of this study is that no attempt was done to elucidate a correlation between interaction energy and C2–H stretching frequency, which could provide opportunities to expand the result of this study to other similar structured ILs.

As mentioned in Chapter 2, Dong *et al.* [19] showed that there is a linear relationship between melting points and interactions energies for some the imidazolium ILs studied. As the interaction between cation and anion becomes stronger (i.e., as the interaction energy becomes smaller (more negative)), the melting point of the corresponding IL increases. However, as the structure of anions gets bulkier, such as when the [Cl]⁻ anion is substituted with [PF₆]⁻ anion, a divergence from linear relationship occurs. The reason is attributed to the presence of more complex interactions between cation and anion in the latter case [19]. Similarly, Ludwig *et al.* [78] elucidated the contribution of hydrogen bonds to the overall interaction energy between anions and cations of the ILs. They reported that although the Coulombic forces dominate the anion-cation interactions, the hydrogen

bonding between anion and cation plays an essential role on the structure and physicochemical properties of ILs as a result of so-called “defect hypothesis”. They further employed this hypothesis on the melting points, viscosities and enthalpies of vaporization of ILs, and illustrated the important contribution of hydrogen bonding on physicochemical properties of ILs [78].

Moreover, Fernandes *et al.* [74] conducted a thorough study on the determination of the interaction energies of between anion cation of the various IL families including imidazolium, pyridinium, pyrrolidinium, and piperidinium by electrospray tandem mass spectrometry (ESI-MS/MS) complemented by DFT calculations. They reported that the structural factors governing the interactions between anions and cation are cation core and ring size, aromaticity, alkyl chain length, anion nature and size, and ion charge densities. For instance, data illustrated that inter-ionic interactions are weaker in the aromatic ILs because of the charge delocalization in the aromatic rings resulting in hindrance in the electrostatic strength. Furthermore, the obtained interaction energies by electrospray ionization tandem mass spectrometry correlated well with the surface tensions of ILs [74].

Here, we report the elucidation of interaction energies between cation and anions of ILs based on 1-butyl-3-methylimidazolium, [BMIM]⁺, which were obtained by DFT calculations. These calculated interaction energies were further correlated with the experimental C2–H stretching frequencies. A direct correlation relating interaction energies with C2–H stretching frequencies was established. This correlation will contribute to the ongoing research studies conducting in our research group.

6.2 Conformational Analysis and Computation of Interaction Energies

A full conformational search was performed for each IL by altering the anion position around [BMIM] cation. Representative structures for [BMIM] cation and six different

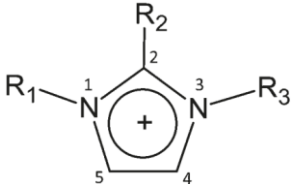
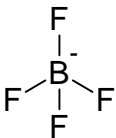
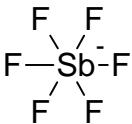
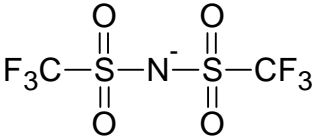
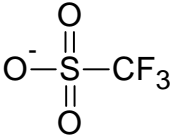
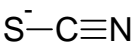
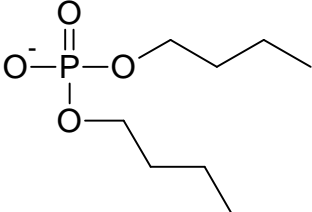
anions are illustrated in Figure 6.1. The energies of all conformers were found using B3LYP/6-31+G(d), except for [BMIM][SbF₆], for which B3LYP/DGDZVP was used. By comparing the energies of all conformers, the lowest energy conformer was assumed as global minimum geometry on its corresponding potential energy surface (PES). Additionally, the relative energies, ΔE , were calculated by subtracting energy of conformers from their corresponding global minimum energy. According to this definition, global minimum geometry has the relative energy of $\Delta E = 0 \text{ kJ mol}^{-1}$ (see Figures 6.2-6.7).

For [BMIM][BF₄], the conformers and their energies relative to lowest energy conformer (i.e., conformer #7) are given in Figure 6.2. The conformational search yielded 7 conformers for [BMIM][BF₄]. As shown in Figure 6.2, the energies of conformers, where the anion is located close to C2–H, are much lower than other conformers. The lowest energy conformer was achieved when the [BF₄] anion is located close to C2–H but below the plane of imidazolium ring. It should be noted that the relative energy increases up to 40 kJ mol^{-1} when the anion is located close to C4–H, C5–H as in the case of conformer 1.

Figure 6.3 represents the conformers and relative low energies for [BMIM][SbF₆]. There are only 5 low energy conformers obtained for [BMIM][SbF₆]. The lowest energy conformer (i.e., conformer 5) was achieved when the anion lies close to C2–H and below plane of the imidazolium ring. When the anion lies close to C2–H but above the plane of the imidazolium ring, the relative energy increases to 5.6 kJ mol^{-1} . Furthermore, the difference in energy increases 36.7 kJ mol^{-1} as the anion is located near C5–H.

As illustrated in Figure 6.4, there are 12 different low energy conformers for [BMIM][NTf₂]. This high number of attainable conformers is specifically derived from the high degree of rotational structure of [NTf₂] anion. Again, the lowest energy conformer (i.e., conformer 12) was obtained when the anion lies near C2–H, but most part of the anion is above the ring plane. Surprisingly, a top conformer (i.e., conformer 1), where the [NTf₂] anion is located at the top of ring plane, can be achieved. However, it is the highest energy

Figure 6.1: Structures of imidazolium ILs based on [BMIM] cation.

Structure	Name	Abbreviation
	<p>1-Butyl-3-methylimidazolium</p> <p>R₁: butyl, R₂: hydrogen, R₃: methyl</p>	[BMIM]
	Tetrafluoroborate	[BF ₄]
	Hexafluoroantimonate	[SbF ₆]
	Bis(trifluoromethylsulfonyl)imide	[NTf ₂]
	Trifluoromethanesulfonate	[TfO]
	Thiocyanate	[SCN]
	Dibutyl phosphate	[DBP]

conformer, and the relative energy increases to 10.5 kJ mol^{-1} .

Figure 6.5 illustrates the relative energies and ion-pair structures of conformers for [BMIM][TfO]. There are 4 lower energy conformers and 3 higher energy conformers, where the anion lies near C2–H and C4–H, C5–H, respectively. In the lowest energy conformer (i.e., conformer 7), the [TfO] anion is located near C2–H, where the O atoms are at the top and at the same plane with the imidazolium ring to enhance the C–H \cdots O bonds ability. The relative energy gets higher as 38.8 kJ mol^{-1} when the anion with the same conformer lies near C4–H, C5–H.

As shown in Figure 6.6, there are 6 lower conformers and 2 higher conformers for [BMIM][SCN]. However, there is only 2.2 kJ mol^{-1} difference in relative energies among the lower conformers. In the lowest energy conformer, the anion lies near the C2–H, but almost above the ring plane. Similarly, in the highest energy conformer, the anion is located towards C4–H, C5–H at the same plane with the imidazolium ring, resulting in an increase in the relative energy to 38 kJ mol^{-1} .

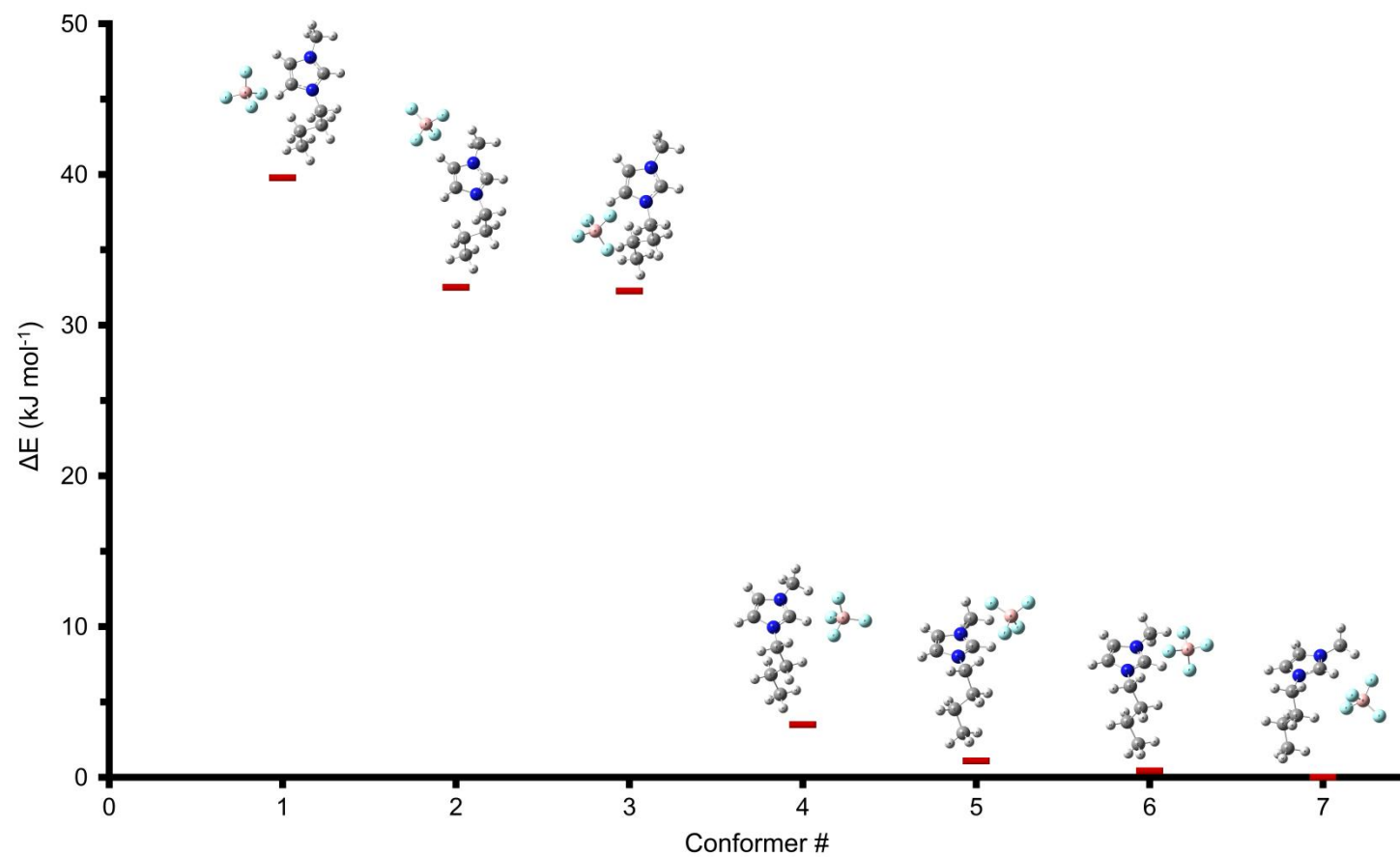
Finally, the low energy conformers for [BMIM][DBP] are given in Figure 6.7. 10 different conformers were found, and 5 of them are in the lower energy conformer region with the anions located towards C2–H. As in the [BMIM][NTf₂], the high number of obtained conformers is because of a high degree of rotational freedom of the relatively bulkier of [DBP] anion. In the lowest energy conformer, the phosphate center is located at the same plane with the imidazolium ring and pointed towards C2–H. On the other hand, in the highest energy conformer, the anion energetically prefers to lie close to methyl and C4–H with the phosphate center lying above the ring plane, and ultimately increasing the relative energy to 59 kJ mol^{-1} .

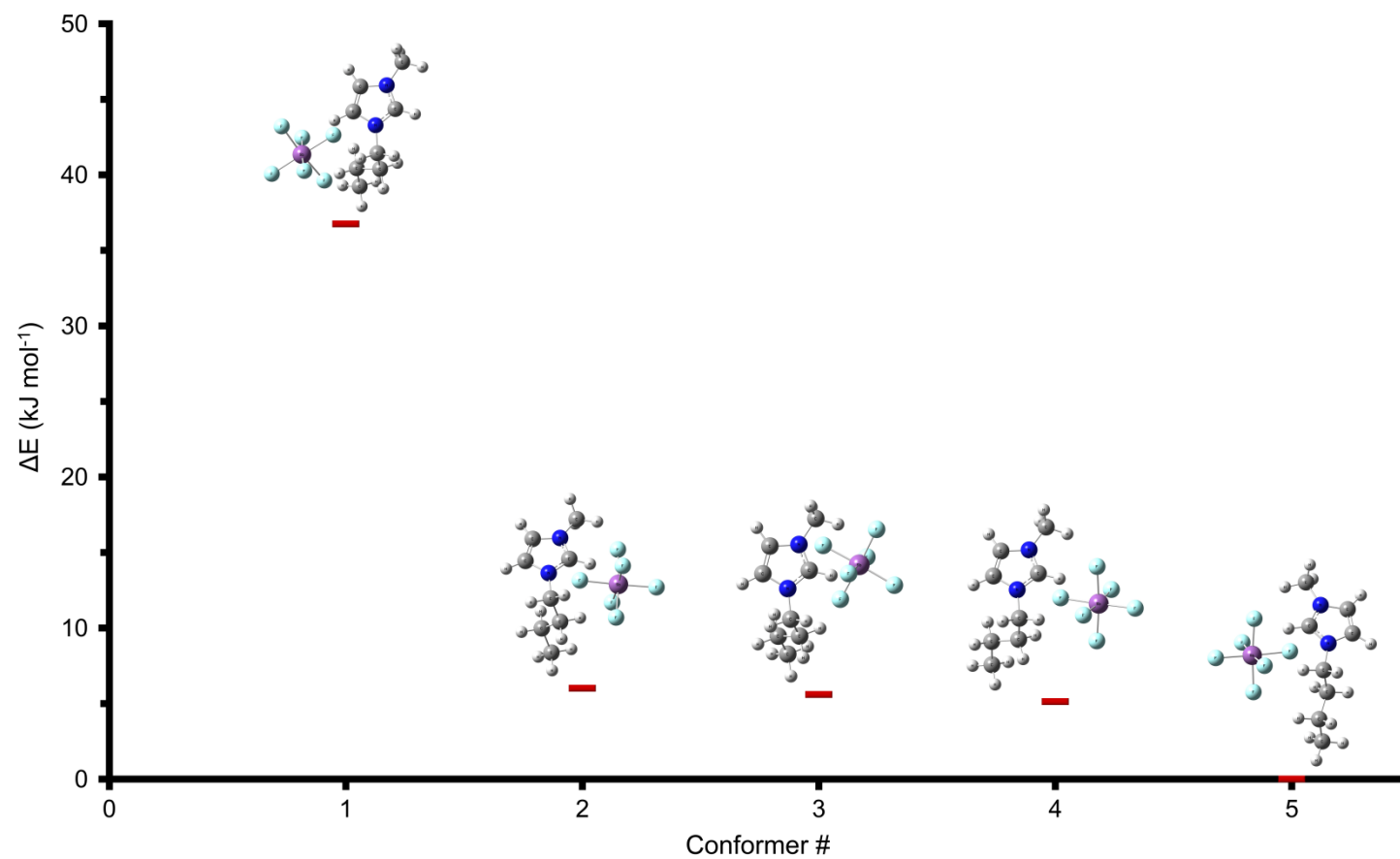
Furthermore, interionic interaction energy, $E_{\text{interaction}}$, was calculated considering the global minimum geometries of each IL and their corresponding anions/cations by using Eq. 3.1. The results of interaction energies along with individual global minimum energies of

ILs, anions and cations are tabulated in Table 6.1. Experimental C2–H stretching frequencies are also given here.

Table 6.1: Interaction energies and experimental C2–H stretching frequencies of ILs.

ILs	E_{IL} (a.u)	E_{cation} (a.u)	E_{anion} (a.u)	$\Delta ZPVE$ (kJ mol ⁻¹)	$E_{interaction}$ (kJ mol ⁻¹)	$\nu(C2-H)$ (cm ⁻¹)
[BMIM][BF ₄]	-847.8825	-423.1851	-424.5670	3.68	-338.86	3114
[BMIM][SbF ₆]	-7338.0852	-423.2113	-6914.7522	3.10	-316.36	3123
[BMIM][NTf ₂]	-2250.5873	-423.1851	-1827.2822	3.64	-311.33	3124
[BMIM][TfO]	-1384.8653	-423.1851	-961.5534	3.01	-330.12	3115
[BMIM][SCN]	-914.4336	-423.1851	-491.1194	2.24	-336.67	3095
[BMIM][DBP]	-1381.4649	-423.1851	-958.1348	3.69	-377.20	3077

Figure 6.2: Conformers and relative energies of [BMIM][BF₄].

Figure 6.3: Conformers and relative energies of [BMIM][SbF₆].

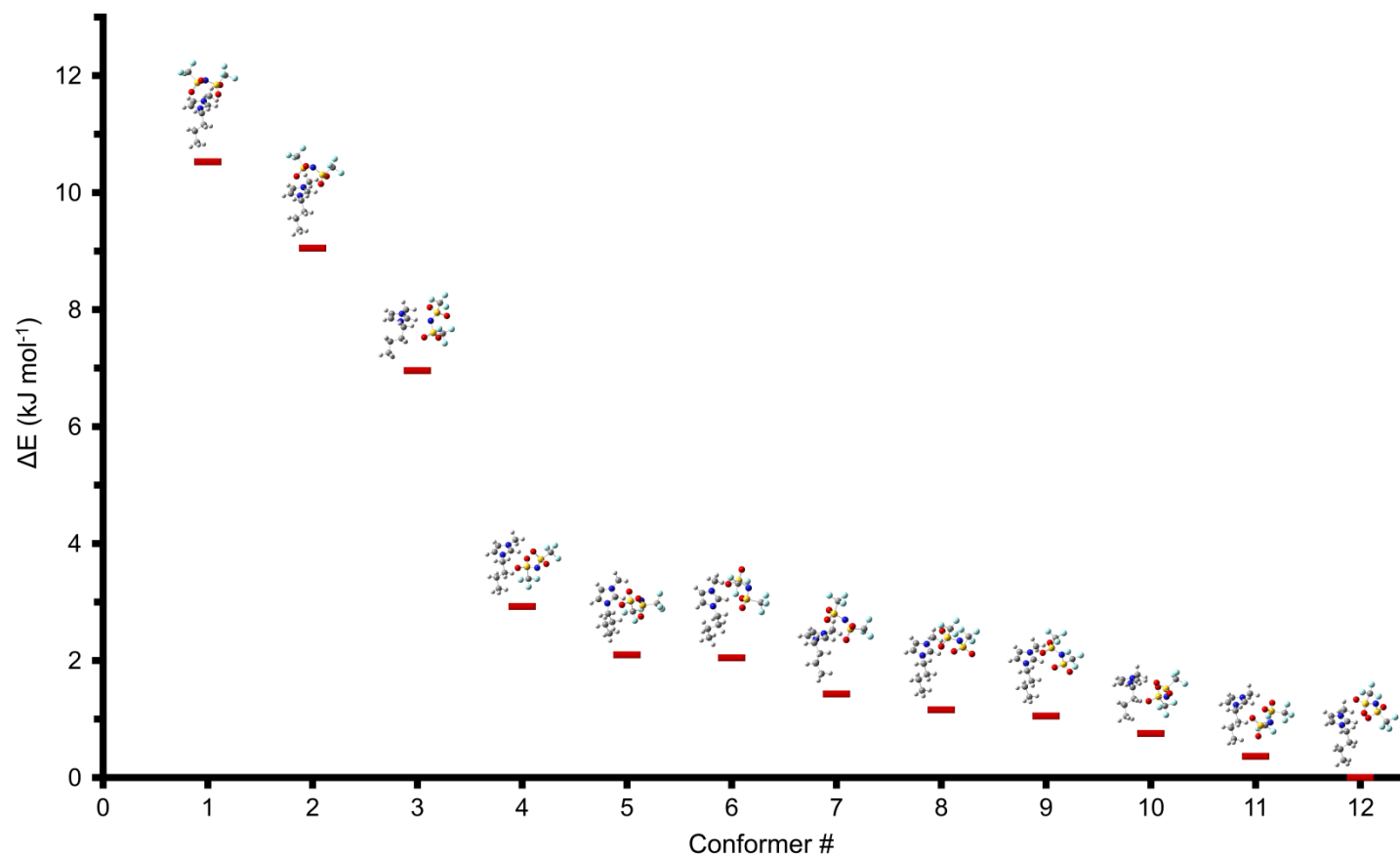


Figure 6.4: Conformers and relative energies of [BMIM][NTf₂].

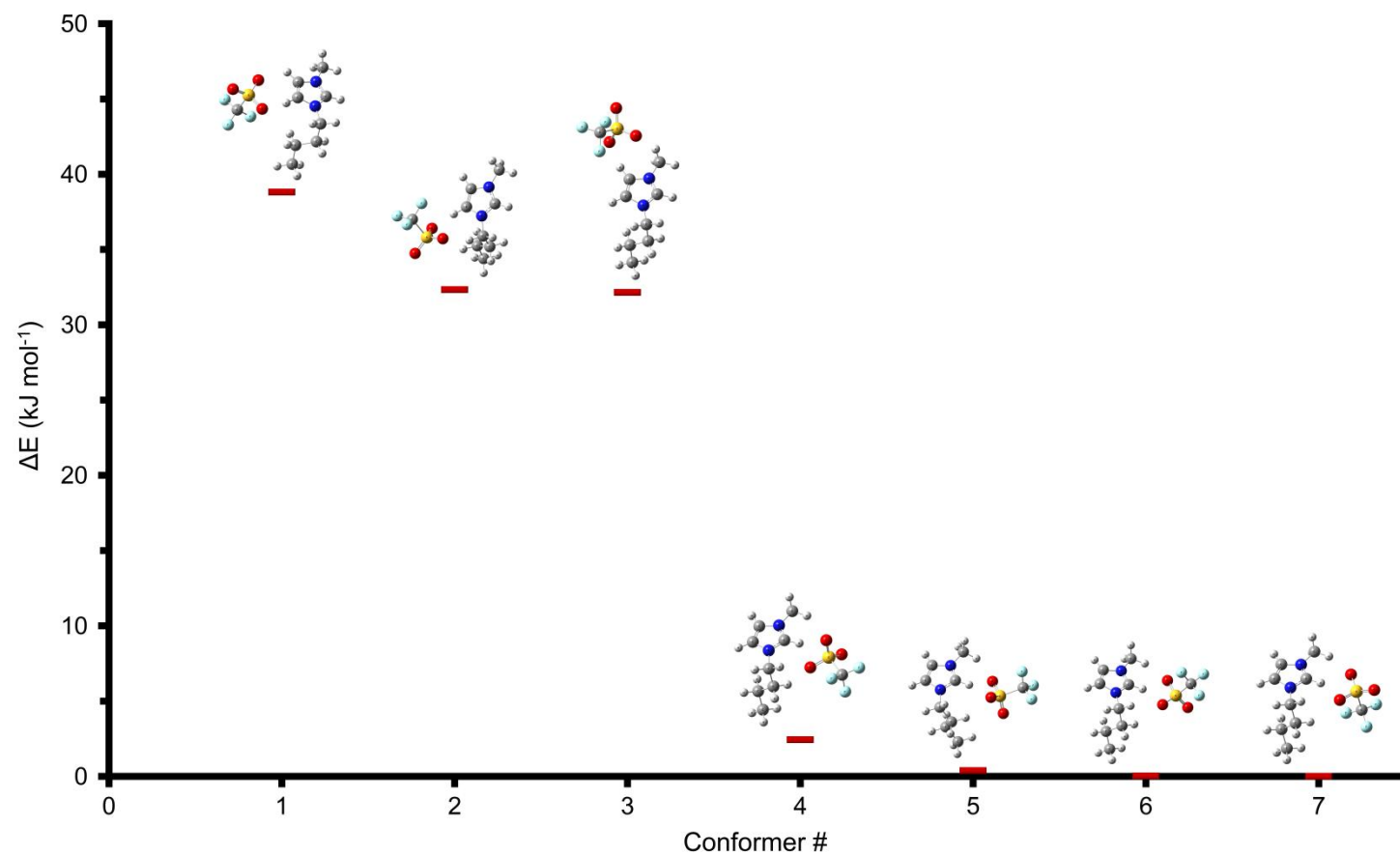


Figure 6.5: Conformers and relative energies of [BMIM][TfO].

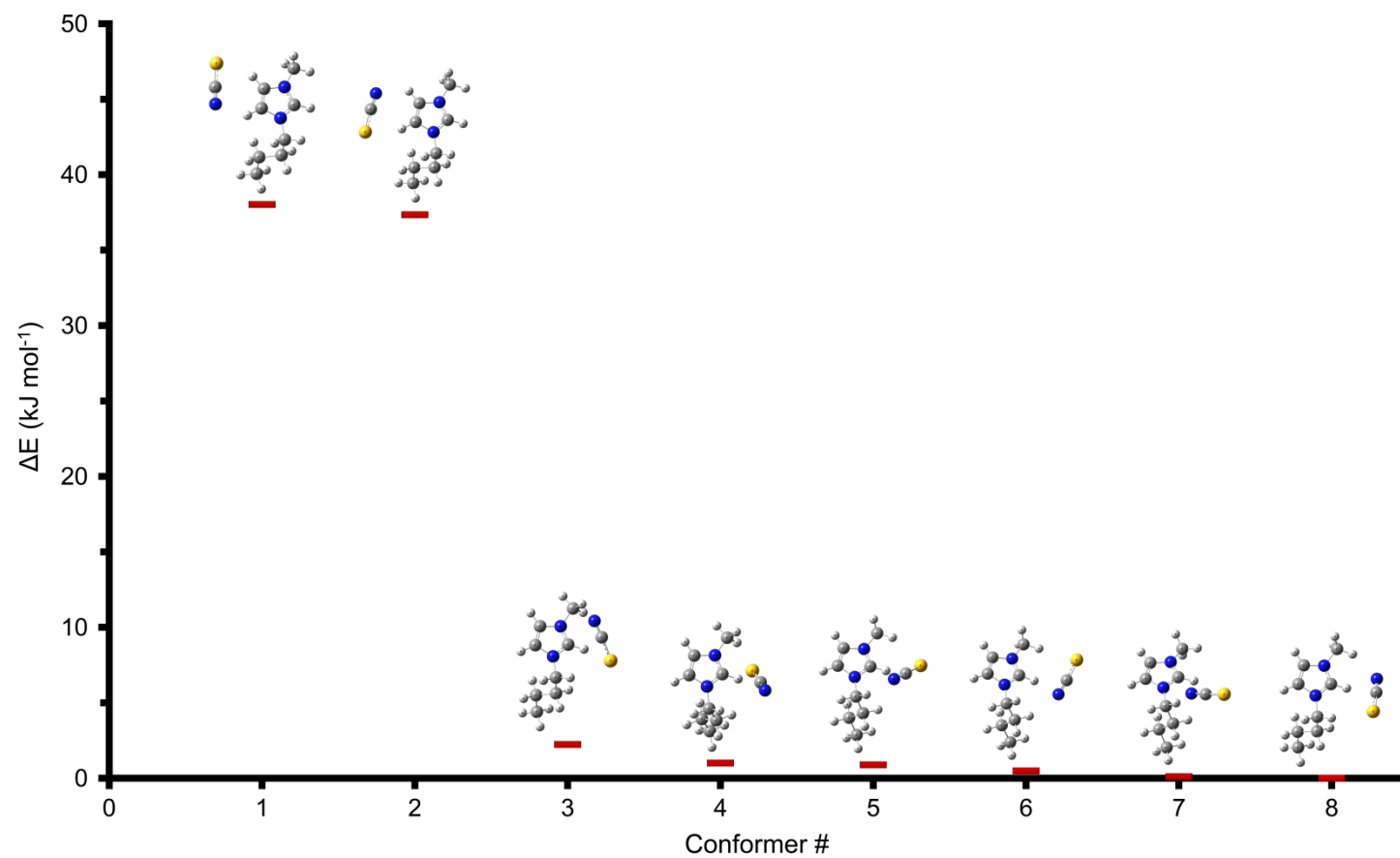


Figure 6.6: Conformers and relative energies of [BMIM][SCN].

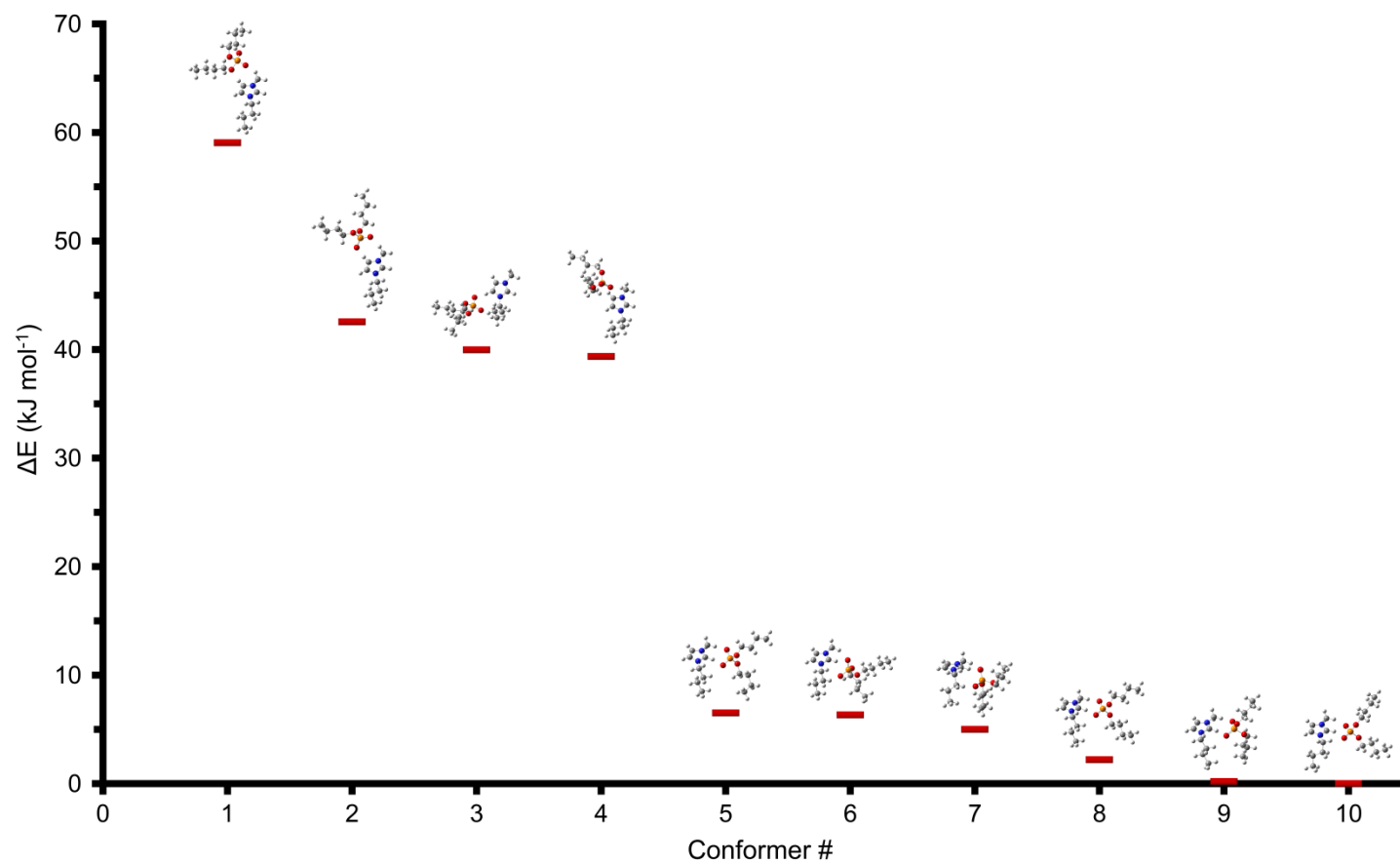


Figure 6.7: Conformers and relative energies of [BMIM][DBP].

6.3. Correlation between Interaction Energy and Vibration Frequency

After structures of ILs were optimized and a full conformational search was performed, interaction energies between anions and cations of the lowest energy conformers were calculated using the corresponding formula (Eq. 3.1). The results demonstrate that the strength of interaction between corresponding anions and [BMIM] cation decreases in the order of:

[BMIM][DBP] > [BMIM][BF₄] > [BMIM][SCN] > [BMIM][TfO] > [BMIM][SbF₆] > [BMIM][NTf₂].

As discussed before, the C2–H stretching frequency determines the electron density of hydrogen-bonding. Furthermore, the determination of interaction energies between anions and cations is quite challenging and highly time-consuming. Therefore, we basically attempted to correlate the experimental C2–H stretching frequencies with their corresponding calculated interaction energies so that one can easily predict the interaction energies using this correlation.

As illustrated in Figure 6.8, there is a linear correlation between experimental C2–H stretching frequencies of ILs and their interaction energies. It is evident that as the C2–H stretching frequency decreases, the interaction energy decreases as well. In other words, the interaction between cation and anion becomes stronger when C2–H stretching frequency becomes lower. For example, [BMIM][DBP] has the lowest C2–H stretching frequency (i.e., 3077 cm⁻¹), hence the strongest cation-anion interaction among other ILs studied here.

These results can be used to predict the interaction energies between cation and anion of ILs. Additionally, this correlation can be used as a tool to correlate the predicted interaction energies with numerous physicochemical and thermochemical properties such as melting point, density, viscosity, surface tension, and thermal decomposition temperatures. Hence, it would be possible to design novel ILs with enhanced properties for a broader operating

limits. Besides, this information can provide preliminary data to describe the interactions of these ILs with the active sites of the catalysts, hence helping the elucidation of structure-performance relationships in IL-assisted catalysts.

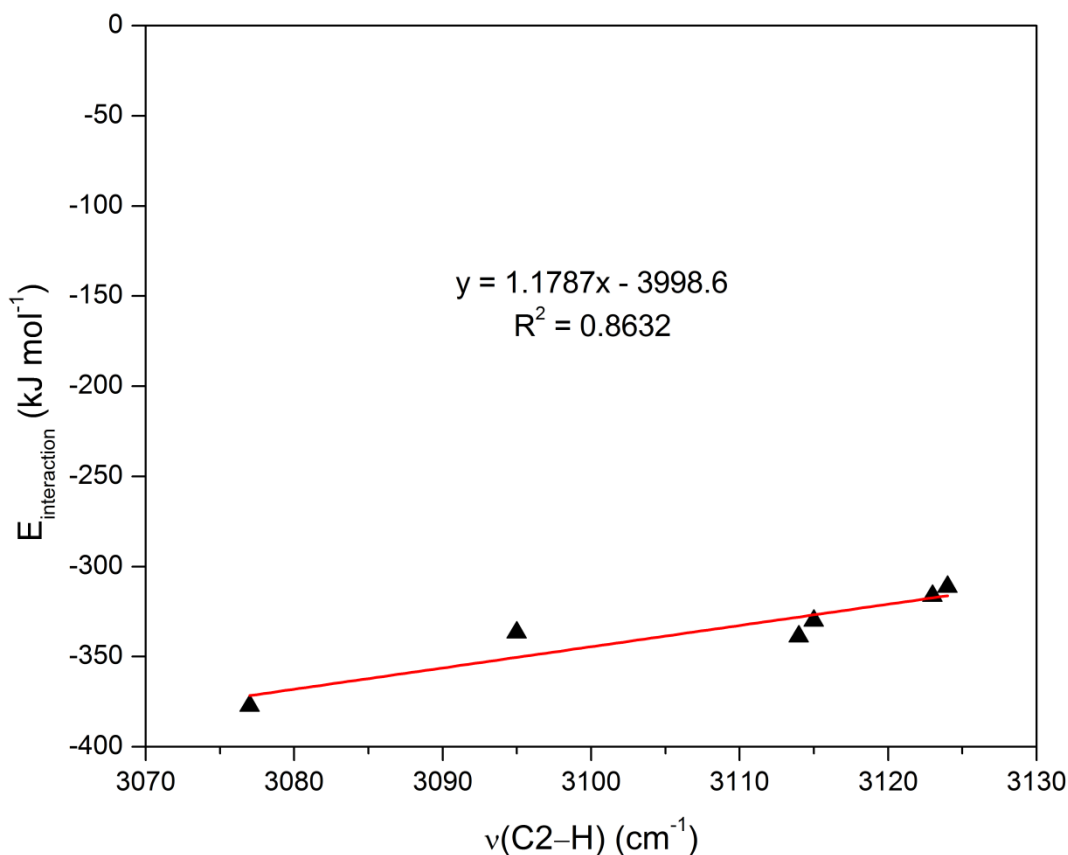


Figure 6.8: Relationship between experimental $\nu(\text{C2-H})$ and interaction energies between cation and anion of corresponding ILs.

In addition, the same regression analysis was performed using experimental C4,5-H stretching frequencies to check if there exists any correlation between C4,5-H stretching frequencies and corresponding interaction energies. As illustrated in Figure 6.9, the R^2 value of 0.4837 confirms that a direct correlation between C4,5-H stretching frequencies

and cation-anion interaction energies cannot be achieved. Considering the location of C4,5-H on [BMIM] cation (Figure 6.1), this result is consistent with the premise that there is no direct interaction between anions and C4,5-H. DFT calculations also suggest that it is energetically not favorable for the anions to be located near C4,5-H as it yielded the highest energy conformers for all the ILs studied here.

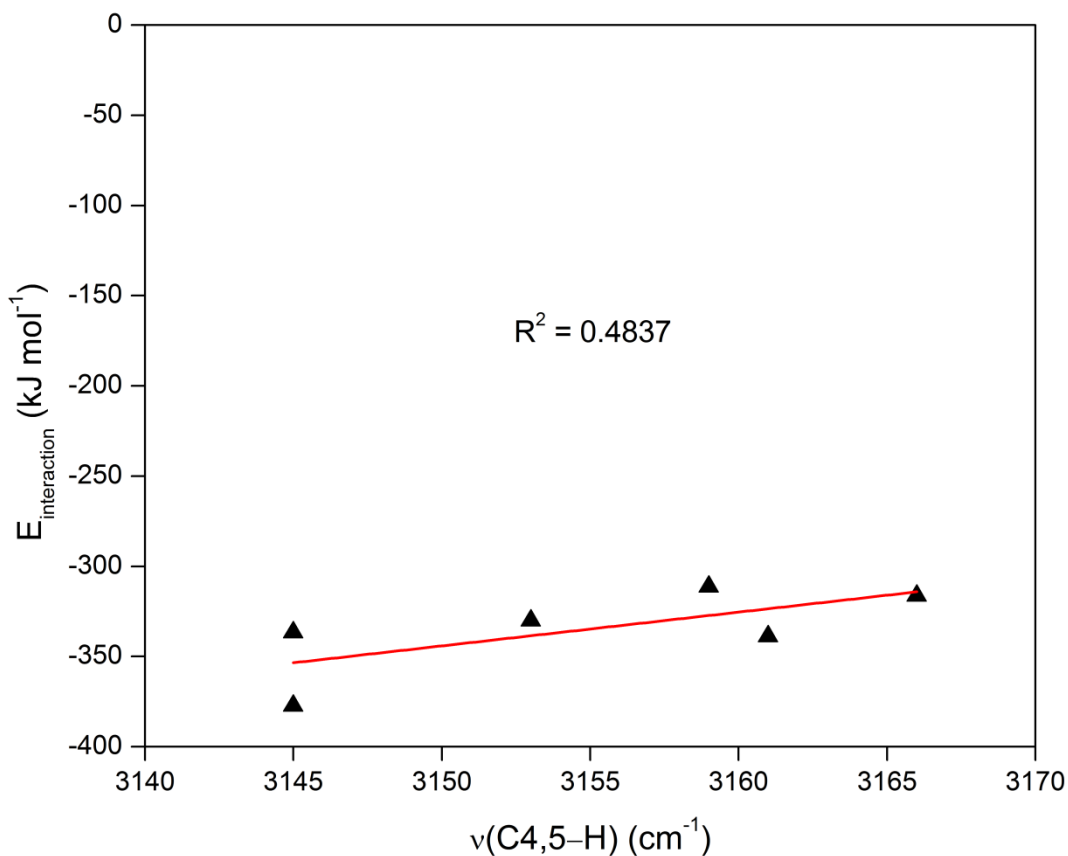


Figure 6.9: Relationship between experimental $\nu(\text{C4,5-H})$ and interaction energies between cation and anion of corresponding ILs.

Chapter 7

CONCLUSIONS AND OUTLOOK

There has been a great attention towards ionic liquids especially in the last decade because of their prominent characteristics, such as extremely low volatility, low melting point, high solvating ability and high thermal stability. Hence, they are considered as green solvents and potential replacement for conventional volatile organic compounds (VOCs).

SCILL and SILP concepts have been developed to exploit their enhanced catalytic performance and tunable selectivity towards desired products. However, thermal stability of ILs determines the upper operating limits for many of IL-integrated processes. Besides, thermal stability limits of bulk ILs are not applicable to the systems where ILs are immobilized on supports. Their thermal stability limits usually decrease on support surfaces because of pronounced tandem interactions among them.

In the first part of this study, thermogravimetric analysis of nine different phosphonium ILs was performed to determine their short-term thermal stability limits. The variation in thermal stability limits of different ILs were analyzed based on DFT calculated ^1H NMR chemical shifts of individual protons on individual alkyl groups of phosphonium cation. Results reveal for the first time a relationship between electron density of individual protons on the tetraalkylphosphonium ILs and their corresponding thermal stability limits. Accordingly, electron density on terminal protons of the alkyl group closest to the anion

controls intrinsically the thermal stability limits of these ILs. Based on these results, a decomposition mechanism involving nucleophilic attack of the anion at the α -carbon of this specific alkyl chain was postulated. These results can be utilized for rational design of phosphonium ILs with superior thermal stability for a wider range of applications by tuning the structures to increase electron density allocated for the bonding between central P atom and its substituents.

Subsequently, the thermogravimetric analysis was also conducted to determine structural parameters controlling the thermal stability limits of phosphonium ILs supported on SiO₂, γ -Al₂O₃, and MgO. Results reveal that thermal stability limits of corresponding ILs deviate highly from bulk thermal stability limits when they are confined on supports, especially on MgO. Furthermore, size of IL, electronegativity of anion, and aromatic ring addition in anion are some of the structural parameters dominating the thermal stability limits. The effect of support on relevant thermal stability limits of ILs is more apparent on MgO. These results can be also used to select a more robust phosphonium IL for supported IL processes, which can withstand the high operating temperatures.

Finally, interaction energies between anions and cations of imidazolium ILs were estimated using experimental C2–H stretching frequencies. Results show that there is a linear correlation between interaction energies and C2–H stretching frequencies. The interaction energy decreases with decreasing C2–H stretching frequency. This linear correlation can be used to estimate the interaction energies between cation and anion of imidazolium ILs bearing the C2–H acidic proton in their structures. These results serve as a valuable tool to relate the estimated interaction energies with their corresponding physicochemical and thermochemical properties, hence rationally design advanced ILs. This information will be a valuable tool in understanding structure-performance relationships in IL-assisted supported metal catalysts. The catalytic performance is directly related to how ILs interact with the active sites. Knowing the changes in interionic

interaction energies can help to correlate the variations in catalytic performance to the IL structure.

Furthermore, results presented in this study will be the basis for future studies to be conducted in our research group. For instance, thermal stability limits of metal-oxide supported phosphonium ILs reported in this study will serve as database in selecting ILs that can sustain their activity at the target reaction temperatures for SCILL and SILP involving catalytic reactions.

For future work, thermal decomposition products of phosphonium ILs on metal oxide supports will be elucidated by mass spectroscopy to postulate a general thermal decomposition mechanism on supports. Additionally, the validity of DFT-calculated ^1H NMR shift values will be confirmed by that of experimental values. Besides, thermal stability limits reported here reflect only short-term limits as they were measured by quick heating measurements. However, it is required to determine long-term stability limits for ILs. Thus, we will determine long-term limits for bulk and metal-oxide supported phosphonium ILs as a part of ongoing project. For this purpose isothermal treatment studies will be conducted.

Moreover, as a suggestion to further extend this study, the effect of metal active sites on stability limits of corresponding IL should be investigated. This information is crucial for SCILL and SILP catalytic concepts. Heat and mass transfer limitations, as well as reaction mechanisms in these IL-assisted catalyst systems should be studied in detail. Thermal stability limits of IL mixtures (i.e., from the same family and/or incorporating ILs from different families) and their potential applications in supported catalytic systems would be an interesting and challenging research topic.

BIBLIOGRAPHY

- [1] P. Wasserscheid, T. Welton, *Ionic Liquids in Synthesis*, Wiley-VCH, Weinheim, (2008).
- [2] C.P. Mehnert, R.A. Cook, N.C. Dispenziere, M. Afeworki, Supported Ionic Liquid Catalysis - a New Concept for Homogeneous Hydroformylation Catalysis, *J. Am. Chem. Soc.*, 124 (2002), 12932-12933.
- [3] U. Kernchen, B. Etzold, W. Korth, A. Jess, Solid Catalyst with Ionic Liquid Layer (SCILL) – a New Concept to Improve Selectivity Illustrated by Hydrogenation of Cyclooctadiene, *Chem. Eng. Technol.*, 30 (2007), 985-994.
- [4] R.D. Rogers, K.R. Seddon, Ionic Liquids--Solvents of the Future?, *Science*, 302 (2003), 792-793.
- [5] T. Welton, Room-Temperature Ionic Liquids. Solvents for Synthesis and Catalysis, *Chem. Rev.*, 99 (1999), 2071-2084.
- [6] K. R. Seddon, in S. Boghosian, V. Dracopoulos, C. G. Kontoyannis, and G. A. Voyiatzis, eds., *The International George Papatheodorou Symposium, Institute of Chemical Engineering and High Temperature Chemical Processes, Patras*, (1999), 131–135.
- [7] B. Kirchner, *Ionic Liquids, Topics in Current Chemistry*, 290, Springer-Verlag, Heidelberg (2009).
- [8] N.V. Plechkova, K.R. Seddon, Applications of Ionic Liquids in the Chemical Industry, *Chem. Soc. Rev.*, 37 (2008), 123-150.
- [9] M. Freemantle, Designer Solvents, *Chem. Eng. News*, 76 (1998), 32-37.
- [10] R. Giernoth, Task-Specific Ionic Liquids, *Angew. Chem. Int. Ed.*, 49 (2010), 2834-2839.

-
- [11] H. Ohno, *Electrochemical Aspects of Ionic Liquids*, John Wiley & Sons, Inc., Hoboken, New Jersey, (2011).
- [12] A. Berthod, M.J. Ruiz-Angel, S. Carda-Broch, *Ionic Liquids in Separation Techniques*, *J. Chromatogr. A*, 1184 (2008), 6-18.
- [13] J.P. Hallett, T. Welton, *Room-Temperature Ionic Liquids: Solvents for Synthesis and Catalysis*. 2, *Chem. Rev.*, 111 (2011), 3508-3576.
- [14] P. Wasserscheid, *Chemistry: Volatile Times for Ionic Liquids*, *Nature*, 439 (2006), 797.
- [15] M.J. Earle, J.M.S.S. Esperanca, M.A. Gilea, J.N. Canongia Lopes, L.P.N. Rebelo, J.W. Magee, K.R. Seddon, J.A. Widegren, *The Distillation and Volatility of Ionic Liquids*, *Nature*, 439 (2006), 831-834.
- [16] S. Zhang, X. Lu, Q. Zhou, X. Li, X. Zhang, S. Li, *Ionic Liquids: Physicochemical Properties*, Elsevier, Amsterdam (2009).
- [17] I. Krossing, J.M. Slattery, C. Daguene, P.J. Dyson, A. Oleinikova, H. Weingartner, *Why Are Ionic Liquids Liquid? A Simple Explanation Based on Lattice and Solvation Energies*, *J. Am. Chem. Soc.*, 128 (2006), 13427-13434.
- [18] S. Zahn, F. Uhlig, J. Thar, C. Spickermann, B. Kirchner, *Intermolecular Forces in an Ionic Liquid ([MMIM][Cl]) Versus Those in a Typical Salt (NaCl)*, *Angew. Chem. Int. Ed.*, 47 (2008), 3639-3641.
- [19] K. Dong, S. Zhang, D. Wang, X. Yao, *Hydrogen Bonds in Imidazolium Ionic Liquids*, *J. Phys. Chem. A*, 110 (2006), 9775-9782.
- [20] V.I. Parvulescu, C. Hardacre, *Catalysis in Ionic Liquids*, *Chem. Rev.*, 107 (2007), 2615-2665.
- [21] R. Knapp, A. Jentys, J.A. Lercher, *Impact of Supported Ionic Liquids on Supported Pt Catalysts*, *Green Chem.*, 11 (2009), 656-661.

- [22] J. Arras, M. Steffan, Y. Shayeghi, P. Claus, The Promoting Effect of a Dicyanamide Based Ionic Liquid in the Selective Hydrogenation of Citral, *Chem. Commun.*, 0 (2008), 4058-4060.
- [23] C. Maton, N. De Vos, C.V. Stevens, Ionic Liquid Thermal Stabilities: Decomposition Mechanisms and Analysis Tools, *Chem. Soc. Rev.*, 42 (2013), 5963-5977.
- [24] C.P. Fredlake, J.M. Crosthwaite, D.G. Hert, S.N.V.K. Aki, J.F. Brennecke, Thermophysical Properties of Imidazolium-Based Ionic Liquids, *J. Chem. Eng. Data*, 49 (2004), 954-964.
- [25] M. Kosmulski, J. Gustafsson, J.B. Rosenholm, Thermal Stability of Low Temperature Ionic Liquids Revisited, *Thermochim. Acta*, 412 (2004), 47-53.
- [26] H.L. Ngo, K. LeCompte, L. Hargens, A.B. McEwen, Thermal Properties of Imidazolium Ionic Liquids, *Thermochim. Acta*, 357 (2000), 97-102.
- [27] W.H. Awad, J.W. Gilman, M. Nyden, R.H. Harris, T.E. Sutto, J. Callahan, P.C. Trulove, H.C. DeLong, D.M. Fox, Thermal Degradation Studies of Alkyl-Imidazolium Salts and Their Application in Nanocomposites, *Thermochim. Acta*, 409 (2004), 3-11.
- [28] K. Tsunashima, S. Kodama, M. Sugiya, Y. Kunugi, Physical and Electrochemical Properties of Room-Temperature Dicyanamide Ionic Liquids Based on Quaternary Phosphonium Cations, *Electrochim. Acta*, 56 (2010), 762-766.
- [29] A.F. Ferreira, P.N. Simões, A.G.M. Ferreira, Quaternary Phosphonium-Based Ionic Liquids: Thermal Stability and Heat Capacity of the Liquid Phase, *J. Chem. Thermodyn.*, 45 (2012), 16-27.
- [30] G. Adamová, R.L. Gardas, L.P. Rebelo, A.J. Robertson, K.R. Seddon, Alkyltrioctylphosphonium Chloride Ionic Liquids: Synthesis and Physicochemical Properties, *Dalton Trans.*, 40 (2011), 12750-12764.

- [31] J. Lemus, J. Palomar, M.A. Gilarranz, J.J. Rodriguez, Characterization of Supported Ionic Liquid Phase (SILP) Materials Prepared from Different Supports, *Adsorption*, 17 (2011), 561-571.
- [32] M.P. Singh, R.K. Singh, S. Chandra, Thermal Stability of Ionic Liquid in Confined Geometry, *J. Phys. D: Appl. Phys.*, 43 (2010), 092001-092005.
- [33] M.T. Clough, K. Geyer, P.A. Hunt, J. Mertes, T. Welton, Thermal Decomposition of Carboxylate Ionic Liquids: Trends and Mechanisms, *Phys. Chem. Chem. Phys.*, 15 (2013), 20480-20495.
- [34] A. Akçay, V. Balci, A. Uzun, Structural Factors Controlling Thermal Stability of Imidazolium Ionic Liquids with 1-*n*-Butyl-3-Methylimidazolium Cation on γ -Al₂O₃, *Thermochim. Acta*, 589 (2014), 131-136.
- [35] National Institute of Standards and Technology (NIST) Chemistry WebBook, <http://webbook.nist.gov/chemistry/>.
- [36] M. J. Frisch, G. W. Trucks, H. B. Schlegel, G. E. Scuseria, M. A. Robb, J. R. Cheeseman, G. Scalmani, V. Barone, B. Mennucci, G. A. Petersson, H. Nakatsuji, M. Caricato, X. Li, H. P. Hratchian, A. F. Izmaylov, J. Bloino, G. Zheng, J. L. Sonnenberg, M. Hada, M. Ehara, K. Toyota, R. Fukuda, J. Hasegawa, M. Ishida, T. Nakajima, Y. Honda, O. Kitao, H. Nakai, T. Vreven, J. A. Montgomery, Jr., J. E. Peralta, F. Ogliaro, M. Bearpark, J. J. Heyd, E. Brothers, K. N. Kudin, V. N. Staroverov, T. Keith, R. Kobayashi, J. Normand, K. Raghavachari, A. Rendell, J. C. Burant, S. S. Iyengar, J. Tomasi, M. Cossi, N. Rega, J. M. Millam, M. Klene, J. E. Knox, J. B. Cross, V. Bakken, C. Adamo, J. Jaramillo, R. Gomperts, R. E. Stratmann, O. Yazyev, A. J. Austin, R. Cammi, C. Pomelli, J. W. Ochterski, R. L. Martin, K. Morokuma, V. G. Zakrzewski, G. A. Voth, P. Salvador, J. J. Dannenberg, S. Dapprich, A. D. Daniels, O. Farkas, J. B. Foresman, J. V. Ortiz, J. Cioslowski and D. J. Fox, *Gaussian 09, Revision D.01*, Gaussian, Inc., Wallingford, CT, 2013.

-
- [37] A.D. Becke, Density-Functional Thermochemistry. III. The Role of Exact Exchange, *J. Chem. Phys.*, 98 (1993), 5648.
- [38] C.T. Lee, W.T. Yang, R.G. Parr, Development of the Colle-Salvetti Correlation-Energy Formula into a Functional of the Electron-Density, *Phys. Rev. B*, 37 (1988), 785-789.
- [39] R. Ditchfield, Self-Consistent Perturbation Theory of Diamagnetism, *Mol. Phys.*, 27 (1974), 789-807.
- [40] E.I. Izgorodina, U.L. Bernard, D.R. MacFarlane, Ion-Pair Binding Energies of Ionic Liquids: Can DFT Compete with Ab Initio-Based Methods?, *J. Phys. Chem. A*, 113 (2009), 7064-7072.
- [41] J.P. Merrick, D. Moran, L. Radom, An Evaluation of Harmonic Vibrational Frequency Scale Factors, *J. Phys. Chem. A*, 111 (2007), 11683-11700.
- [42] J.D. Holbrey, K.R. Seddon, Ionic Liquids, *Clean Prod. Process.*, 1 (1999), 223-236.
- [43] D.R. MacFarlane, N. Tachikawa, M. Forsyth, J.M. Pringle, P.C. Howlett, G.D. Elliott, J.H. Davis, M. Watanabe, P. Simon, C.A. Angell, Energy Applications of Ionic Liquids, *Energy Environ. Sci.*, 7 (2014), 232.
- [44] C.J. Bradaric, A. Downard, C. Kennedy, A.J. Robertson, Y. Zhou, Industrial Preparation of Phosphonium Ionic Liquids, *Green Chem.*, 5 (2003), 143-152.
- [45] K.J. Fraser, D.R. MacFarlane, Phosphonium-Based Ionic Liquids: An Overview, *Aust. J. Chem.*, 62 (2009), 309-321.
- [46] R.E. Del Sesto, C. Corley, A. Robertson, J.S. Wilkes, Tetraalkylphosphonium-Based Ionic Liquids, *J. Organomet. Chem.*, 690 (2005), 2536-2542.
- [47] T. Ramnial, D.D. Ino, J.A. Clyburne, Phosphonium Ionic Liquids as Reaction Media for Strong Bases, *Chem. Commun.*, (2005), 325-327.

- [48] L.S. Ott, M.L. Cline, M. Deetlefs, K.R. Seddon, R.G. Finke, Nanoclusters in Ionic Liquids: Evidence for *N*-Heterocyclic Carbene Formation from Imidazolium-Based Ionic Liquids Detected by ^2H NMR, *J. Am. Chem. Soc.*, 127 (2005), 5758-5759.
- [49] J.S. Luo, O. Conrad, I.F.J. Vankelecom, Physicochemical Properties of Phosphonium-Based and Ammonium-Based Protic Ionic Liquids, *J. Mater. Chem.*, 22 (2012), 20574-20579.
- [50] Y. Cao, T. Mu, Comprehensive Investigation on the Thermal Stability of 66 Ionic Liquids by Thermogravimetric Analysis, *Ind. Eng. Chem. Res.*, 53 (2014), 8651-8664.
- [51] T. Erdmenger, J. Vitz, F. Wiesbrock, U.S. Schubert, Influence of Different Branched Alkyl Side Chains on the Properties of Imidazolium-Based Ionic Liquids, *J. Mater. Chem.*, 18 (2008), 5267.
- [52] A. Wulf, K. Fumino, D. Michalik, R. Ludwig, IR and NMR Properties of Ionic Liquids: Do They Tell Us the Same Thing?, *ChemPhysChem*, 8 (2007), 2265-2269.
- [53] H.B. Schlegel, Geometry Optimization on Potential Energy Surfaces, in: *Modern Electronic Structure Theory*, 459-500, World Scientific, Singapore (1995).
- [54] Dwan, D. Durant, K. Ghandi, Nuclear Magnetic Resonance Spectroscopic Studies of the Trihexyl (Tetradecyl) Phosphonium Chloride Ionic Liquid Mixtures with Water, *Cent. Eur. J. Chem.*, 6 (2008), 347-358.
- [55] K.J. Fraser, E.I. Izgorodina, M. Forsyth, J.L. Scott, D.R. MacFarlane, Liquids Intermediate between “Molecular” and “Ionic” Liquids: Liquid Ion Pairs?, *Chem. Commun.*, (2007), 3817-3819.
- [56] M.G. Benavides-Garcia, M. Monroe, Molecular Models and IR Spectra of Asymmetric Tetraalkyl Phosphonium Iodide Ionic Liquids, *Chem. Phys. Lett.*, 479 (2009), 238-243.

- [57] D.R. MacFarlane, M. Forsyth, E.I. Izgorodina, A.P. Abbott, G. Annat, K. Fraser, On the Concept of Ionicity in Ionic Liquids, *Phys. Chem. Chem. Phys.*, 11 (2009), 4962-4967.
- [58] R.P. Morco, A.Y. Musa, J.C. Wren, The Molecular Structures and the Relationships between the Calculated Molecular and Observed Bulk Phase Properties of Phosphonium-Based Ionic Liquids, *Solid State Ionics*, 258 (2014), 74-81.
- [59] D.J. Abdallah, R.E. Bachman, J. Perlstein, R.G. Weiss, Crystal Structures of Symmetrical *Tetra-n*-Alkyl Ammonium and Phosphonium Halides. Dissection of Competing Interactions Leading to “Biradial” and “Tetradial” Shapes, *J. Phys. Chem. B*, 103 (1999), 9269-9278.
- [60] A. Bagno, F. D'Amico, G. Saielli, Computing the ^1H NMR Spectrum of a Bulk Ionic Liquid from Snapshots of Car-Parrinello Molecular Dynamics Simulations, *ChemPhysChem*, 8 (2007), 873-881.
- [61] T. Cremer, C. Kolbeck, K.R. Lovelock, N. Paape, R. Wolfel, P.S. Schulz, P. Wasserscheid, H. Weber, J. Thar, B. Kirchner, F. Maier, H.P. Steinruck, Towards a Molecular Understanding of Cation-Anion Interactions--Probing the Electronic Structure of Imidazolium Ionic Liquids by NMR Spectroscopy, X-Ray Photoelectron Spectroscopy and Theoretical Calculations, *Chem.–Eur. J.*, 16 (2010), 9018-9033.
- [62] A. Cieniecka-Rosłonkiewicz, J. Pernak, J. Kubis-Feder, A. Ramani, A.J. Robertson, K.R. Seddon, Synthesis, Anti-Microbial Activities and Anti-Electrostatic Properties of Phosphonium-Based Ionic Liquids, *Green Chem.*, 7 (2005), 855-862.
- [63] D.M. Fox, W.H. Awad, J.W. Gilman, P.H. Maupin, H.C. De Long, P.C. Trulove, Flammability, Thermal Stability, and Phase Change Characteristics of Several Trialkylimidazolium Salts, *Green Chem.*, 5 (2003), 724-727.

- [64] F. Heym, B.J. Etzold, C. Kern, A. Jess, An Improved Method to Measure the Rate of Vaporisation and Thermal Decomposition of High Boiling Organic and Ionic Liquids by Thermogravimetric Analysis, *Phys. Chem. Chem. Phys.*, 12 (2010), 12089-12100.
- [65] P.G. Rickert, M.R. Antonio, M.A. Firestone, K.A. Kubatko, T. Szreder, J.F. Wishart, M.L. Dietz, Tetraalkylphosphonium Polyoxometalates: Electroactive, "Task-Specific" Ionic Liquids, *Dalton Trans.*, (2007), 529-531.
- [66] A.M. Dias, S. Marceneiro, M.E. Braga, J.F. Coelho, A.G. Ferreira, P.N. Simões, H.I. Veiga, L.C. Tomé, I.M. Marrucho, J.M. Esperança, A.A. Matias, C.M. Duarte, L.P. Rebelo, H.C. de Sousa, Phosphonium-Based Ionic Liquids as Modifiers for Biomedical Grade Poly(Vinyl Chloride), *Acta Biomater.*, 8 (2012), 1366-1379.
- [67] T.J. Wooster, K.M. Johanson, K.J. Fraser, D.R. MacFarlane, J.L. Scott, Thermal Degradation of Cyano Containing Ionic Liquids, *Green Chem.*, 8 (2006), 691.
- [68] A.L. Allred, Electronegativity Values from Thermochemical Data, *J. Inorg. Nucl. Chem.*, 17 (1961), 215-221.
- [69] M.D. Green, C. Schreiner, T.E. Long, Thermal, Rheological, and Ion-Transport Properties of Phosphonium-Based Ionic Liquids, *J. Phys. Chem. A*, 115 (2011), 13829-13835.
- [70] M.C. Kroon, W. Buijs, C.J. Peters, G.-J. Witkamp, Quantum Chemical Aided Prediction of the Thermal Decomposition Mechanisms and Temperatures of Ionic Liquids, *Thermochim. Acta*, 465 (2007), 40-47.
- [71] W. Xie, R. Xie, W.-P. Pan, D. Hunter, B. Koene, L.-S. Tan, R. Vaia, Thermal Stability of Quaternary Phosphonium Modified Montmorillonites, *Chem. Mater.*, 14 (2002), 4837-4845.
- [72] J.H. Gross, Liquid Injection Field Desorption/Ionization-Mass Spectrometry of Ionic Liquids, *J. Am. Soc. Mass. Spectrom.*, 18 (2007), 2254-2262.

-
- [73] C.G. Cassity, A. Mirjafari, N. Mobarrez, K.J. Strickland, R.A. O'Brien, J.H. Davis, Jr., Ionic Liquids of Superior Thermal Stability, *Chem. Commun.*, 49 (2013), 7590-7592.
- [74] A.M. Fernandes, M.A. Rocha, M.G. Freire, I.M. Marrucho, J.A. Coutinho, L.M. Santos, Evaluation of Cation-Anion Interaction Strength in Ionic Liquids, *J. Phys. Chem. B*, 115 (2011), 4033-4041.
- [75] K. Fumino, R. Ludwig, Analyzing the Interaction Energies between Cation and Anion in Ionic Liquids: The Subtle Balance between Coulomb Forces and Hydrogen Bonding, *J. Mol. Liq.*, 192 (2014), 94-102.
- [76] K. Fumino, A. Wulf, R. Ludwig, The Cation-Anion Interaction in Ionic Liquids Probed by Far-Infrared Spectroscopy, *Angew. Chem. Int. Ed.*, 47 (2008), 3830-3834.
- [77] Y. Gao, L. Zhang, Y. Wang, H. Li, Probing Electron Density of H-Bonding between Cation-Anion of Imidazolium-Based Ionic Liquids with Different Anions by Vibrational Spectroscopy, *J. Phys. Chem. B*, 114 (2010), 2828-2833.
- [78] K. Fumino, T. Peppel, M. Geppert-Rybczynska, D.H. Zaitsau, J.K. Lehmann, S.P. Verevkin, M. Kockerling, R. Ludwig, The Influence of Hydrogen Bonding on the Physical Properties of Ionic Liquids, *Phys. Chem. Chem. Phys.*, 13 (2011), 14064-14075.

APPENDIX

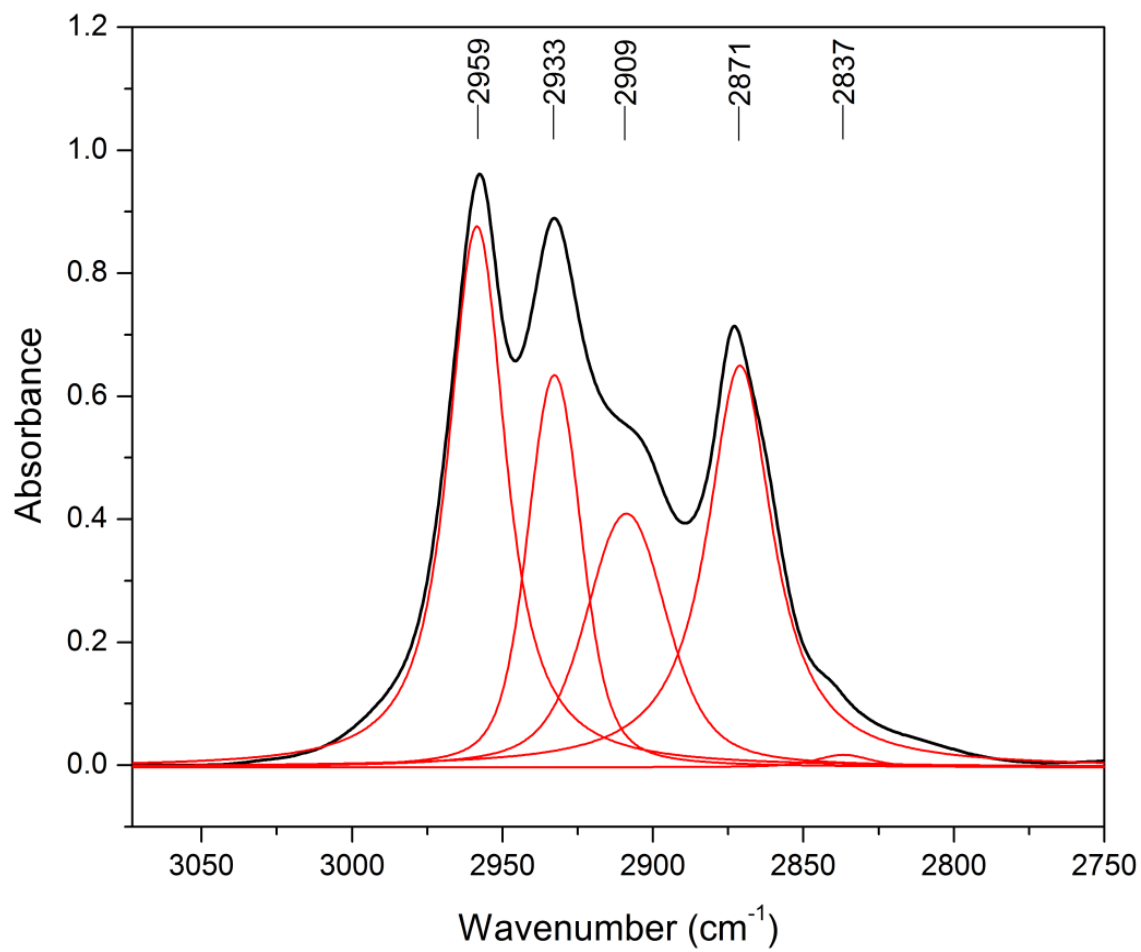


Figure A1: Deconvoluted IR spectrum of [P₄₄₄₁][DBP] in CH stretching region.

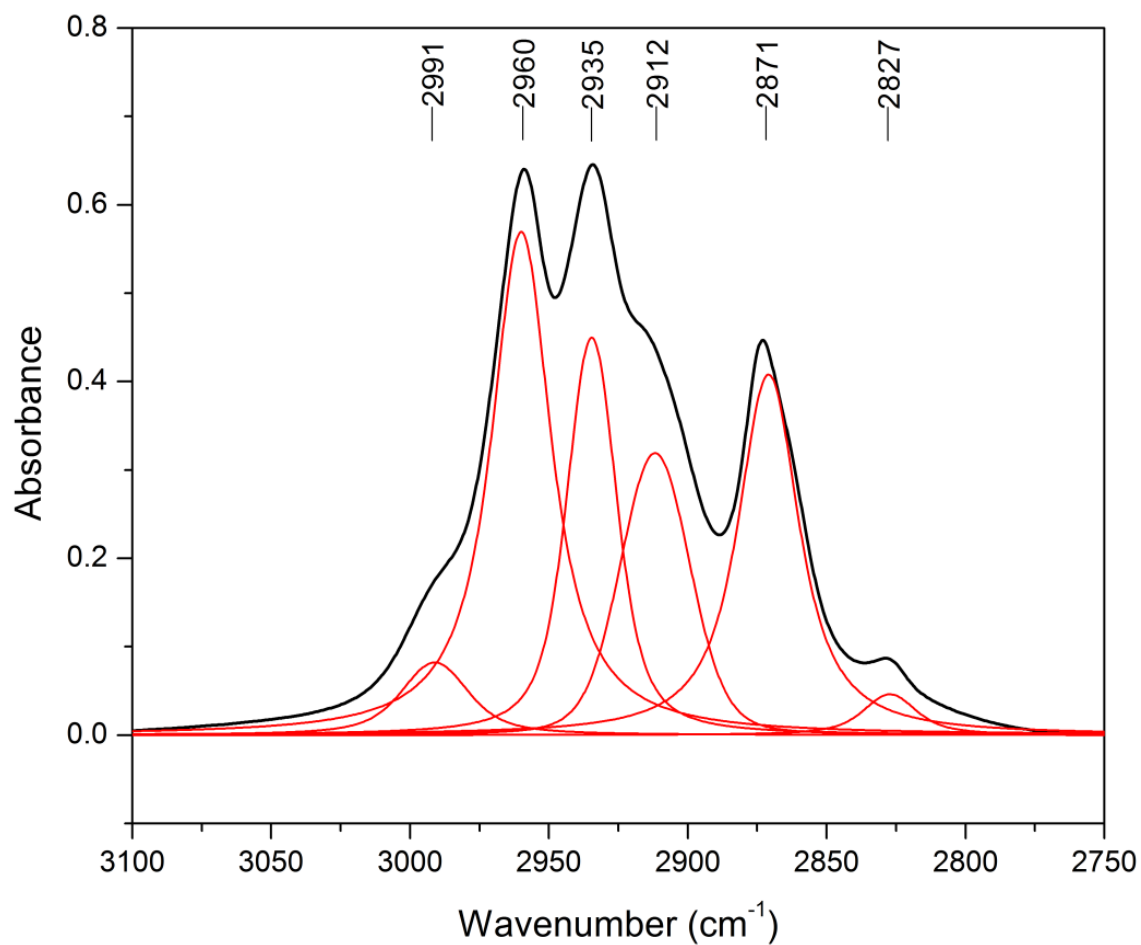


Figure A2: Deconvoluted IR spectrum of [P₄₄₄₁][MeSO₄] in CH stretching region.

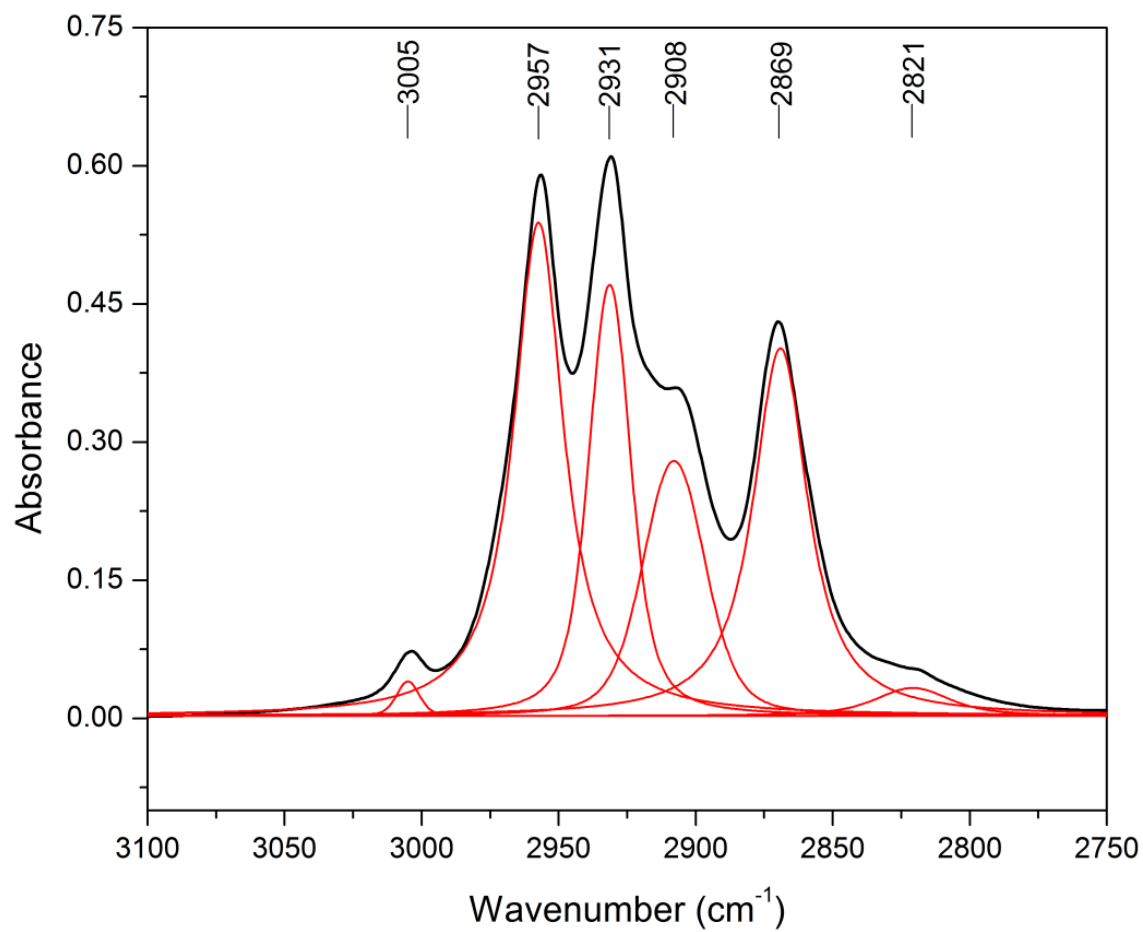


Figure A3: Deconvoluted IR spectrum of [P₄₄₄₄][MeSO₃] in CH stretching region.

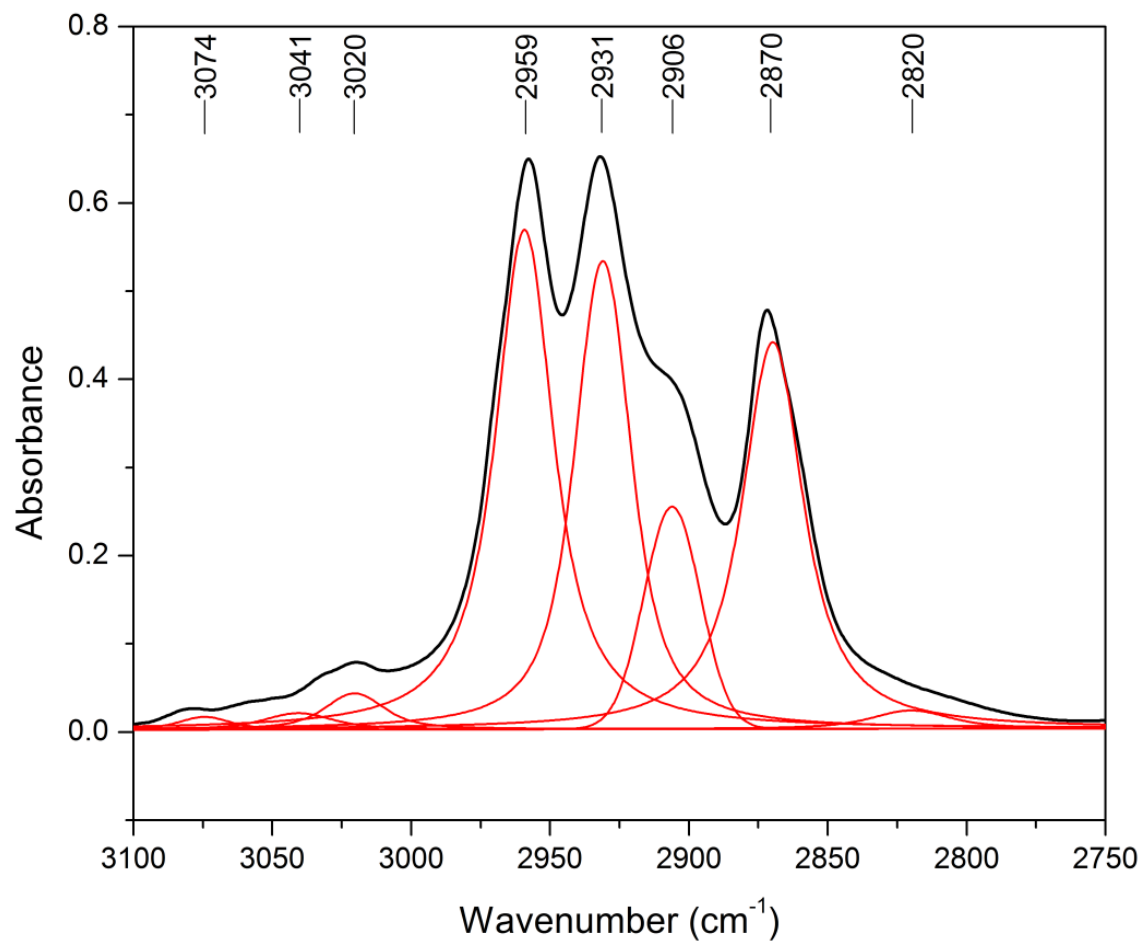


Figure A4: Deconvoluted IR spectrum of [P₄₄₄₄][TOS] in CH stretching region.

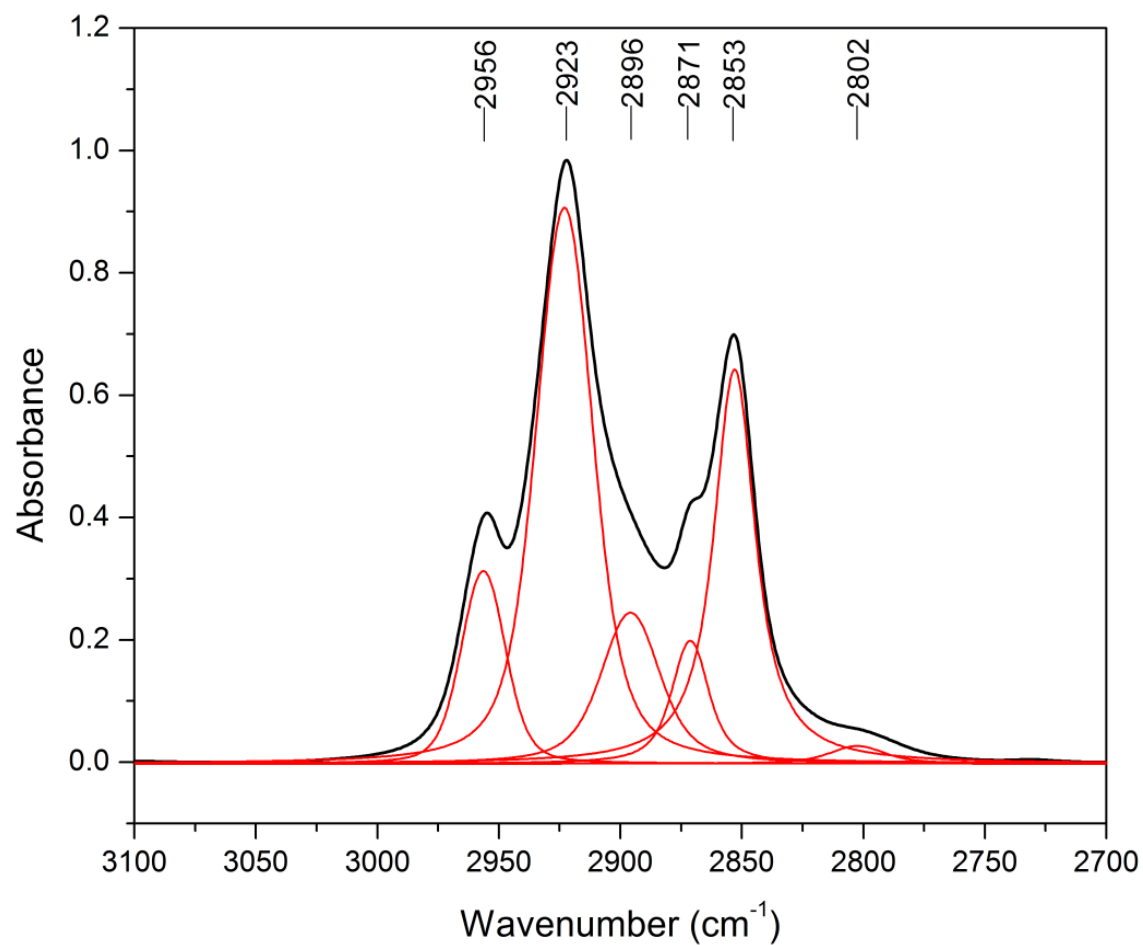


Figure A5: Deconvoluted IR spectrum of [P₆₆₆₍₁₄₎][Br] in CH stretching region.

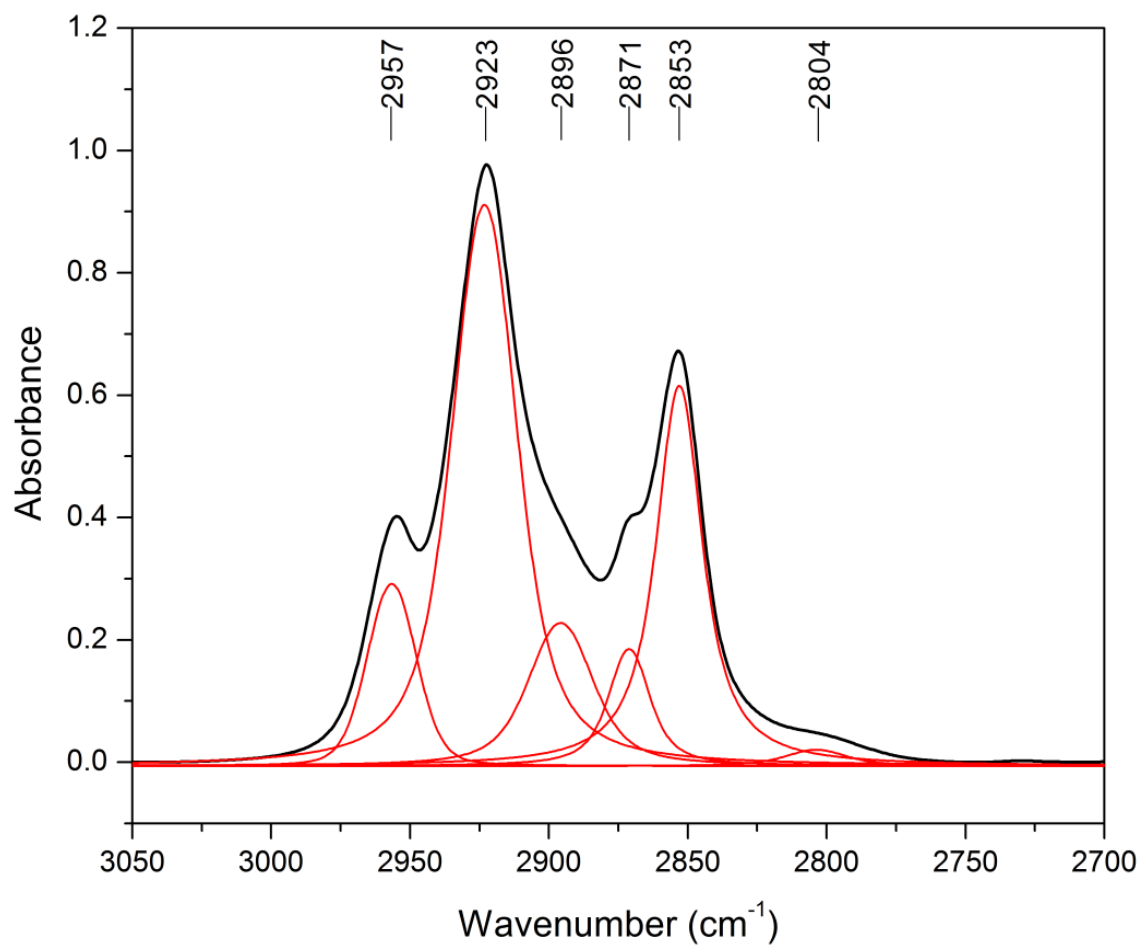


Figure A6: Deconvoluted IR spectrum of [P₆₆₆₍₁₄₎][Cl] in CH stretching region.

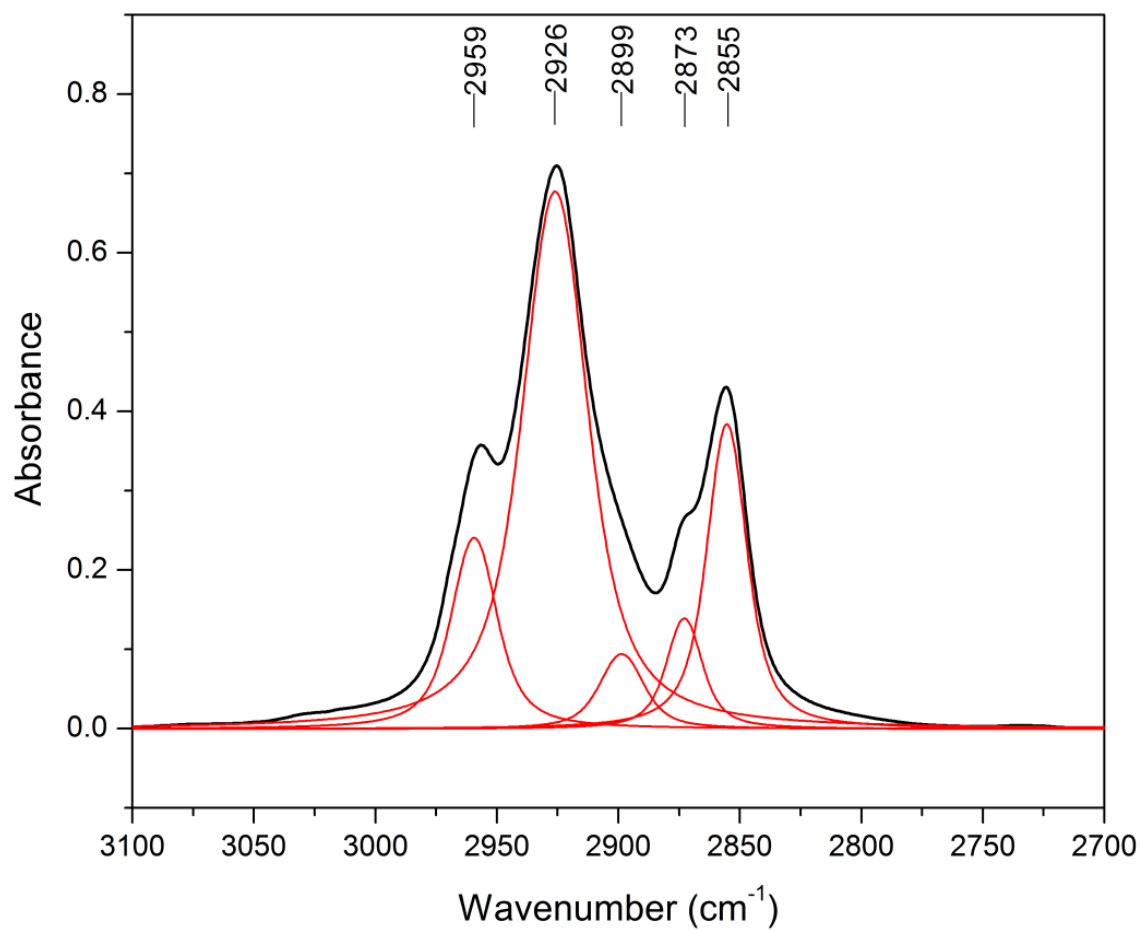


Figure A7: Deconvoluted IR spectrum of $[P_{666(14)}][NTf_2]$ in CH stretching region.

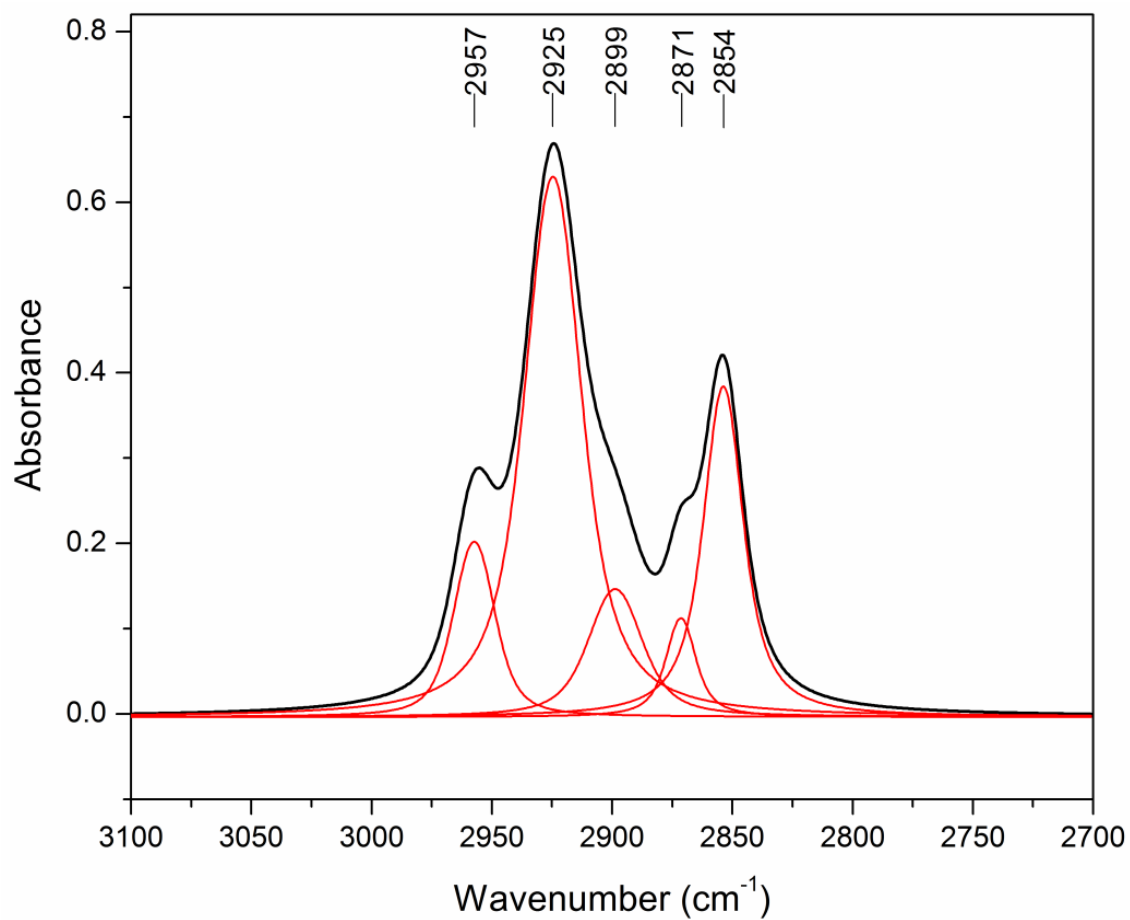


Figure A8: Deconvoluted IR spectrum of [P₆₆₆₍₁₄₎][DCA] in CH stretching region.

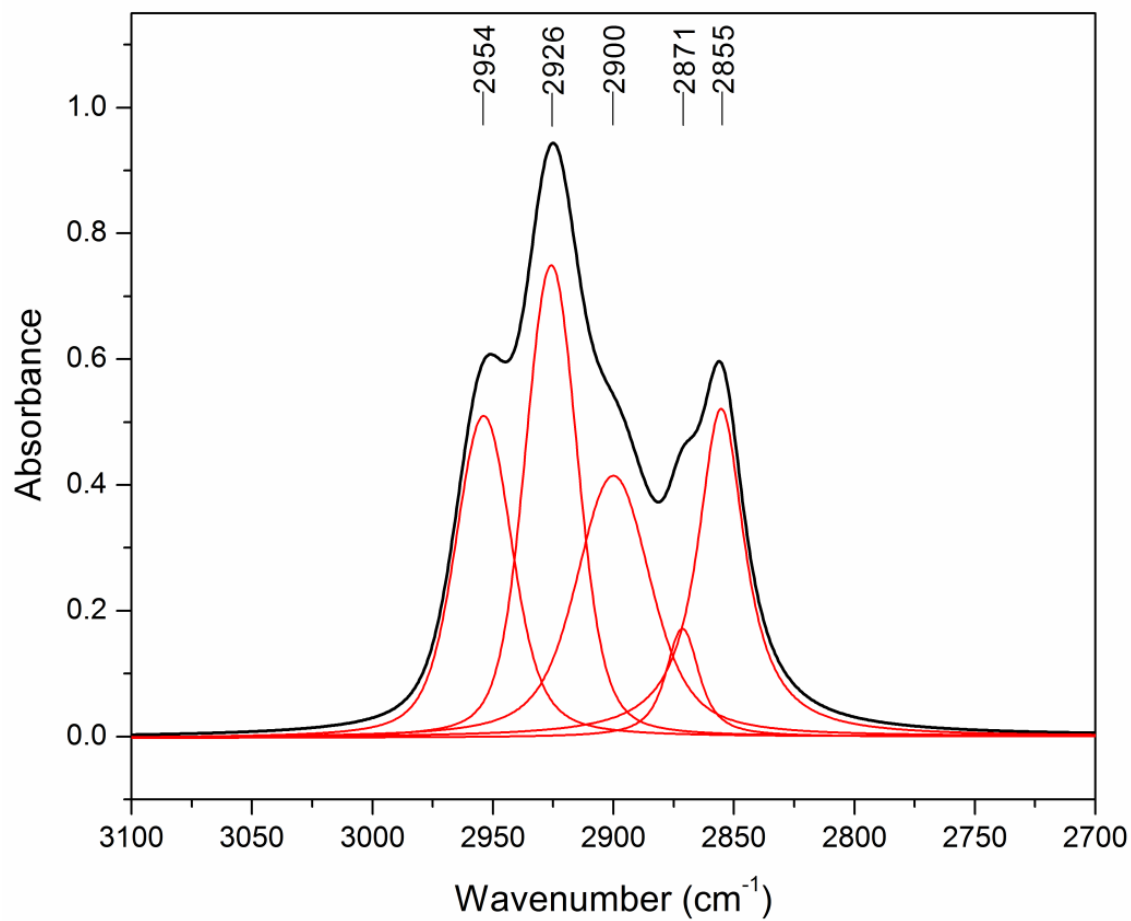


Figure A9: Deconvoluted IR spectrum of [P₆₆₍₁₄₎][TMPP] in CH stretching region.

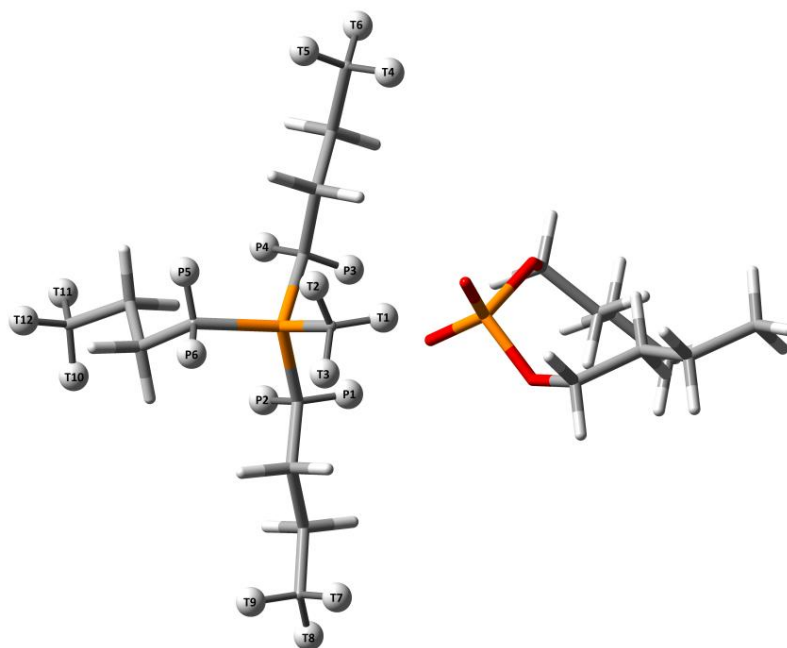


Figure A10: Local minima geometry of $[P_{4441}][DBP]$.

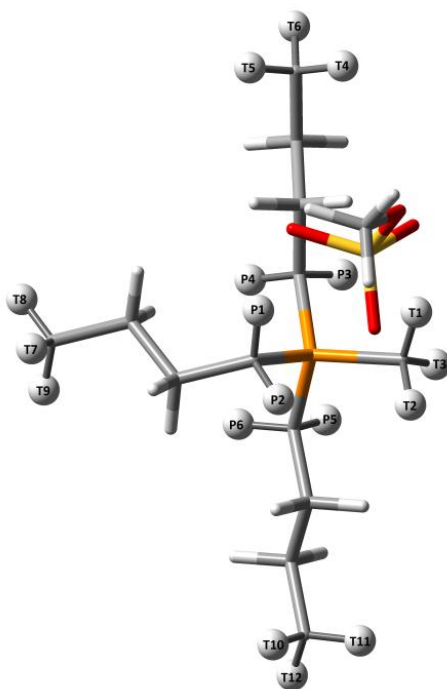


Figure A11: Local minima geometry of $[P_{4441}][MeSO_4]$.

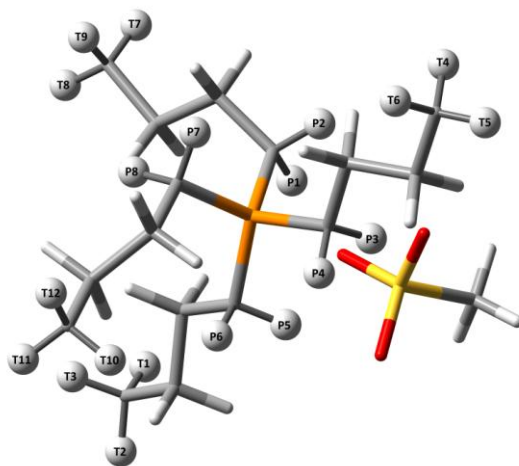


Figure A12: Local minima geometry of $[P_{4444}][MeSO_3]$.

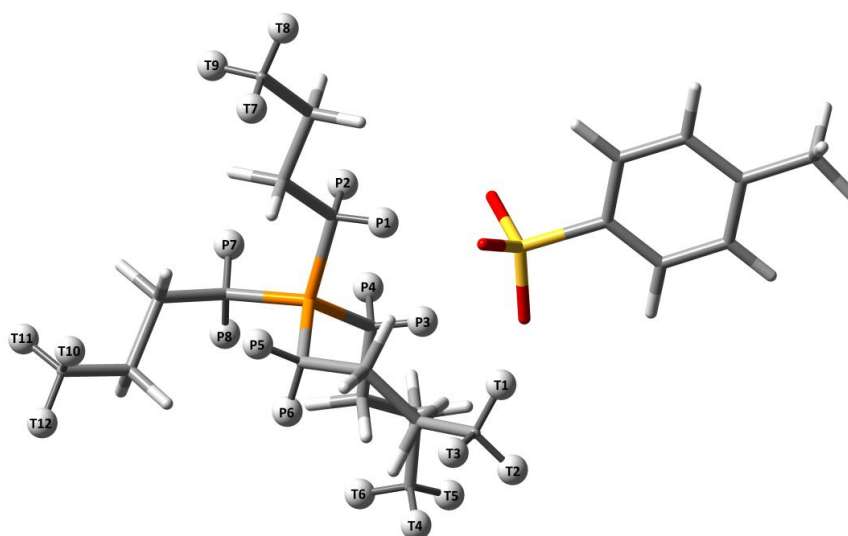


Figure A13: Local minima geometry of [P₄₄₄][TOS].

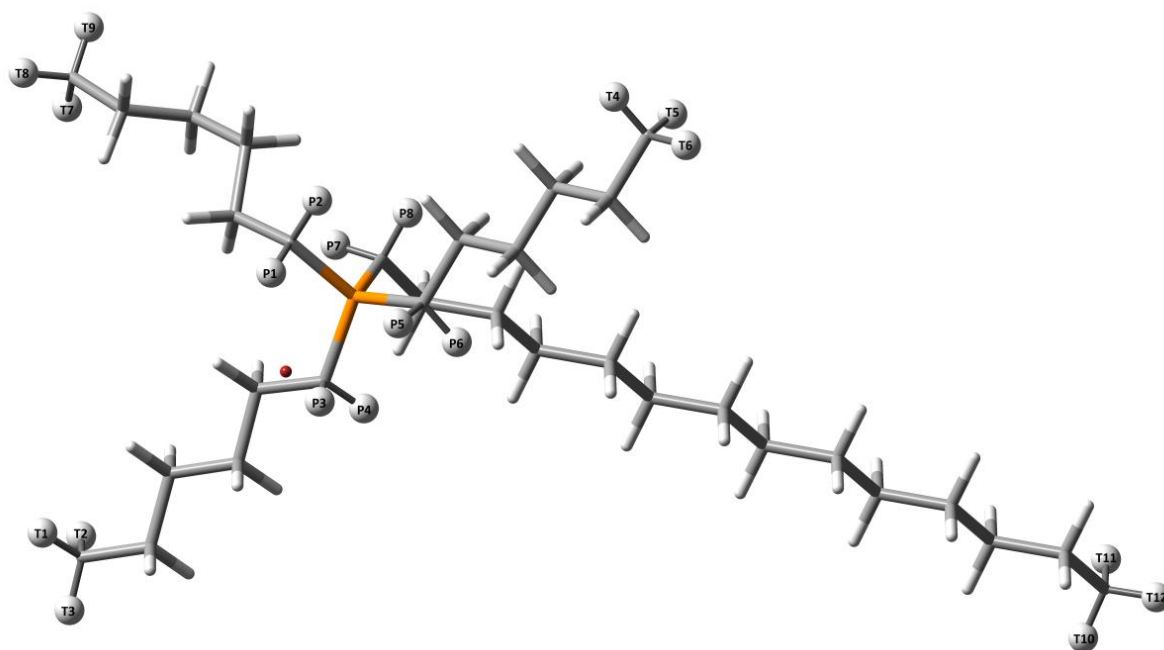


Figure A14: Local minima geometry of [P₆₆₆₍₁₄₎][Br].

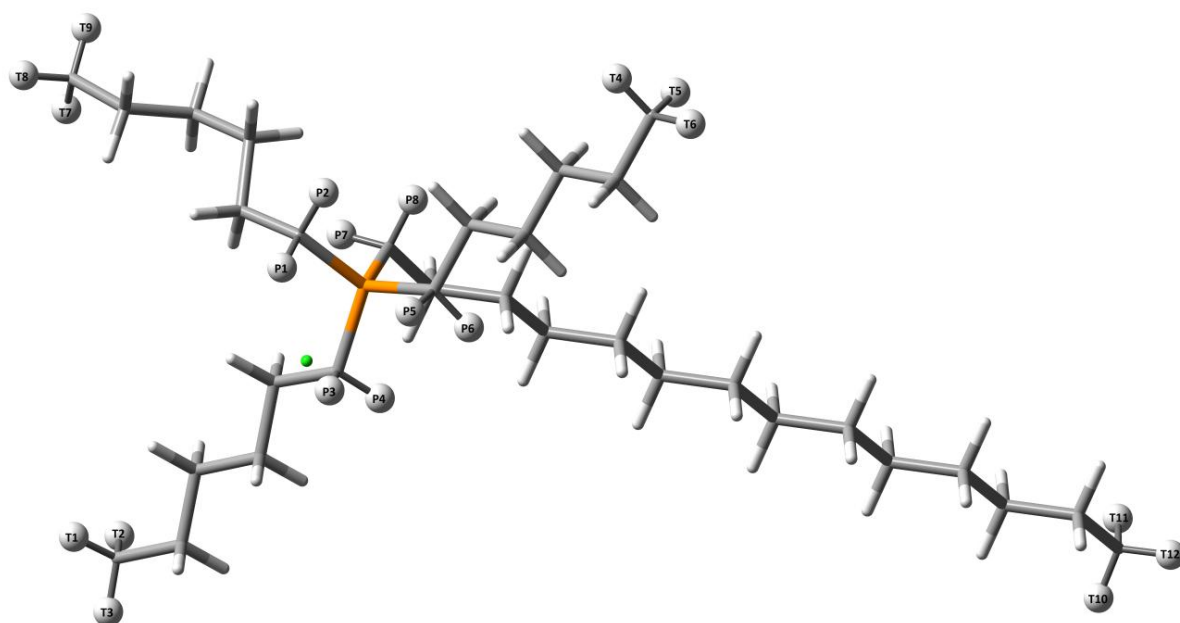


Figure A15: Local minima geometry of $[P_{666(14)}][Cl]$.

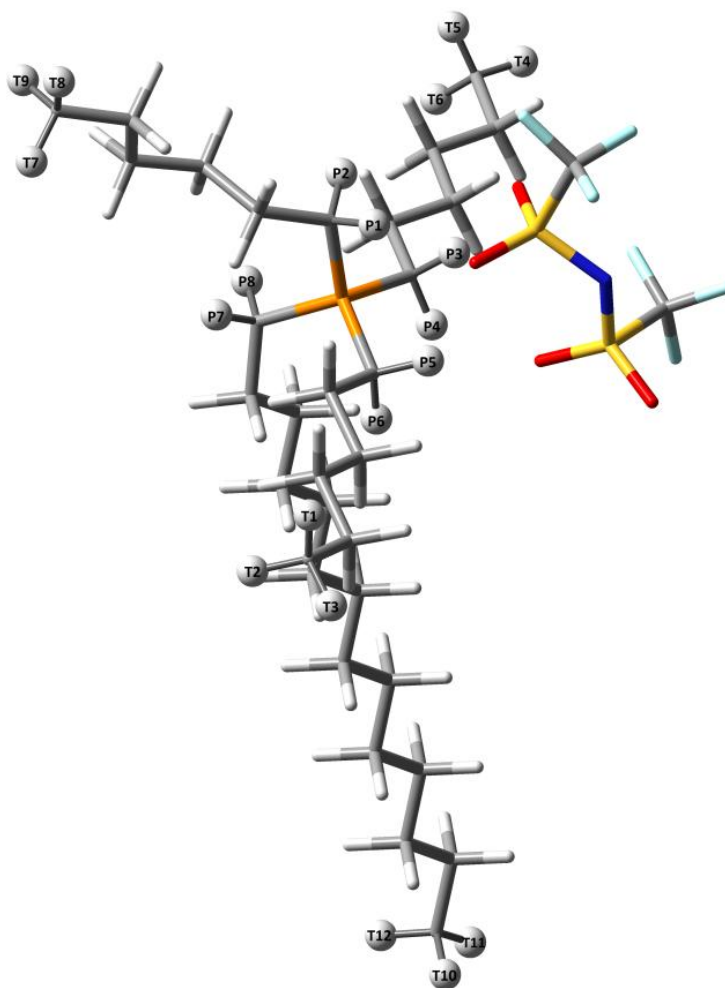


Figure A16: Local minima geometry of $[P_{66(14)}][NTf_2]$.

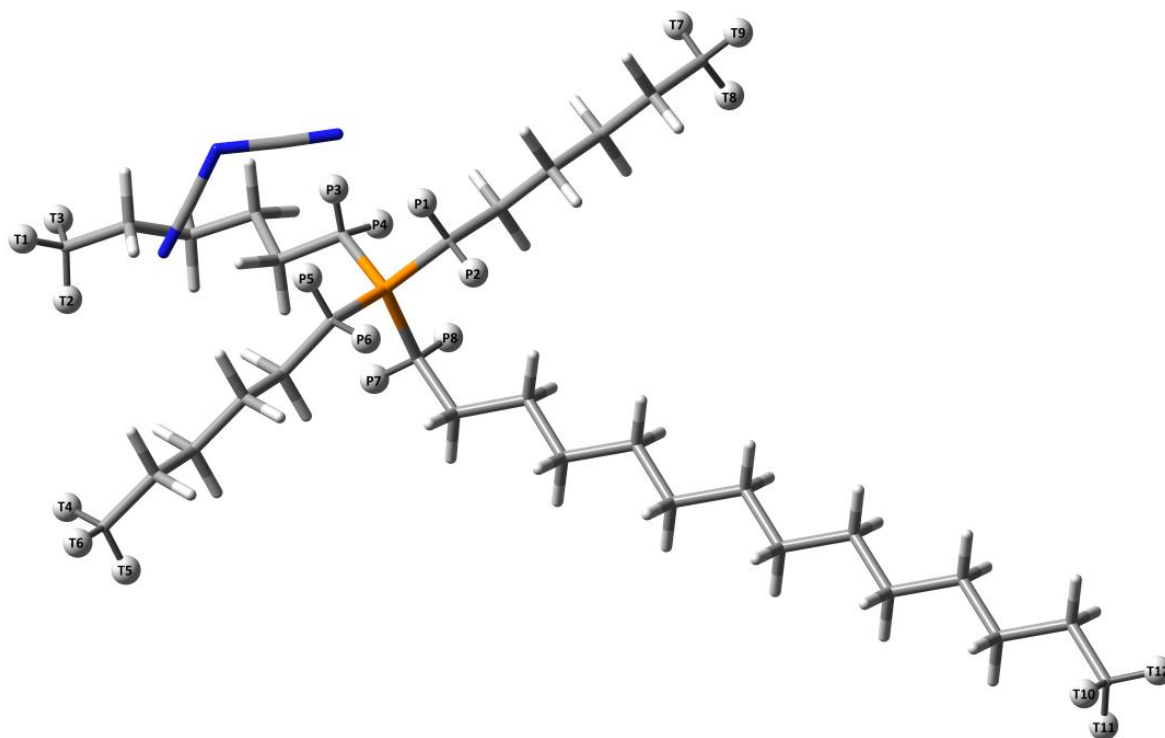


Figure A17: Local minima geometry of [P₆₆₆₍₁₄₎][DCA].

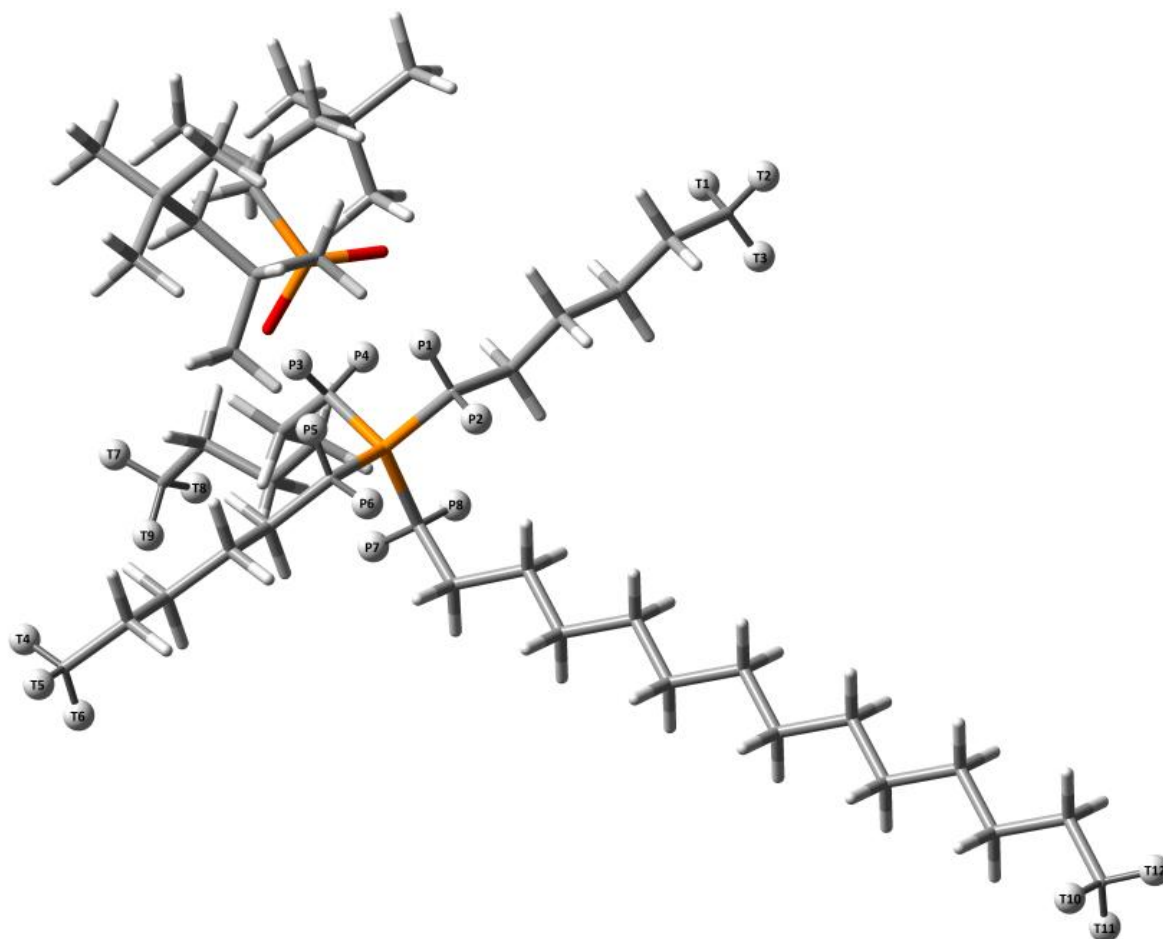


Figure A18: Local minima geometry of $[P_{66(14)}][TMPP]$.

Table A1: DFT calculated ^1H NMR chemical shifts of the individual terminal protons (see Figure A10 to A18 for labeling).

Ionic Liquids	Calculated ^1H NMR chemical shifts (ppm)											
	T1	T2	T3	T4	T5	T6	T7	T8	T9	T10	T11	T12
[P ₄₄₄₁][DBP]	5.28	0.53	0.56	1.01	0.63	0.98	0.83	1.06	0.67	0.78	1.05	0.62
[P ₄₄₄₁][MeSO ₄]	4.66	1.34	0.35	1.22	0.93	0.91	0.84	1.07	0.67	0.88	0.89	1.11
[P ₄₄₄₄][MeSO ₃]	0.95	1.00	0.62	0.79	1.07	0.68	0.74	1.00	0.74	0.73	1.03	0.72
[P ₄₄₄₄][TOS]	1.33	0.87	0.39	0.82	1.15	0.67	0.81	1.18	0.75	0.70	0.74	1.00
[P ₆₆₆₍₁₄₎][Br]	0.75	0.69	0.97	0.78	0.69	1.00	0.63	1.04	0.70	0.71	0.66	0.94
[P ₆₆₆₍₁₄₎][Cl]	0.80	0.71	0.99	0.77	0.69	0.99	0.62	1.04	0.70	0.70	0.67	0.94
[P ₆₆₆₍₁₄₎][NTf ₂]	0.78	0.69	1.00	1.02	0.81	0.73	0.67	1.05	0.72	0.71	0.92	0.62
[P ₆₆₆₍₁₄₎][DCA]	1.09	0.61	0.61	0.83	0.61	0.95	0.80	1.01	0.72	0.74	0.77	0.94
[P ₆₆₆₍₁₄₎][TMPP]	0.74	0.96	0.67	0.75	0.98	0.68	1.03	0.70	0.65	0.70	0.78	0.93

Table A2: DFT calculated ^1H NMR chemical shifts of individual α -protons (see Figure A10 to A18 for labeling).

Ionic Liquids	Calculated ^1H NMR chemical shifts (ppm)							
	P1	P2	P3	P4	P5	P6	P7	P8
[P ₄₄₄₁][DBP]	-	-	5.27	1.11	4.32	1.06	1.65	1.46
[P ₄₄₄₁][MeSO ₄]	-	-	4.66	2.07	1.38	1.43	1.19	1.56
[P ₄₄₄₄][MeSO ₃]	4.79	1.87	4.35	1.21	4.66	0.96	1.63	1.45
[P ₄₄₄₄][TOS]	5.28	1.55	5.05	1.17	1.78	1.53	1.55	1.42
[P ₆₆₆₍₁₄₎][Br]	5.91	0.77	5.46	1.19	4.89	1.05	1.74	1.25
[P ₆₆₆₍₁₄₎][Cl]	5.54	0.90	5.26	1.13	4.84	0.94	1.78	1.21
[P ₆₆₆₍₁₄₎][NTf ₂]	3.67	1.22	3.23	1.34	3.44	1.47	1.74	1.40
[P ₆₆₆₍₁₄₎][DCA]	3.99	1.02	3.10	1.29	2.85	1.12	1.87	1.19
[P ₆₆₆₍₁₄₎][TMPP]	6.02	0.71	5.39	1.24	5.10	0.96	1.60	1.46

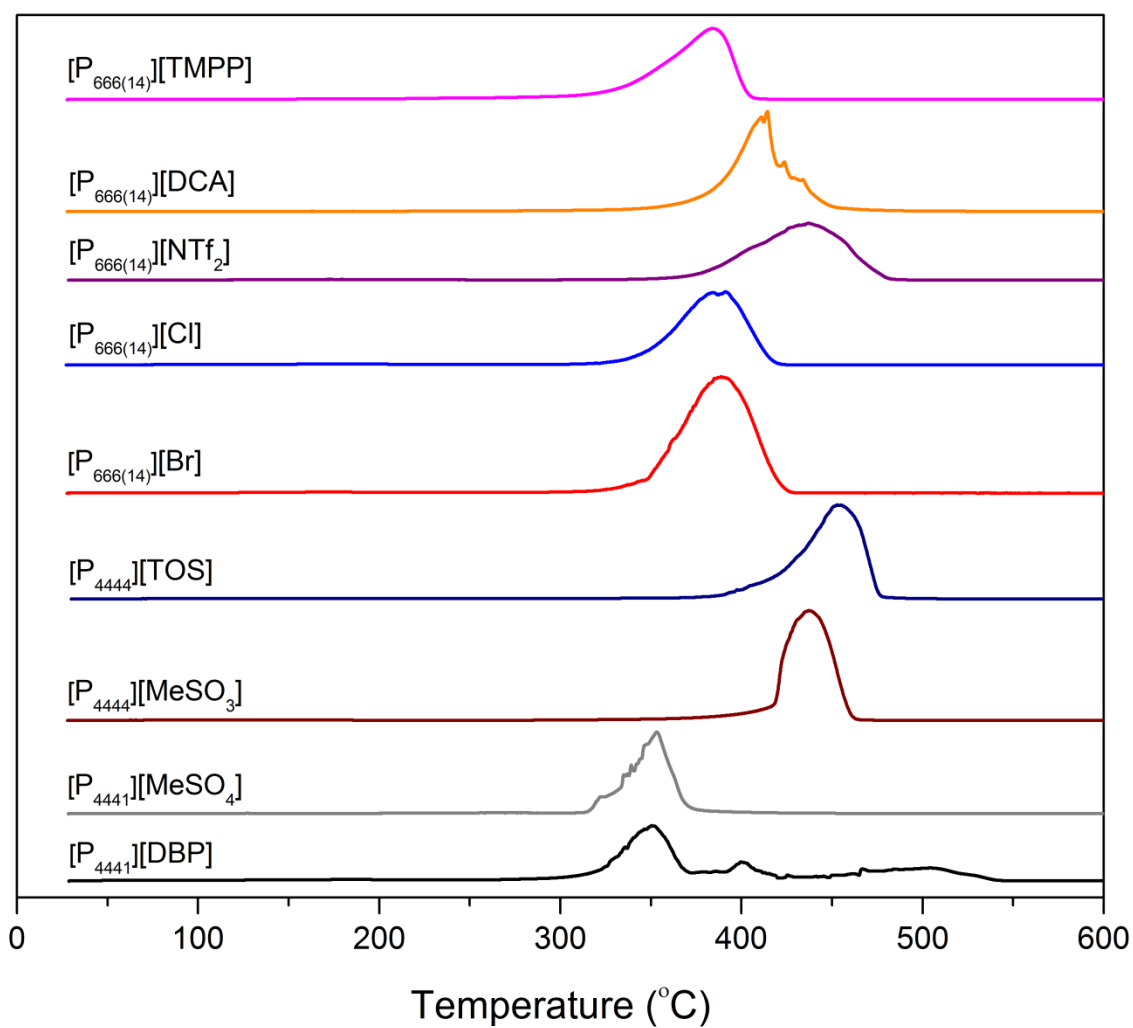


Figure A19: Comparison of fast-scan DTG results of phosphonium ILs.

Table A3: Molar volumes of ILs at 25 °C.

Ionic Liquids	Molar Volume (cm ³ mol ⁻¹)
[P ₄₄₄₁][DBP]	439.74 [1]
[P ₄₄₄₁][MeSO ₄]	308.06 [2]
[P ₄₄₄₄][MeSO ₃]	387.30 [3]
[P ₄₄₄₄][TOS]	458.70 [4]
[P ₆₆₆₍₁₄₎][Br]	590.32 [5]
[P ₆₆₆₍₁₄₎][Cl]	582.74 [2]
[P ₆₆₆₍₁₄₎][NTf ₂]	716.30 [2]
[P ₆₆₆₍₁₄₎][DCA]	611.44 [2]
[P ₆₆₆₍₁₄₎][TMPP]	866.89 [5]

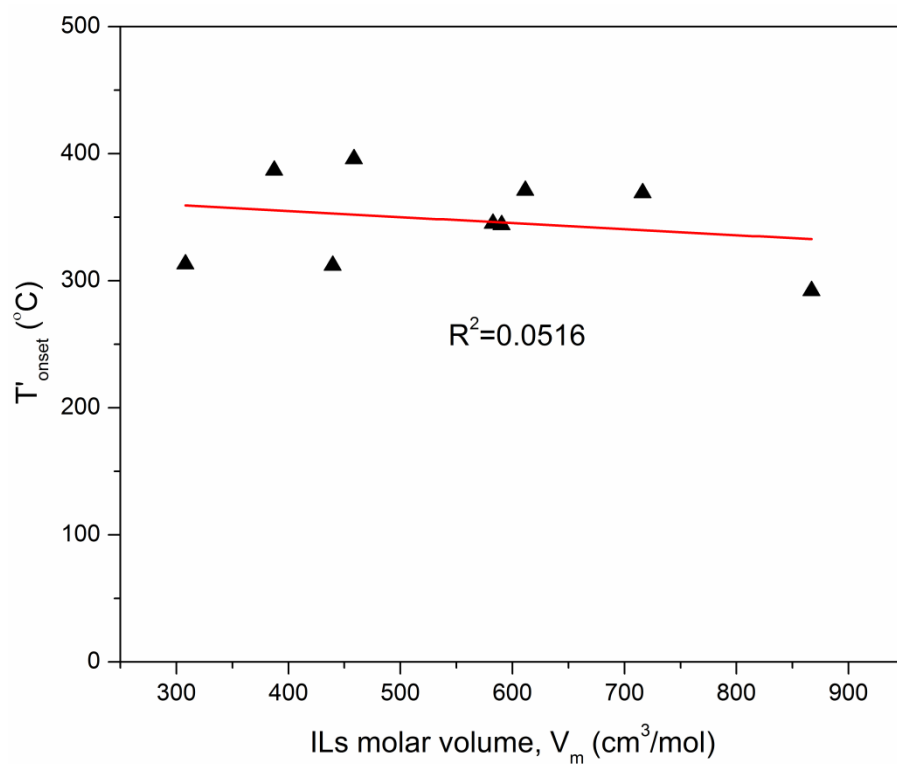


Figure A20: Relationship between size of ILs in terms of molar volumes at 25 °C and their corresponding thermal stability limits: Data show that there is no direct correlation between the size of ILs and their stability limits.

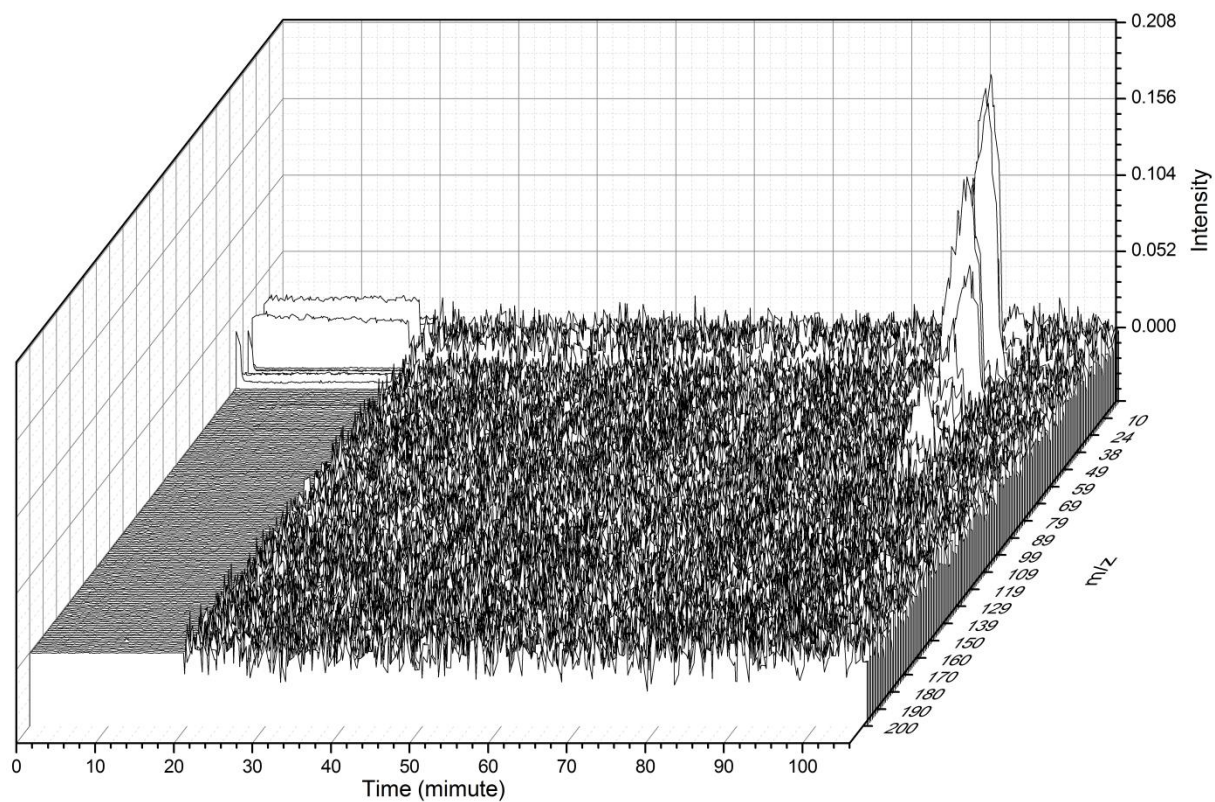


Figure A21: Mass spectra monitoring the effluent gas stream during temperature programmed decomposition of $[P_{666(14)}][Cl]$ in flowing nitrogen covering whole range of m/z values, from 1 to 200 (m/z values for nitrogen and moisture are excluded for clarity).

REFERENCES

- [79] Sigma-Aldrich customer support.
- [80] A.F. Ferreira, P.N. Simões, A.G.M. Ferreira, Quaternary Phosphonium-Based Ionic Liquids: Thermal Stability and Heat Capacity of the Liquid Phase, *J. Chem. Thermodyn.*, 45 (2012), 16-27.
- [81] U. Domanska, L.M. Casas, Solubility of Phosphonium Ionic Liquid in Alcohols, Benzene, and Alkylbenzenes, *J. Phys. Chem. B*, 111 (2007), 4109-4115.
- [82] U. Domanska, K. Paduszynski, Phase Equilibria Study in Binary Systems (Tetra-N-Butylphosphonium Tosylate Ionic Liquid + 1-Alcohol, or Benzene, or N-Alkylbenzene), *J. Phys. Chem. B*, 112 (2008), 11054-11059.
- [83] K.J. Fraser, D.R. MacFarlane, Phosphonium-Based Ionic Liquids: An Overview, *Aust. J. Chem.*, 62 (2009), 309-321.